Undulatory Locomotion in Freshwater Stingray Potamotrygon Orbignyi: Kinematics, Pectoral Fin Morphology, and Ground Effects on Rajiform Swimming

Professor George V. Lauder Erin Leigh Blevins

Undulatory locomotion in freshwater stingray *Potamotrygon orbignyi*: kinematics, pectoral fin morphology, and ground effects on rajiform swimming

Abstract

Fishes are the most speciose group of living vertebrates, making up more than half of extant vertebrate diversity. They have evolved a wide array of swimming modes and body forms, including the batoid elasmobranchs, the dorsoventrally flattened skates and rays, which swim via oscillations or undulations of a broad pectoral fin disc. In this work I offer insights into locomotion by an undulatory batoid, freshwater stingray *Potamotrygon orbignyi* (Castelnau, 1855), combining studies of live animals, physical models, and preserved specimens.

In Chapter 1, I quantify the three-dimensional kinematics of the *P. orbignyi* pectoral fin during undulatory locomotion, analyzing high-speed video to reconstruct three-dimensional pectoral fin motions. A relatively small portion (~25%) of the pectoral fin undulates with significant amplitude during swimming. To swim faster, stingrays increase the frequency, not the amplitude of propulsive motions, similar to the majority of studied fish species. Intermittently during swimming, a sharp, concave-down lateral curvature occurred at the fin margin; as the fin was cupped against the pressure of fluid flow this curvature is likely to be actively controlled.

Chapter 2 employs a simple physical model of an undulating fin to examine the ground effects that stingrays may experience when swimming near a substrate. Previous research considering static air- and hydrofoils indicated that near-substrate locomotion offers a benefit to propulsion. Depending on small variations in swimming kinematics, undulating fins can swim

faster near a solid boundary, but can also experience significant increases (~25%) in cost-of-transport.

In Chapter 3, I determine how pectoral and pelvic fin locomotion are combined in *P. orbignyi* during augmented punting, a hybrid of pectoral and pelvic fin locomotion sometimes employed as stingrays move across a substrate. The timing of pectoral and pelvic fin motions is linked, indicating coordination of thrust production. Chapter 4 discusses pectoral fin structure and morphological variations within the fin, correlating morphology with the swimming kinematics observed in Chapter 1. Passive and active mechanisms may stiffen the anterior fin to create the stable leading edge seen during swimming; stingrays have converged on several structural features (fin ray segmentation and branching) shared by actinopterygian fishes.

Table of Contents

For my teachers.

Acknowledgements

I am extraordinarily lucky to have been advised by Dr. George V. Lauder. Thanks to the advice of Dr. Alison Sweeney, I attended the 2005 meeting of the Society for Integrative and Comparative Biology, walked into a few presentations about fish swimming, and the rest was history. Drs. Andrew Biewener, Stacey Combes, Farish Jenkins, Jr., and Karel Liem (in body and spirit) have offered great advice on my research and career as members of my thesis committee, as have past and present members of the Lauder Lab. In particular, my experience as a graduate student and teacher would not have been the same without my labmate Jeanette Lim. I am grateful to my students for everything I learned while standing at the front of a classroom, and through work with the Derek Bok Center for Teaching and Learning; to poets Joanna Klink and Liza Flum; and to Katie Humphry and the incomparable Nora Lally-Graves, my friends. Because it doesn't go without saying, I am deeply thankful for the love and support of my partner, Anton Dorokhin, and my parents, Shelley and David Blevins, who have been with me all the way.

My interest in biology is grounded in respect for and curiosity about animal life, and so in addition to the people mentioned above I honor the contributions of the stingrays and other fish involved in this work.

Introduction

Fishes move through the water by using their bodies and fins to push on the fluid that surrounds them, accelerating flows backward and creating thrust opposite to their direction of travel. Swimming fishes are able to create such thrust due to the density and viscosity of water, as they push off of a medium roughly eight hundred times more dense than air, and over an order of magnitude more viscous—but the same properties that allow fish to generate thrust lead to the creation of drag forces that resist motion (Vogel, 2003). Fishes have evolved myriad ways to accomplish locomotion, generating thrust and overcoming drag to move through the water and accomplish other necessary behaviors such as prey detection, predator avoidance, and breeding.

Fish body forms are as diverse as their swimming modes. More than half of extant vertebrate species are fish, and within this diversity fish species span orders of magnitude in size and body flexibility, from microscopic larvae to giant whale sharks, and from the nearly-boneless hagfish that ties itself into knots, to the stiff-bodied boxfish with its unbending carapaces (Helfman, 2009). Classical descriptions of swimming modes grouped fishes by the predominant fins used to power propulsion, and the degree to which body undulation was involved in swimming (Breder, 1926). Subsequent research has expanded and revised these descriptions for many species, as new techniques such as high-speed videography, particle image velocimetry, robotic and computer modeling have allowed researchers to examine in greater detail the kinematics with which fish move, and the hydrodynamics that result from their interactions with the surrounding fluid. As three-dimensional analyses have become possible, the importance of considering 3-D interactions between fish and fluid has become increasingly apparent (Tytell et al., 2008; Flammang et al., 2011). At the same time, robotic models offer the

opportunity to simplify biological systems into physical models, studying the effects of particular parameters (e.g. shapes, movement patterns) in isolation (Lauder et al, 2011).

Among Breder's original classifications of fish swimming was the eponymous rajiform locomotion, which included swimming by skates (Rajidae) and other batoid elasmobranchs that swim via undulations or oscillations of expanded pectoral fins (Breder, 1926). Undulation and oscillation were initially considered as discrete modes, termed rajiform (after the skates) and mobuliform (after Mobulidae, the manta and devil rays) respectively (Webb, 1994). More recently, they have been recognized as two poles of a continuum defined by the number of waves present on a batoid's pectoral fin during swimming (wavelength/pectoral disc length; Rosenberger, 2001). Batoids also exhibit a range of pectoral fin shapes, from the triangular fins of mobulids and other oscillators, with a high ratio of fin span to chord, to the rounder shapes of undulators, with a low ratio of fin span to chord (Webb, 1994; Rosenberger, 2001). The combination of diversity in pectoral disc shape and swimming kinematics results in a large parameter space for batoid locomotion.

Even within a single undulatory species, the broad, flexible pectoral surface undulates in three dimensions, with the potential for waveforms to vary along fin chord and span. The ability to vary pectoral fin locomotor patterns is important for batoids. In many fishes, separate fin and body surfaces control separate aspects of locomotion: some may control torques while others produce thrust, and others are involved in maneuvering. In sharks, the body provides lift while the caudal fin drives propulsion, and the pectoral fins add additional lift during ascents (Wilga and Lauder, 2002). In batoids, the body and pectoral fins are essentially fused into one surface (Compagno, 1999). All locomotor functions and some besides, from steady swimming to maneuvering and even prey capture (Wilga et al., 2012) must be achieved by modulating the

shape of the pectoral waveform. However, there is one notable exception –despite the dominance of the pectoral disc, batoids retain pelvic fins, which are often employed by benthic species in punting locomotion along the substrate (Lucifora and Vassallo, 2002; Koester and Spirito, 2003) Undulatory batoids can combine pectoral undulation with pelvic fin punting, adding yet another dimension to locomotion (Macesic and Kajiura,2010).

In this work I offer insights into locomotion by an undulatory batoid, freshwater stingray *Potamotrygon orbignyi* (Castelnau, 1855), combining studies of live animals, physical models, and preserved specimens. In Chapter 1, I quantify the three-dimensional kinematics of the pectoral fin during undulatory locomotion by *P. orbignyi*, including the waveform changes associated with increases in swimming speed. Chapter 2 employs a simple physical model of an undulating fin to examine the ground effects swimming stingrays may experience when swimming near a substrate. Chapter 3 determines how pectoral and pelvic fin locomotion are combined in *P. orbignyi* during augmented punting (a hybrid of pectoral and pelvic fin locomotion), and Chapter 4 discusses pectoral fin structure and morphological variations within the fin, correlating morphology with the swimming kinematics observed in Chapter 1.

References

Breder, C. M. (1926). The locomotion of fishes. *Zoologica* **50**, 159–297.

Flammang, B. E., **Lauder, G. V., Troolin, D. R., and Strand, T.E**. (2011). Volumetric imaging of fish locomotion. *Biology Letters* **7**,695-698.

Helfman, G., Colette, B. B., Facey, D.E., and Bowen, B.W. (1999). *The Diversity of Fishes: Biology, Evolution, and Ecology, 2nd edition.* Chichester, UK: Wiley-Blackwell.

Koester, D. M. and Spirito, C. P. (2003). Punting: An unusual mode of locomotion in the Little Skate, *Leucoraja erinacea* (Chondrichthyes: Rajidae). *Copeia.* **3**, 553-561.

Lauder, G., Tangorra, J., Lim, J., Shelton, R., Witt, C., and Anderson, E.J. (2011). Robotic models for studying undulatory locomotion in fishes. *Marine Tech. Soc J.* **45**, 41-55.

Lucifora, L.O. and Vassallo, A.I. (2002). Walking in skates (Chondrichthyes, Rajidae): Anatomy, behaviour and analogies to tetrapod locomotion. *Biol. J. Linn. Soc.* **77**, 35–41.

Macesic, L. J. and Kajiura, S. M. (2010). Comparative punting kinematics and pelvic fin musculature of benthic batoids. *J. Morph.* **271**, 1219-1228.

Rosenberger, L. J. (2001). Pectoral fin locomotion in Batoid fishes: undulation versus oscillation. *J. Exp. Biol.* **204**, 379-394.

Tytell, E. D., Standen, E. M. and Lauder, G. V. (2008). Escaping flatland: three-dimensional kinematics and hydrodynamics of median fins in fishes. *J. Exp. Biol.* **211**, 187-195.

Vogel, S. (2003). *Comparative Biomechanics: Life's Physical World*. New Jersey: Princeton University Press.

Webb, P. W. (1994). The biology of fish swimming. In *Mechanics and Physiology of Animal Swimming* (ed. L. Maddock, Q. Bone and J. M. V. Rayner), pp. 45–62. Cambridge: Cambridge University Press.

Wilga, C. D. and Lauder, G. V. (2002). Function of the heterocercal tail in sharks: quantitative wake dynamics during steady horizontal swimming and vertical maneuvering. *J. Exp. Biol.* **205**, 2365-2374.

Wilga, C. D., Maia, A., Nauwelaerts, S. and Lauder, G. V. (2012) Prey handling using whole body fluid dynamics in batoids. *Zoology.* **115**, 47-57.

Chapter 1

Rajiform locomotion: three-dimensional kinematics of the pectoral fin surface during swimming by freshwater stingray *Potamotrygon orbignyi*

Abstract

Rajiform locomotion in fishes is dominated by distinctive undulations of expanded pectoral fins. Unlike other fishes which typically interact with the fluid environment via multiple fins, undulating rays modulate a single control surface, the pectoral disc, to perform pelagic locomotion, maneuvering, and other behaviors. Complex deformations of the broad, flexible pectoral fins occur as the undulating wave varies in three dimensions (3-D); pectoral fin kinematics and changes in waveform with swimming speed cannot be fully quantified by two-dimensional analyses of the fin margin. We present a 3-D analysis of undulatory rajiform locomotion in a batoid, the freshwater stingray *Potamotrygon orbignyi*. Using three video cameras (250 fs^{-1}), we gathered 3-D excursion data from 29 points on the pectoral fin during swimming at 1.5 and 2.5 disc-lengths per second, describing the propulsive wave and contrasting waveforms between swimming speeds. Only a relatively small region of the pectoral fin (~25%) undulates with significant amplitude (>0.5 cm). Stingrays can maintain extreme lateral curvature of the distal fin margin in opposition to induced hydrodynamic loads, "cupping" the edge of the pectoral fin into the flow, with implications for drag reduction. Wave amplitude increases across anteroposterior and mediolateral fin axes. Along the anteroposterior axis, amplitude increases until the wave reaches mid-disc and then remains constant, in contrast to angulliform patterns of continuous amplitude increase. Increases in swimming speed are driven by both wave frequency and wavespeed, though multivariate analyses reveal a secondary role for amplitude.

Introduction

Fish interact with the fluid environment using a variety of surfaces—paired fins, median fins, and the body itself (Harris, 1936; Standen and Lauder, 2005; Standen and Lauder, 2007; Tytell et al., 2008; Webb, 2006). These multiple control surfaces work in combination to produce thrust and balance torques in steady swimming, to maneuver, and at evolutionary timescales may offer redundant systems, allowing one set of fins to specialize for a particular function while others drive locomotion (e.g. pelvic "sucker discs" in Liparidae, dorsal fin "fishing lures" in Lophiidae). In contrast, rays (Batoidea) perform virtually all behaviors using a single broad surface: the distinctive, expanded pectoral fins. Pelvic fins are also employed by benthic skates and rays as they move along the substrate (Macesic and Kajiura, 2010), but the pectoral fins control functions that range from epibenthic and pelagic locomotion to prey capture and camouflage, as rays bury themselves or search for food in the substrate (Wilga et al., 2012).

Locomotion by rays and skates has been set apart since early classifications of swimming modes, with the eponymous "rajiform mode" originally encompassing locomotion by any elasmobranch with expanded pectoral fins, from mantas (Myliobatidae: Mobulinae) to stingrays (Dasyatidae) (Breder, 1926). Most batoids do use their pectoral fins to swim, with the exception of body-caudal fin propulsion by guitarfish (Rhiniformes and Rhynchobatiformes; Klausewitz, 1965) and torpedo rays (Torpediniformes; Roberts, 1969). However, even among pectoral-fin swimmers, fin morphology and kinematics vary widely. More recent work has recognized the diversity of locomotion within the group, distinguishing two modes: (1) mobuliform oscillation, underwater flapping flight dominated by dorsoventral excursion; and (2) rajiform undulation, via a propulsive wave of bending that passes from anterior to posterior along the pectoral fin (Webb, 1994). Rosenberger (2001) identified a continuum of batoid locomotion between oscillation and

undulation, with species' position between the two extremes defined by the number of waves present on the pectoral fin at one time; undulators have more than one wave, oscillators less than one. The distinction is more than kinematic: oscillators are typically pelagic, and have high-aspect-ratio fins, while undulators are primarily benthic, with a low-aspect-ratio pectoral disc (Rosenberger, 2001). Skeletal morphology also reflects locomotor mode, with areas of increased fin stiffness and preferential axes of bending created by the arrangement of fin-radial joints and variations in calcification pattern (Schaefer and Summers, 2005).

Both oscillatory and undulatory rays are popular inspirations for biomimetic designs. Studies of mobuliform locomotion have found surprising maneuverability and efficiency in mantas and other, typically large, "underwater fliers" (Heine, 1992; Parson et al., 2011); the charismatic manta is the basis of several bio-inspired robots (e.g. Moored et al., 2011). Mathematical models suggest interesting fluid properties for undulating rays as well; vortices may be retained in the troughs of an undulating fin, acting as "fluid roller bearings" that reduce drag (Wu et al., 2007), while stingray-like "waving plates" may relaminarize flow (Taneda and Tomonari, 1974). Opportunities to investigate these phenomena are increasing as advances in robotics and new, flexible biomaterials make undulatory locomotion a practical model for biomimesis. Models of knifefish (Curet et al., 2011), undulatory rays and ray-like fins (Low, 2006; Clark and Smits, 2006) may be based on different organisms, but they share the same underlying principle: locomotion is controlled by a single undulating surface, with modulations of the wave function producing steady swimming, acceleration, or more complex maneuvers.

The fins of undulating rays and their robotic counterparts are both broad and highly flexible, as they must have sufficient area to generate thrust and the capacity to bend into various waveforms. This combination of flexibility and breadth creates a large parameter space of

possible waves; waveforms are truly three-dimensional, and may vary along both anteroposterior and mediolateral axes (i.e., both fin chord and span). Changes in waveform may occur via the direct action of dorsal and ventral fin muscles during wave propagation, as seen in the blue-spot stingray *Taenuria lymma* (Rosenberger and Westneat, 1999). They could also result from variations in overall fin structure (Schaefer and Summers, 2005) or the shape and stiffness of individual fin elements, as Taft et al. (2008) found to influence pectoral fin motion in sculpin.

In this study, we analyze pectoral fin undulation in three dimensions, determining the kinematics of the propulsive wave in steady swimming by freshwater stingray *Potamotrygon orbignyi* (Castelnau, 1855), an undulatory swimmer. Previous work on undulating rays has described the propulsive wave in terms of the motion of a single point at the fin margin (Rosenberger, 2001), or several points along the margin (Rosenberger and Westneat, 1999), but has not explored the pectoral fin as an undulating *surface*. Here, we ask how the propulsive wave changes as it propagates across the pectoral fin, and determine what modulations occur with increased swimming speed. In most fishes, increases in the frequency of propulsive motions drive increases in swimming speed (e.g. increased tailbeat frequency) while amplitude remains constant (Bainbridge, 1958; Drucker and Jensen, 1996). However, in the only detailed study of stingray swimming kinematics, Rosenberger and Westneat (1999) find that the swimming speed of *T. lymma* is frequency-modulated in some cases, and amplitude-modulated in others, depending on the individual. We therefore expect similar individual variation in *P. orbignyi,* with swimming speed driven by either the frequency or amplitude of the pectoral wave. Within speeds, we predict that amplitude will increase along both anteroposterior and mediolateral axes, and that the wave will accelerate as it propagates. To test our hypotheses and describe the three-dimensional wave, we gathered detailed 3D excursion data from 29 points

across the pectoral fin surface, determining wave properties and values for fin curvature. We compare and contrast waveforms between the two swimming speeds, discovering how pectoral undulations are modulated to increase velocity.

Materials and Methods

Animals

Juvenile freshwater stingrays, *Potamotrygon orbignyi* (Castelnau, 1855), were purchased from a local importer and transported to Harvard University, MA, USA. We chose to work with juvenile potamotrygonids as their small size (mean pectoral disc length (DL) 12.8±0.8 cm, mean disc width (DW) 11.27±0.99 cm) allowed the study of undulatory swimming in a small, controlled volume, yielding high-resolution kinematic data. In the lab, stingrays were housed in individual 100 liter aquaria with >2 cm of sandy substrate (grain size 1-3mm). Animals were maintained at 27±1º C under a 12 h:12 h photoperiod, and were fed live blackworms six times per week. Three individuals were used in our experiments, with all animal care performed according to Harvard University IACUC protocols (no. 20-03).

Swimming protocol and videography

Stingrays were filmed while swimming in a calibrated, variable-speed flow tank (as in Tytell & Lauder, 2004), heated to 27±1º C, at a Reynolds number of approximately 10,000. Baffles constructed of plastic mesh (0.5 cm mesh size) were positioned upstream and downstream to restrict stingrays to the working section (28 cm wide, 28 cm high and 66 cm long). A third, angled baffle was placed ventral to the stingray to encourage swimming, preventing stingrays from settling to the flat flow tank bottom where they could remain motionless even in high flow.

The baffle was positioned with its upstream end higher than its downstream end, forming an angle of approximately 20 degrees with the tank bottom. We verified that fluid maintained micro-turbulent flow and steady velocity as it passed through the angled baffle, and analyzed only swimming sequences where stingrays swam well clear of all baffles and flow tank surfaces. We used a wooden dowel to maneuver animals away from the sides of the flow tank, but removed it before filming. Individual stingrays were filmed during steady swimming at two speeds, 1.5 and 2.5 disc-lengths (DL) per second (approximately 0.20 and 0.33 m/s, respectively).

Swimming sequences were recorded at 250 frames per second by three synchronized, one-megapixel high speed video cameras (FASTCAM 1024 PCI; Photron USA, Inc., San Diego, CA, USA). One camera captured a dorsal view via a 45º angled mirror positioned above the flow tank, and the remaining two cameras were set off-axis from dorsal and lateral positions. Camera height and angles ensured that all portions of the stingray fin were visible in at least two camera views throughout each finbeat. (One finbeat was defined as a full cycle of the propulsive wave.) As cameras were widely-spaced to film stingrays from different angles, this allowed kinematics to be reconstructed in three dimensions. Cameras were calibrated using direct linear transformation (DLT) to remove image distortion and align camera views in three-space, using the DLT Calibration 3 program in MATLAB version 7.10 (Mathworks, Natick, MA, USA; Hedrick, 2008).

Kinematic measurements and analysis

To determine the three-dimensional kinematics of undulation and variations with swimming speed, we analyzed four finbeats from each of three individuals for two speeds, for a total of 24

sequences. Finbeats were defined as a full cycle of the propulsive wave, from the initiation of a wave at the anterior edge of the fin through completion as the wave passed off the posterior edge. Using the DLT Dataviewer 2 program in MATLAB version 7.10 (Hedrick, 2008), we digitized 31 points across the right pectoral fin and along the body midline, determining the x, y, and z coordinates of each point in every frame via direct linear transformation to give fin surface deformations in 3D (Figure 1.1). Natural pigmentation markings on the dorsal surface of the pectoral fin allowed the same points to be reliably identified in each camera view. After initial analysis confirmed that the body midline does not undulate, we slightly reduced the number of midline points analyzed, and present results based on 29 digitized points.

Throughout the paper, we present standardized measurements relative to disc length (DL), disc width (DW), and disc perimeter, corresponding to Rosenberger and Westneat (1999) and Rosenberger (2001). Disc length was measured from the most anterior point on the stingray snout to the posterior margin of the pectoral fin disc, and is equivalent to chord-length. Disc width was determined as the distance from the lateral edge of one pectoral fin to the other, at the widest part of the pectoral fin disc, equivalent to fin span. For each swimming sequence, mean values were determined for kinematic variables including the amplitude, frequency, wavespeed, and wavelength of the propulsive wave, plus whole-body angle of attack and fin curvature. These variables (frequency, amplitude, wavespeed, and wavelength) allow us to characterize the pectoral fin wave as it propagates across the surface of the fin, and determine additional features of stingray locomotion (angle of attack, fin curvature) that influence the interactions of fish and fluid. We compare these variables between speeds to quantify the kinematic changes that increase thrust and allow stingrays to swim faster. Amplitude was calculated for each point as

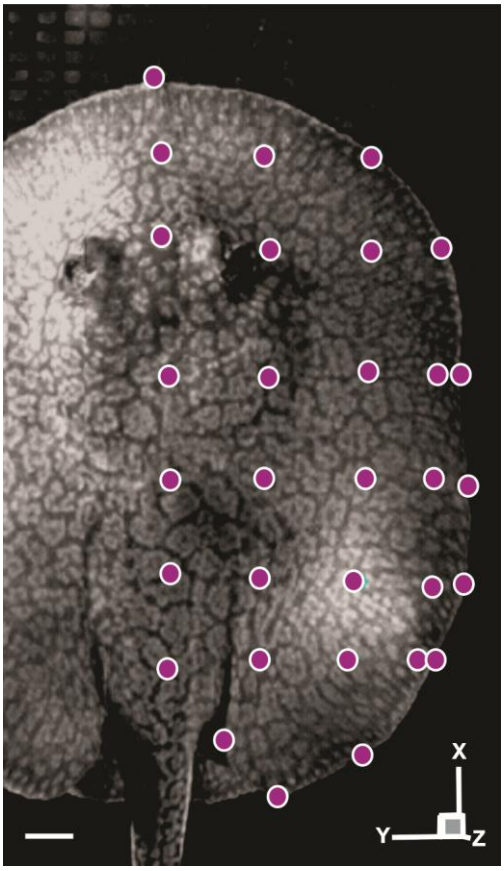

Figure 1.1. Dorsal view of freshwater stingray *Potamotrygon orbignyi* (anterior at top); purple circles indicate the locations of the thirty-one points digitized on the dorsal surface of the right pectoral fin. Scale bar=1 cm.

half of the total dorsoventral excursion. We determined amplitude variation along the fin, and also compared total amplitude (the sum of average amplitudes for all points) between swimming speeds, as a metric to represent the volume through which the fin travels during one wave cycle. For comparison with 2D data as in Rosenberger (2001), we determined a mid-disc value amplitude at 0.5 DL, corresponding to maximum disc width. Frequency (*f*) was determined as the number of wave cycles per second at mid-disc. To determine wavespeed (*v*), we chose a known distance between points along an anteroposterior axis, then divided that distance by the time required for a given wave (e.g. crest or trough) to travel that distance. We calculated a mid-disc wavespeed at 0.5 DL along the distal margin of the fin and, to examine variation across the fin surface, determined local wavespeeds at points along three anteroposterior transects spaced at different distances from the midline. Wavespeed and frequency are not reported for every point individually as variations are subtle and require a pronounced (high amplitude) wave for reliable calculation. Wavelength (λ) was determined by dividing mid-disc wavespeed (*v*) by mid-disc frequency (*f*), according to the wave function $\lambda = v/f$. We calculated slip and stride length as two common measures of propulsive efficiency, which relate the motion of the pectoral fin to the overall forward progress of the stingray body (as in Rosenberger, 2001). Slip was calculated as the ratio of overall swimming speed (*U*) to the velocity of the propulsive wave (*v*); stride length was defined as the distance travelled per wave cycle, the ratio of forward swimming speed (*U*) to propulsive wave frequency (*f*). Strouhal number was determined by fL/U, with disc length used as the characteristic length L. Wave number, defined as the number of waves present on the fin at one time, was calculated relative to both disc length and disc perimeter. To find body angle, the angle between the body and oncoming water flow, we performed a linear regression of at least five digitized points along the stingray midline, then determined the angle between the

regression line and the horizontal axis (x-axis, parallel to the direction of flow) in each video frame. Fin curvature (κ) was determined at each timestep for three-point mediolateral transects in the mid-disc region (middle third of the fin), at the distal margin of the fin. We calculated curvature using standard methods as in Standen and Lauder (2005) and Taft et al. (2008), using the following equation:

$$\kappa = |dT/ds|$$

where s is the arc length of a curve connecting all three points in the transect, and T is the unit tangent vector of that curve. We determine values for maximum positive (concave up) and negative (concave down) curvature. The percentage of a wave cycle spent in negative curvature was determined by dividing the time spent in negative curvature by total cycle time. Beyond the results presented here, we offer detailed kinematic datasets as supplemental materials.

Statistical Analysis

A mixed-model two-factor analysis of variance (ANOVA) was performed in JMP 9 to test effects of swimming speed and individual on all kinematic variables. To compare local wavespeeds determined at different points across the fin surface, and test for differences in wavespeed based on position, we used a second ANOVA and post-hoc Tukey test. To examine multivariate differences between swimming speeds, we performed a principal components analysis (PCA) on eleven variables: mid-disc amplitude, frequency, wavespeed and wavelength; body angle; maximum amplitude; location of maximum amplitude; maximum negative curvature; maximum positive curvature; portion of cycle spent in negative curvature; and total excursion. A multivariate analysis of variance (MANOVA) was performed to test for group separation along PCA axes. All variables except the location of maximum amplitude were major

elements of the first four principal components, and were retained in a discriminant function analysis (DFA). Analyses were performed in JMP 9.0.2 (SAS Institute, Cary, NC, USA); values are given as mean ± standard error of measurement.

Results

Pectoral wave and body kinematics

Pectoral fin locomotion in *P. orbignyi* occurs via a propulsive wave passing from anterior to posterior along the fin (Figures 1.2, 1.3). At mid-disc (maximum disc width), the wave has an average amplitude of 1.41±0.06 cm (mean±s.e.m.), increasing to a maximum amplitude of 1.66±0.04 cm approximately 2 cm posterior to mid-disc; neither mid-disc nor maximum amplitude changes significantly with speed (Figure 1.4A; ANOVA, $p=0.74$ and 0.88, respectively). The location of maximum amplitude also remains constant across speeds, occurring at approximately 0.7 DL (ANOVA, $p=0.90$). Frequency, mid-disc wavespeed, and body angle all increase significantly with swimming speed (Figure 1.4B,C,D). Frequency increases from 2.53±0.16 Hz to 3.80±0.18 Hz (ANOVA, $p<0.0001$) and mid-disc wavespeed from 31.00±2.53 cm s^{-1} to 46.02±3.25 cm s^{-1} (ANOVA, $p<0.01$): a 50% increase in each value with a 65% increase in swimming speed. We calculated a mean wavelength of 12.5±0.7 cm, which did not vary across speeds (ANOVA, $p=0.89$); standardized to disc length (DL) and disc perimeter (DP), this equates to a wave number of 1.10±0.08 (DL) or 1.65±0.12 (DP). Body angle increases as stingrays swim faster, from 5.1±1.1^{o} to 7.8±0.7^{o} (ANOVA, $p<0.05$), though this finding is not illustrated by the particular sample images and view angles depicted in Figure 1.2. Stingrays swam with a slip of 0.7±0.04 and a stride length of 8.7±0.3 cm, at Strouhal

Figure 1.2. Illustration of *P. orbignyi* swimming at (A) 1.5 disc-lengths per second (DLs^{-1}) and (B) 2.5 DLs^{-1}, at intervals of 25% of one finbeat. Stingrays are shown in a three-quarter lateral view, angled slightly toward the dorsal and posterior to best show the propulsive wave. In the first row of images, a propulsive wave is initiated at the anterior edge of the pectoral fin (0% of the finbeat). As the cycle progresses, the wave passes along the pectoral fin, increasing in amplitude (25-75% of the finbeat), then passing off the posterior margin of the disc (100% of the finbeat). Note differences in wave timing between swimming speeds. However, overall findings for body angle are not reflected by the particular sample images and view angles used here.

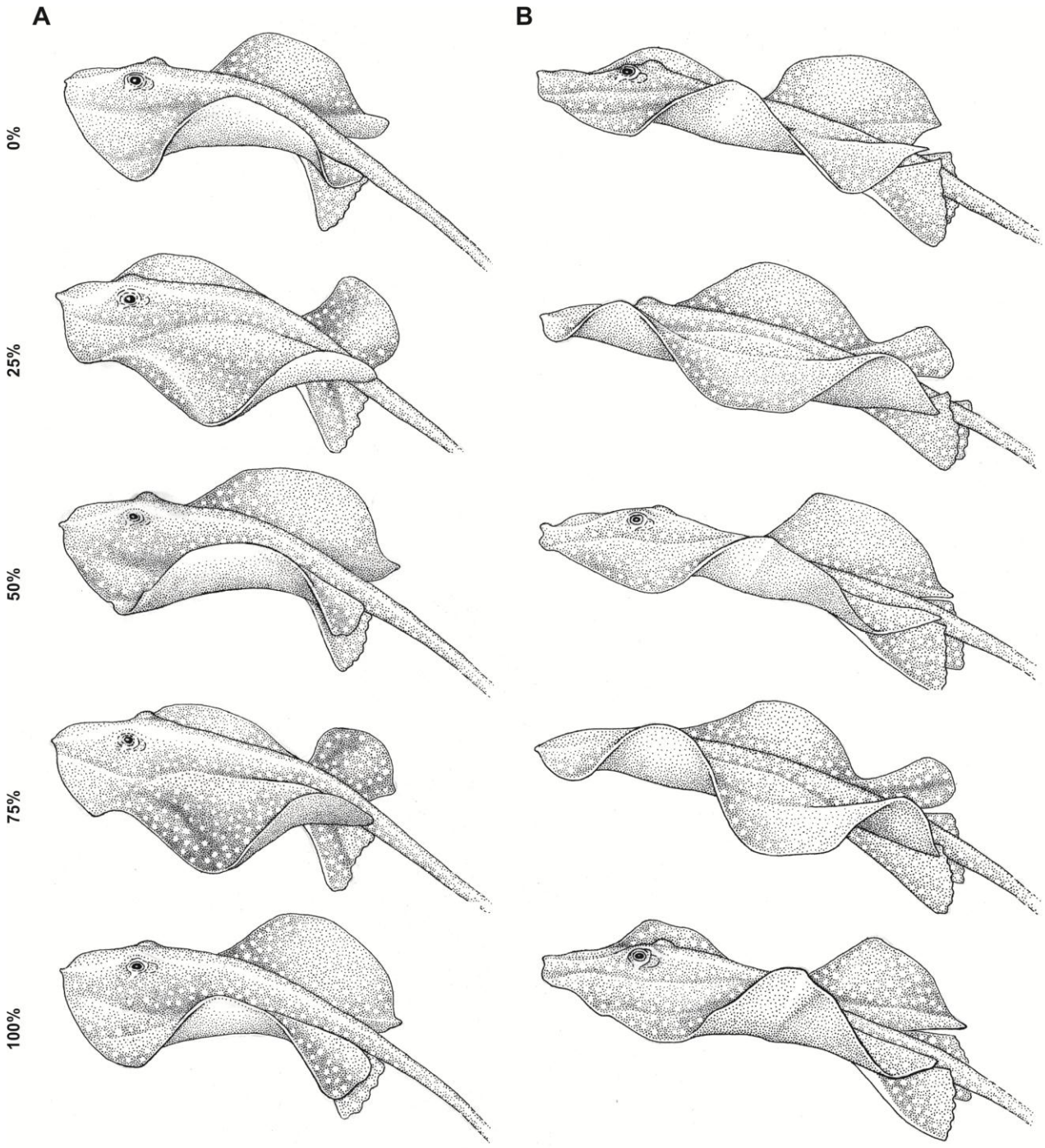

Figure 1.2 (Continued)

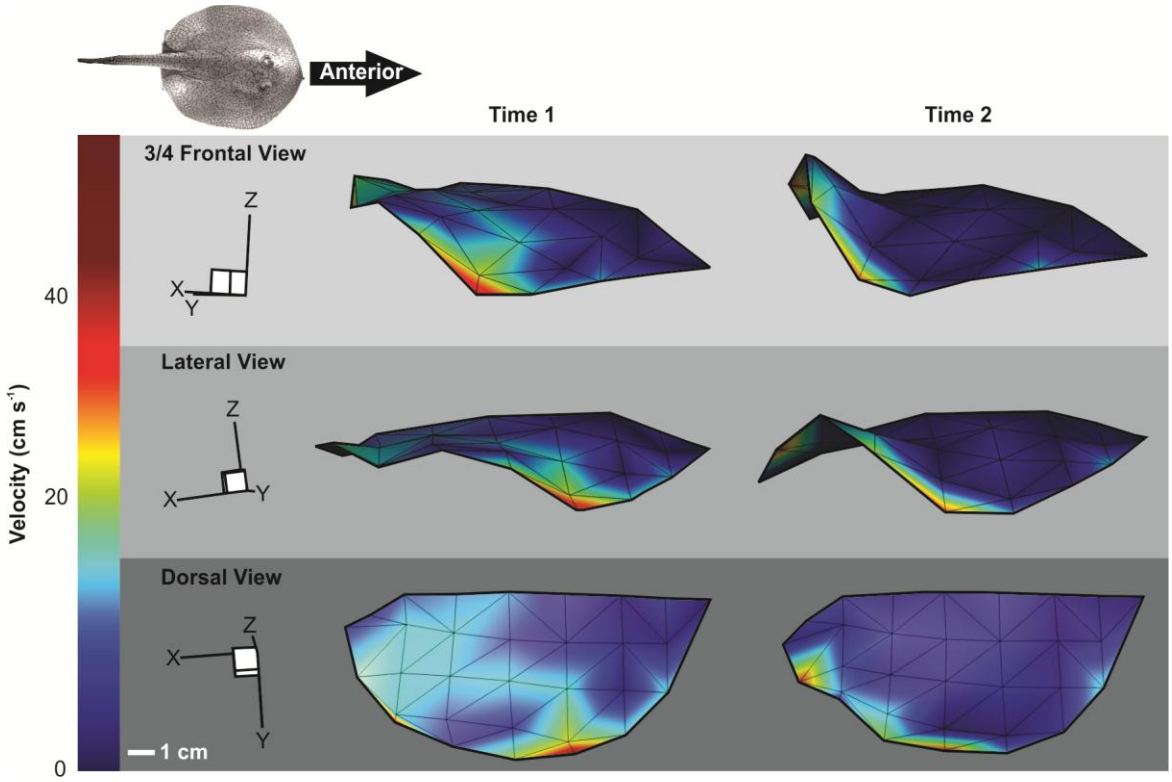

Figure 1.3. Sample images showing pectoral fin motion in three dimensions, in three-quarter frontal, lateral, and dorsal views, at two points in the wave cycle. To best portray the propulsive wave of the right pectoral fin, non-orthogonal perspectives are shown, and anterior is to the right. Images are reconstructed from digitized data points connected into a triangular mesh to model the fin surface. Colors indicate velocity magnitudes relative to the motion of the head, with greater magnitudes represented by warmer colors. Anterior is to the right. Scale bar represents 1 cm.

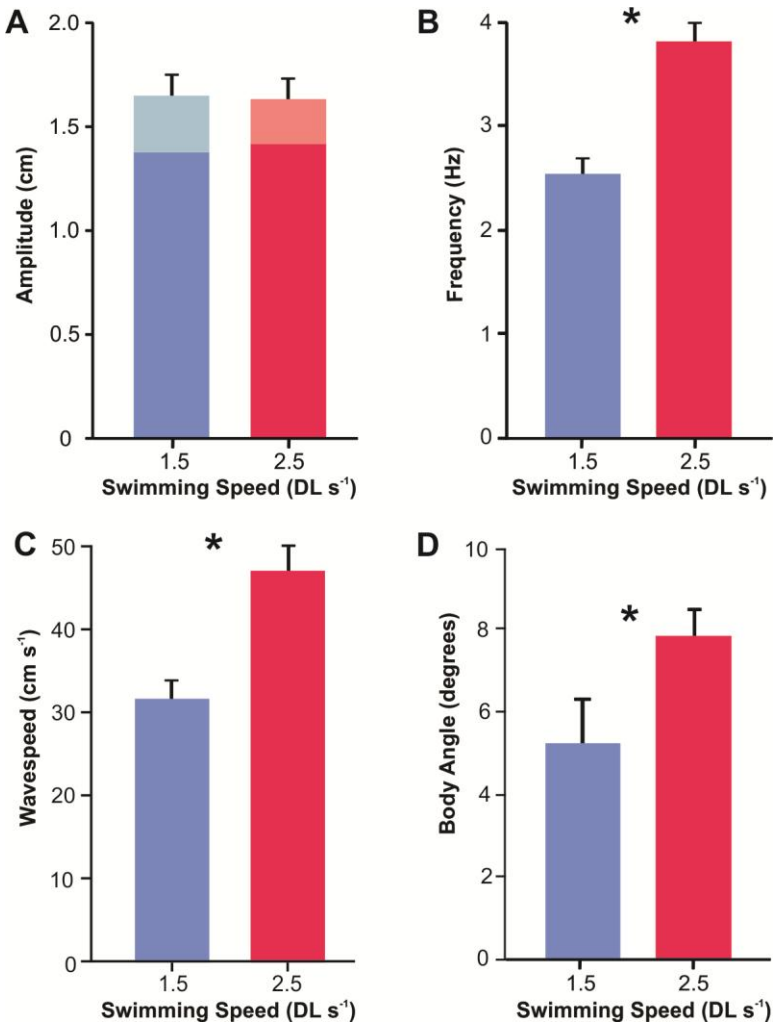

Figure 1.4. Mean values of major kinematic variables at each swimming speed, 1.5 DLs^{-1} (blue) and 2.5 DLs^{-1} (red). (A) Amplitude, as mid-disc value (deep blue/red) and maximum amplitude (light blue/red); (B) frequency; (C) mid-disc wavespeed; and (D) body angle, the incline of the dorsal midline relative to the horizontal. Asterisks indicate significant differences between swimming speeds ($p<0.05$); error bars represent one standard error. N=12 for all variables at each swimming speed.

number 0.2±0.01; none of these values differed significantly with swimming speed (ANOVA, $p>0.2$).

Kinematic variation across the fin surface

We examined variation in amplitude and wavespeed across the fin surface. Amplitude increases along both anteroposterior and mediolateral axes, with the highest excursion occurring in the distal posterior region of the fin (Figures 1.2, 1.5A). Total amplitude, the sum of pectoral fin amplitude at all positions, is 16.82±0.62 cm, and does not vary with swimming speed (Figure 1.5B; ANOVA, $p=0.48$). The mediolateral trend reflects increasing angular displacement with distance from the midline (Figure 1.6). Along the anteroposterior axis, amplitude is negligible from the anterior margin until approximately 0.3 DL (i.e., values within the margin of experimental measurements, as demonstrated by the amplitude measured at non-oscillating midline points) (Figure 1.7). Amplitude increases between 0.3 DL and approximately 0.5 DL; the rate of increase slows as the wave moves toward the posterior region of the fin, approaching an asymptote. The magnitude of the asymptote depends on distance from the midline, with points further from the midline having a higher asymptote (and greater maximum amplitude) due to increasing angular displacement along the fin's span. For all points except one, amplitudes remain constant across swimming speeds (ANOVA, $p>0.05$); the exceptional point is located just distal to the tail where the pectoral fin forms a lobe at its posterior margin, and has an amplitude inversely correlated to swimming speed, decreasing from 0.88±0.07 cm to 0.58±0.05 cm (ANOVA, $p<0.01$). In addition to the data discussed here, supplemental materials provide mean excursion data for all points (S1) and a sample dataset (x, y, and z coordinates) for one wave cycle (S2, with animation S3).

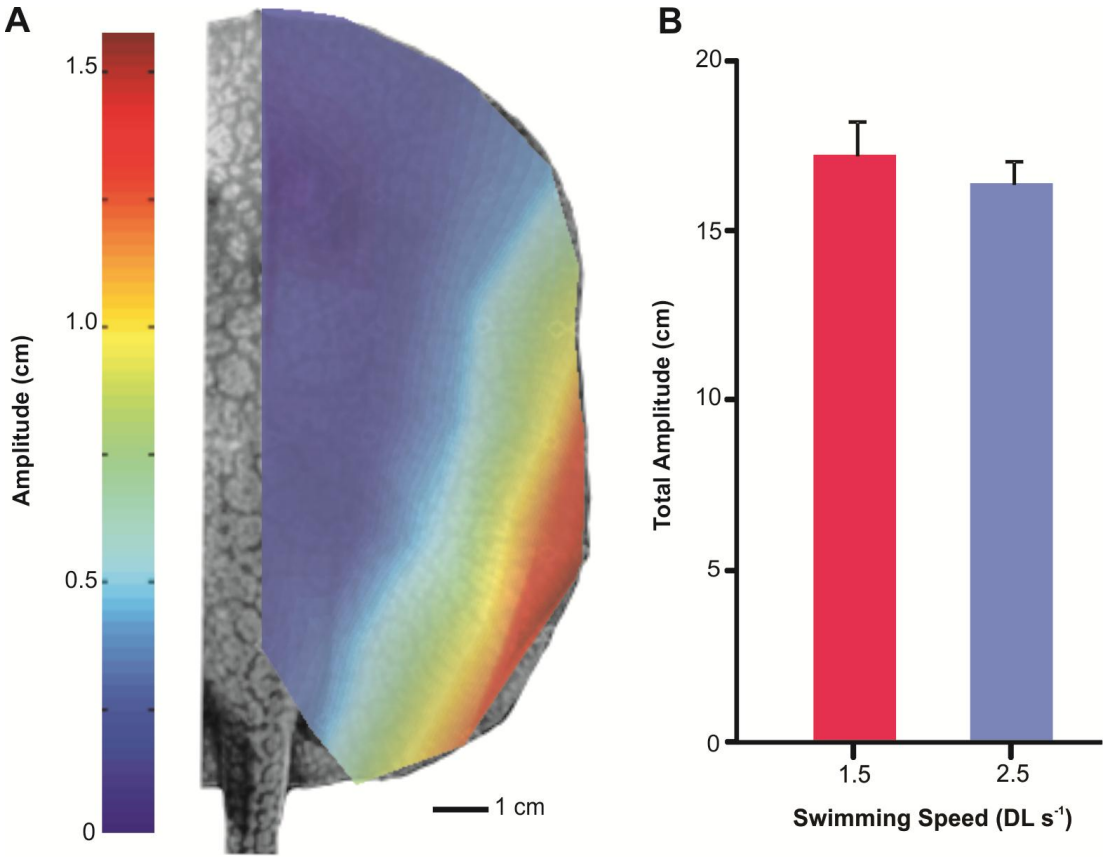

Figure 1.5. (A) Amplitude variation across the pectoral fin surface; warmer colors represent greater magnitudes. Amplitude values represent ½ of the maximum excursion occurring at each point during one wave cycle. As no significant differences in amplitude were found between swimming speeds, data were pooled (N=24). (B) Total amplitude, defined as the sum of the amplitudes of all points on the fin, at each speed (N=12; $p>0.05$); error bars indicate one standard error. Scale bar for stingray image is 1 cm.

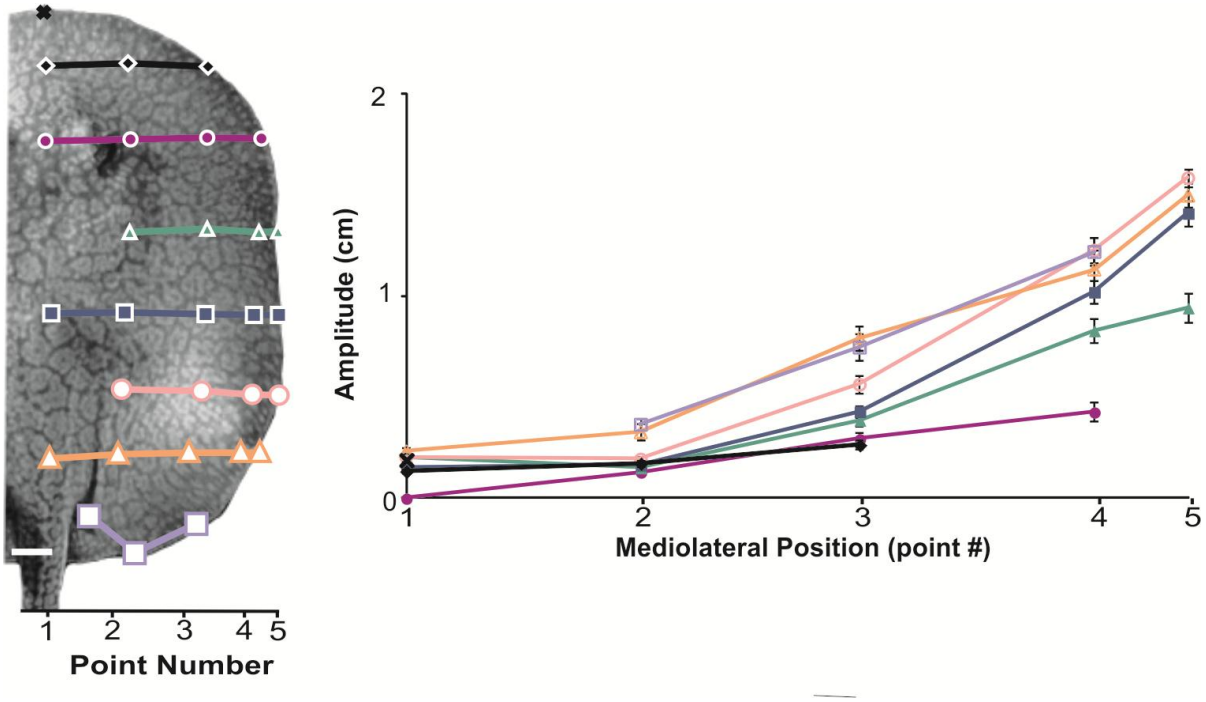

Figure 1.6. Spanwise amplitude variation along the mediolateral axis at positions indicated on stingray image. For clarity, the vertical axis is elongated by a factor of three relative to true aspect ratio. As no significant differences in amplitude were found between swimming speeds, data were pooled (N=24). Error bars represent ± standard error; some are obscured by symbols. Scale bar for stingray image is 1 cm.

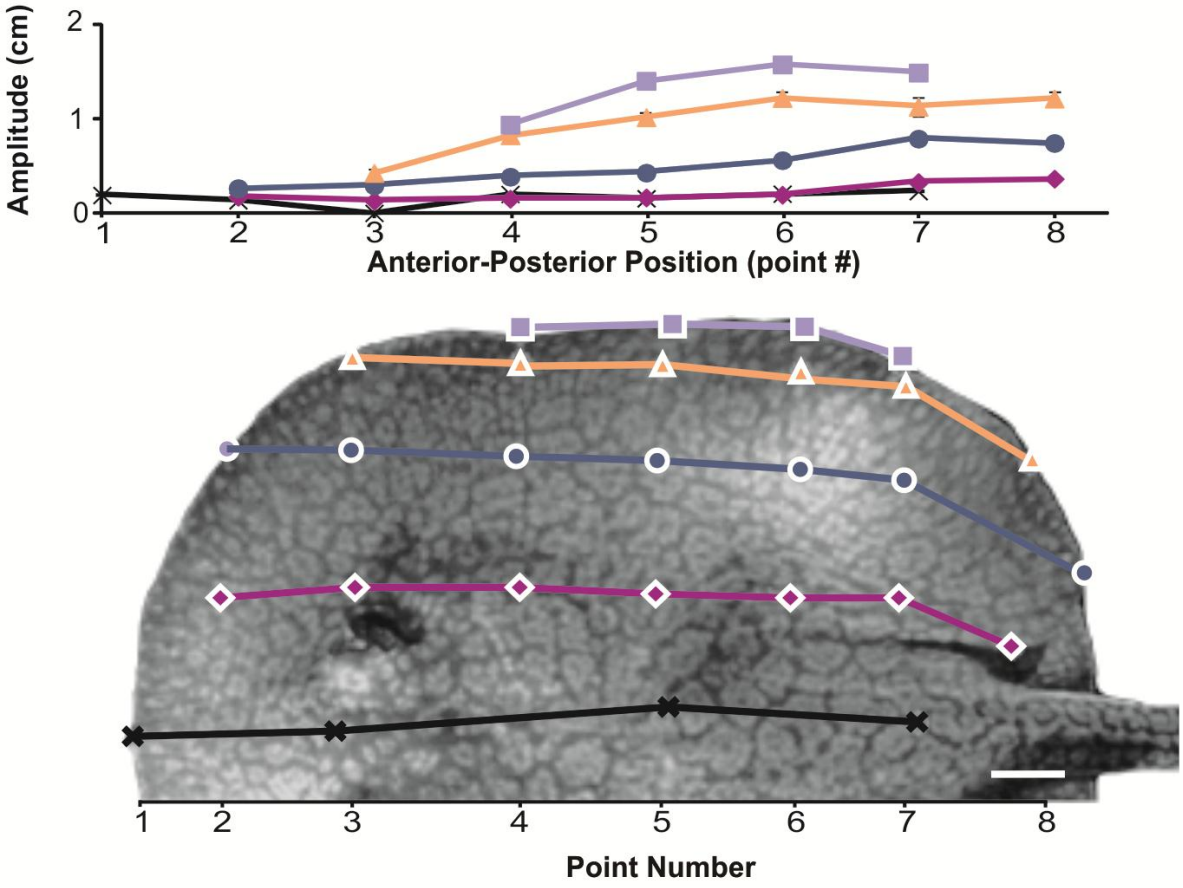

Figure 1.7. Chordwise amplitude variation along the anteroposterior axis at positions indicated on stingray image. As no significant differences in amplitude were found between swimming speeds, data were pooled (N=24). Error bars represent ± standard error; some are obscured by symbols. Scale bar for stingray image is 1 cm.

Local wavespeeds determined at points from 0.4 to 0.7 DL generally reflect the mid-disc value and do not vary significantly with swimming speed (Figure 1.8). Distal wavespeeds show no variation along the anteroposterior axis (ANOVA, $p>>0.05$). Medially, however, wavespeeds do vary along the length of the disc (ANOVA, $p=0.0001$); a post-hoc Tukey test identified the medial, posterior wavespeed as significantly different from medial-anterior and medial-intermediate wavespeeds. At both swimming speeds, medial wavespeeds show a similar pattern, decreasing (though not significantly) from anterior to intermediate positions, then increasing posteriorly.

Mediolateral fin curvature

In addition to the anteroposterior bending that accompanies the propulsive wave, stingray fins show mediolateral curvature, with a maximum of 0.06 ± 0.02 mm^{-1} in both positive (concave up) and negative (concave down) directions (Figure 1.9A). No significant differences in the magnitude of curvature exist between swimming speeds, curvature direction (positive or negative), or along an anteroposterior axis from 0.4 DL to 0.7 DL (ANOVAs, $p>0.1$ for all comparisons). High-speed video stills from some sequences reveal extreme negative curvature of the distal fin, with a smaller radius than could be resolved given the limited number of points digitized in this region (Fig 9B). The proportion of a wave cycle spent in negative curvature is highly variable. Although the mean value of $59\pm4\%$ suggests a relatively even division of cycle time between positive and negative curvature, values range widely from 30% to 93%, and in almost one-third of sequences the fin is negatively curved for more than 75% of the cycle. There is no clear relationship between fin curvature and wave phase, and curvature can clearly persist across phases (Figure 1.9B). However, two major patterns of curvature emerge. As the fin

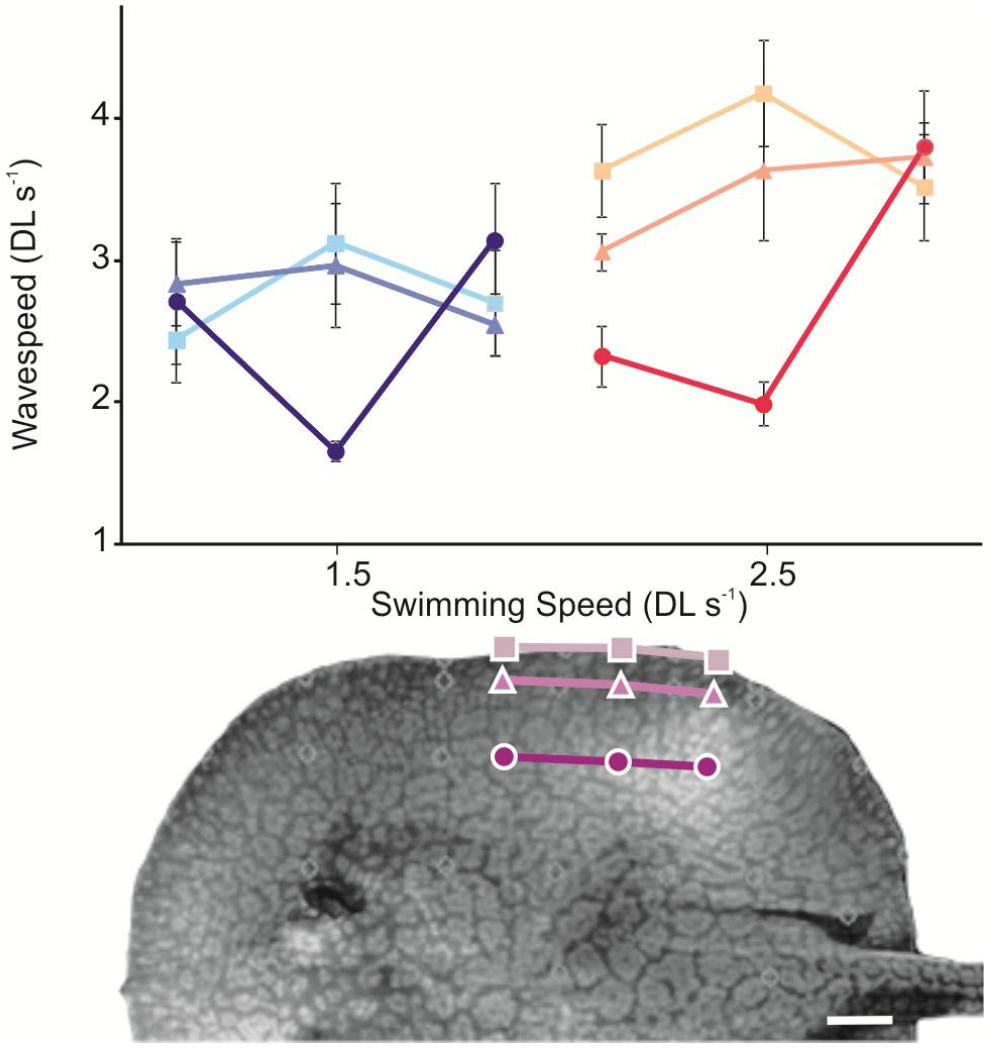

Figure 1.8. Wavespeed variation along the anteroposterior axis of the pectoral disc for each swimming speed, at distal (light blue/red), intermediate (medium blue/red) and near-medial (dark blue/red) positions as indicated on the stingray image. Position markers are positioned halfway between the two digitized points used to calculate each local wavespeed. Error bars represent ± standard error; N=12. Scale bar for stingray image is 1 cm.

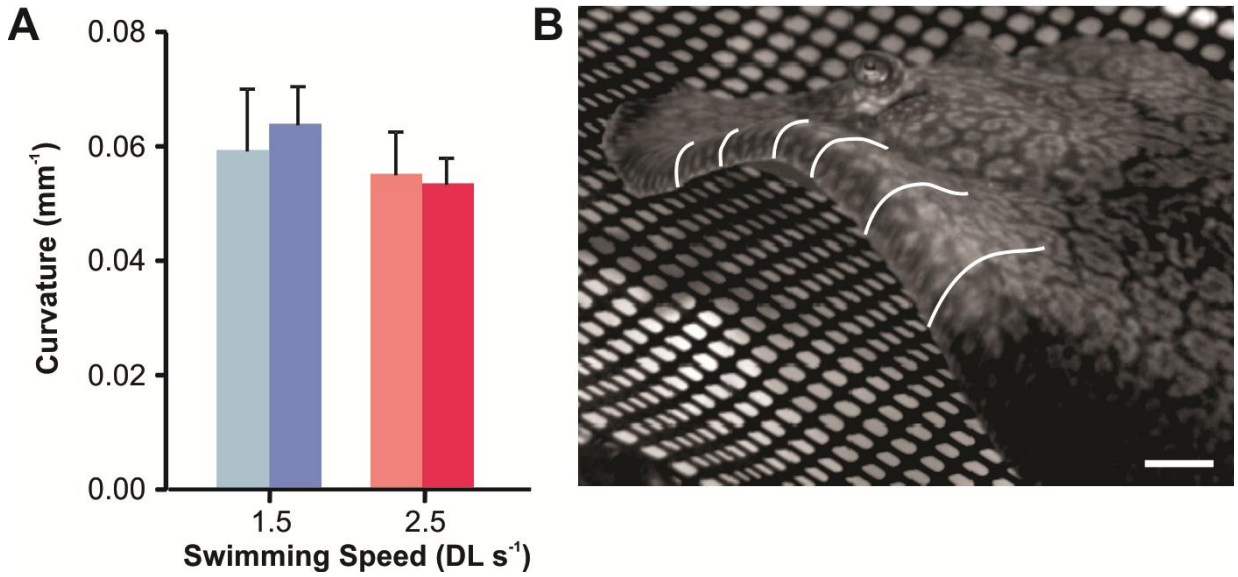

Figure 1.9. (A) Magnitude of positive (light blue/red) and negative (deep blue/red) mediolateral fin curvature at both swimming speeds, with no significant differences by curvature sign or speed ($p>0.05$). (B) Sample frame from high-speed video sequence of stingray swimming. White lines highlight extreme negative curvature at the distal margin of the fin. Scale bar=1 cm.

moves through a wave cycle, it may bend in the opposite direction to fin motion—concave down during the "upstroke," as the wave moves from trough to crest, and concave up during the crest-to-trough "downstroke" (Figure 1.10A,B). Alternatively, the fin may retain concave down curvature on both upstroke and downstroke (Figure 1.10A, C). Concave upward curvature does not persist for any major portion of the upstroke.

Multivariate kinematic changes with swimming speed

A single principal component showed significant separation of groups by swimming speed (MANOVA, $p<0.05$), explaining 16.8% of sequence variation (Figure 1.11A). Mid-disc wavespeed, mid-disc frequency, and the proportion of the cycle spent in negative curvature loaded high on this axis. Groups were successfully separated by speed along the first canonical axis of the discriminant function analysis (100% correct classifications), based on mid-disc wavespeed and mid-disc frequency, and (to a lesser degree) mid-disc amplitude, body angle, and wavelength (Figure 1.11B).

Discussion

Undulatory swimmers propel themselves by passing a wave of bending along a flexible fin or body surface; modulations of the wave produce changes in swimming speed or instigate maneuvers. In undulating rays, the broad, flexible pectoral fins allow for substantial variation in waveform as the propulsive wave propagates across the fin surface. These three-dimensional deformations cannot be described by a single point or the motion of the fin margin alone. Here we present the first three-dimensional kinematic analysis of undulatory locomotion in stingrays, determining the properties of the pectoral wave across the entire fin surface, and identifying the

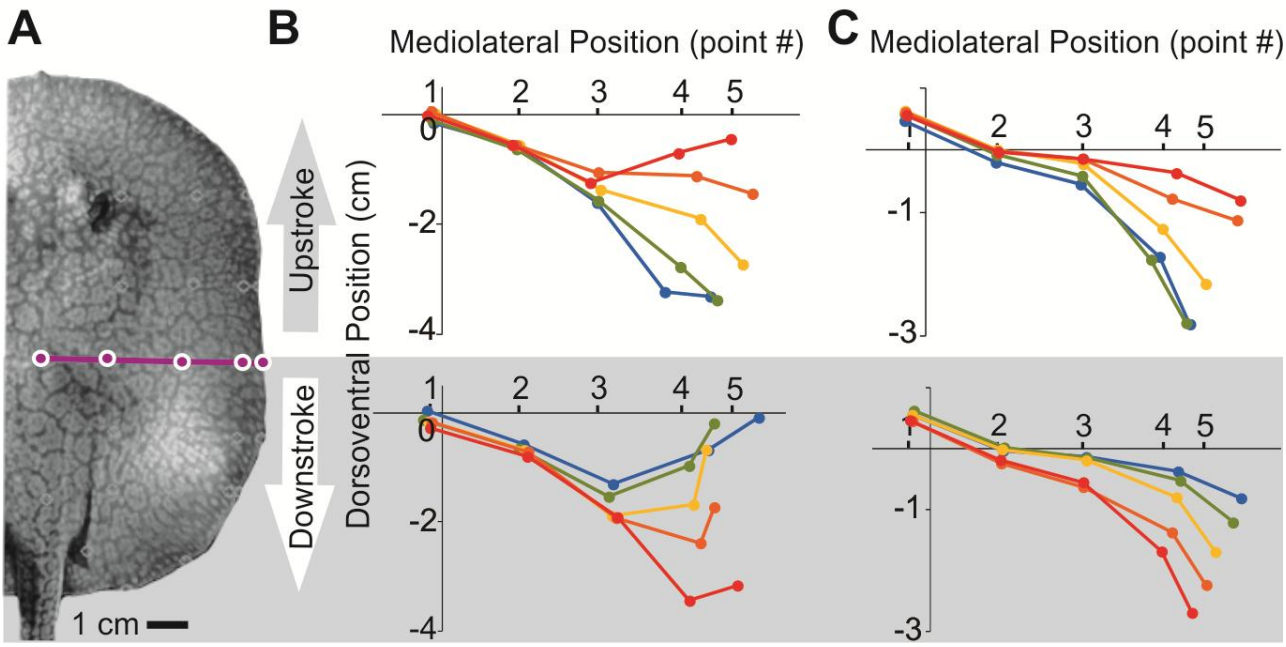

Figure 1.10. Sample plots showing fin curvature at the mid-disc mediolateral position indicated on the stingray image (A), as the fin moves dorsoventrally during one wave cycle. Cycles are divided into upstrokes (top row, white background) defined as the portion of the wave cycle where the fin moves from trough to crest, and downstrokes (bottom row, grey background), defined from crest to trough. On each plot, colors move from cool to hot (blue to red) through time. Columns illustrate the two major patterns of curvature through one wave cycle: (B) concave down on upstroke, concave up on downstroke, and (C) concave down on upstroke and downstroke. Scale bar for stingray image is 1 cm.

Figure 1.11. Multivariate analysis of kinematic variables at swimming speeds of 1.5 DLs^{-1} (blue) and 2.5 DLs^{-1} (red). Each point represents one swimming sequence (N=21). (A) Principal component plot with significant separation of swimming speeds along principal component 2 ($p<.001$), an axis mainly described by mid-disc wavespeed, mid-disc frequency, and the proportion of the cycle spend in negative curvature. Reference lines indicate mean values for each swimming speed on each axis. (B) Discriminant function plot separating swimming speeds along canonical 1 (100% correct classifications), with major influences of mid-disc wavespeed and mid-disc frequency, and secondary influences of mid-disc amplitude, body angle, and wavelength. All variables increase from left to right along canonical 1. Ellipses represent 95% confidence intervals with crosshairs at mean values for each speed.

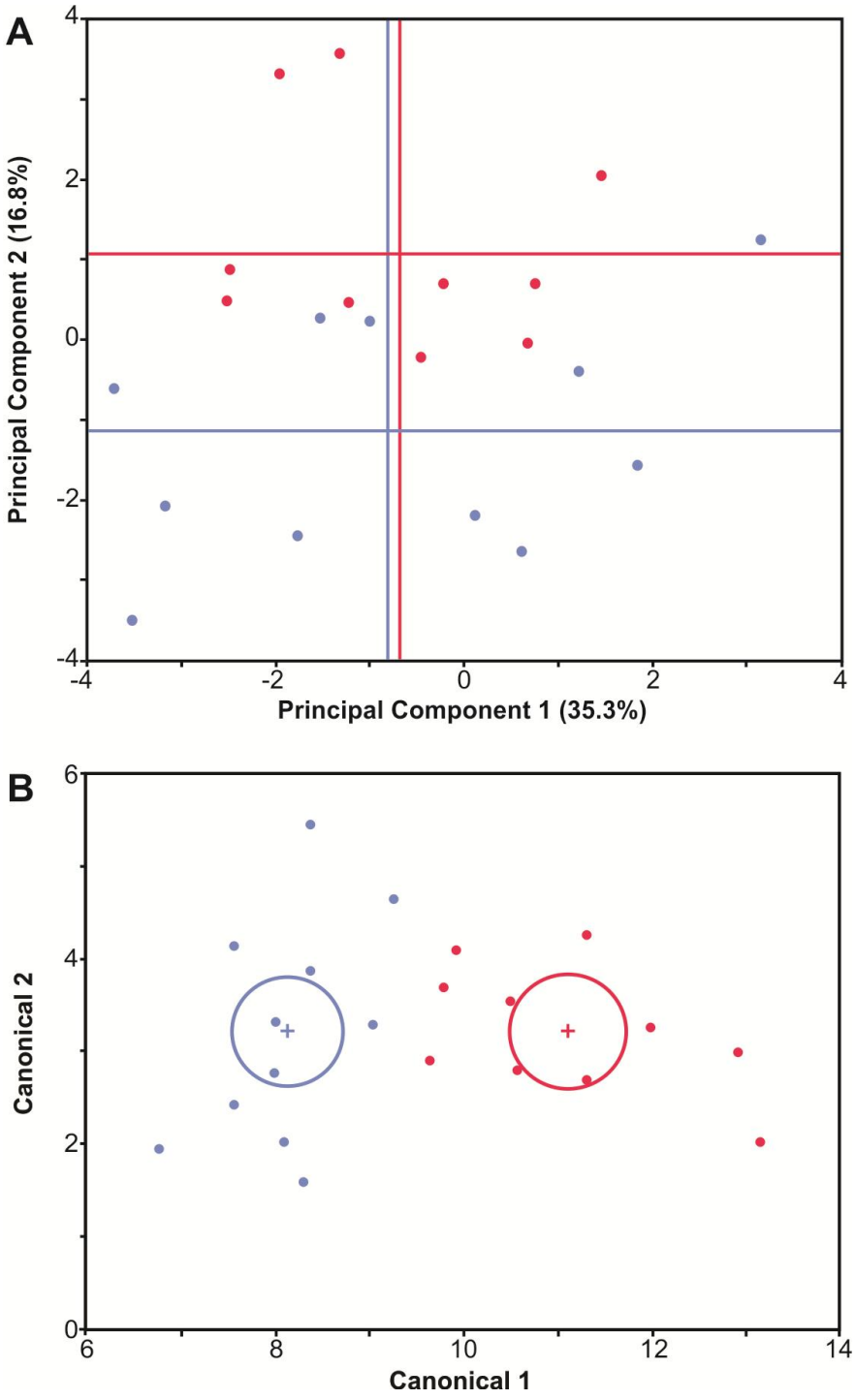

Figure 1.11 (Continued)

changes in waveform that drive increased swimming speed (Figures 1.2, 1.3, 1.4). In addition, we provide supplemental data sets (S1, S2) describing excursions of the entire pectoral fin surface, which may be useful for future robotic works drawing inspiration from undulating, rajiform swimmers.

Undulations of the pectoral surface

The dramatic undulations of stingray pectoral fins draw attention from any observer—the entire fin initially appears to be involved in a high-amplitude wave (Figures 1.2, 1.3). Yet, our analysis of three-dimensional fin surface kinematics reveals that wave amplitude reaches a maximum of 1.66±0.04 cm, or 0.15 disc widths (DW), and that significant undulations (amplitude >0.5 cm) are restricted to a relatively small portion of the fin—roughly one quarter to one third of the total surface, centered on the distal mid-disc and distal posterior quadrants of the disc (Figure 1.5). Given the size of the fin, a maximum amplitude of less than 2 cm seems small, but still represents a significant fraction of disc width, and is in the range of standardized mid-disc amplitudes found for other batoids (Rosenberger, 2001). Constraints in fin undulation result from a combination of morphological and hydrodynamic factors. First, the central portion of a stingray's body cannot undulate (in dorsoventral or mediolateral directions), due to stiffening of the vertebral column and fusion of the pectoral girdles with axial cartilages (Compagno, 1999); motion of the medial fin is limited by its attachment to the fixed midline. Further, anterior portions of the disc which move freely during other behaviors, such as foraging (Wilga et al., 2012) do not do so during undulatory locomotion. Minimizing the undulation of the anterior fin during locomotion creates a stable leading edge, streamlining the shape of the body as projected into the water flow, reducing flow separation and drag.

The motion of the pectoral fin increases at mid-disc and posterior regions (Figure 1.5). Amplitude increase is nearly linear along the mediolateral axis of the fin, except at the distal margin where the rate of increase becomes steeper (Figure 1.6). This distal increase is an effect of lateral curvature of the fin margin, discussed below. Along the anteroposterior axis, amplitude increases to its maximum value just posterior to mid-disc (at 0.7 DL), and remains near this asymptote from 0.5-1.0 DL (Figure 1.7). The magnitude of the asymptote varies with position from the midline (due to varying angular displacement), but the pattern holds across for the entire disc, in an interesting complement to patterns of amplitude increase found for other undulating swimmers. In eels, amplitude increases continuously along the entire length of the body, without asymptote (Gillis, 1996; Gray, 1933); in undulating blue-spot stingray *Taenuria lymma* amplitude at the fin margin increases toward the mid-disc, then decreases as the wave moves further posterior (Rosenberger and Westneat, 1999). Rosenberger and Westneat (1999) describe the *T. lymma* pattern of amplitude increase and decrease as a form of "narrow-necking," a phenomenon discussed by Lighthill (1975) in relation to the caudal peduncle of fish swimming via body-caudal fin propulsion: a reduction in body depth in regions of high amplitude motion, and/or an increased body depth at the center of mass reduces recoil forces and yawing moments, reducing drag. Rosenberger and Westneat (1999) suggest that the posterior amplitude decrease seen in *T. lymma* might have a similar effect to reduced body depth, decreasing drag. However, the broad, dorsoventrally compressed stingray body has ample inertia and hydrodynamic added mass to resist recoil forces, and any drag reduction benefit from restricted amplitude is more likely to result from a decrease in projected area, compared to the anguilliform pattern of continuous amplitude increase. The asymptotic amplitude pattern we observe in *P. orbignyi* would reduce projected area, even without the posterior decrease seen in *T. lymma*: as amplitude

nears the asymptote, projected area does not further increase. Most importantly, though, the amplitude pattern presented for *T. lymma* highlights the limitations of two-dimensional analyses when interpreting three-dimensional waveforms. In Rosenberger and Westneat (1999), measurements are made along the curved fin margin only; the decrease in amplitude between mid-disc (the location of maximum disc width) and the posterior fin may represent nothing more than geometry, since the angular displacement of the fin margin will decrease as the disc narrows. By analyzing points across the fin surface, and comparing points with similar potential for angular displacement, we verify an asymptotic amplitude pattern for *P. orbignyi*: amplitude is constrained, but not reduced, as the propulsive wave crosses the posterior portion of the disc.

Stingrays swim with a mean slip (swimming speed/propulsive wavespeed) of 0.7±0.04, within the 0.6-0.9 range determined for stingray *T. lymma* (Rosenberger and Westneat, 1999), similar to skates (Daniel, 1988) and eels (Gillis, 1996). Our results for wave frequency and mid-disc wavespeed also fall in the range for species studied by Rosenberger (2001). We further examined wavespeed in detail, calculating distal, intermediate, and medial wavespeeds for the mid-disc region. Within this small region of the fin we found only one significant difference—a posterior increase in medial wavespeed (ANOVA, $p=0.0001$)—but the overall trend speaks to the path of the propulsive wave across the fin surface (Figure 1.8). At both distal and intermediate positions, wavespeeds remain constant across the anteroposterior axis of the examined region. However, at both swimming speeds medial wavespeeds show the same trend, decreasing from anterior to mid-disc, then increasing from mid-disc toward the posterior. Though the wavespeed "trough" does not differ from surrounding values by a statistically significant margin, it does suggest the radial path taken by the propulsive wave, which moves around the perimeter of the disc rather than parallel to the midline. As local wavespeeds were

calculated between points on a direct anteroposterior axis, a propulsive wave moving parallel to the midline should have constant wavespeed between all points. A radially-propagating wave, however, when measured along a direct anteroposterior axis, would appear to have greater wavespeed when traveling at a greater angle to that axis, i.e., anterior or posterior to the mid-disc region where fin margin and midline are parallel. This is the pattern we observe for medial wavespeeds; we were unable to detect a similar trend for more distal regions of the fin, but the medial pattern corresponds to our direct observations of propulsive wave travel. Frames from a sample sequence, color-coded for velocity, also show heightened wavespeeds along the perimeter of the disc compared to medial regions, further illustrating the radial path of the propulsive wave (Figure 1.3).

The importance of considering the direction of wave propagation also emerges in the calculation of wave number, the major metric of batoid locomotion used by Rosenberger (2001) to describe the oscillatory-undulatory continuum. When calculated as in Rosenberger (2001), our data yield a wave number of 1.10±0.08 for *P. orbignyi*, representing just over one complete wave on the pectoral fin at one time, barely above the cutoff for oscillatory rays at 1. *P. orbignyi* is clearly an undulatory swimmer; images of swimming rays reveal significantly more than one wave present on the pectoral fin (Figure 1.2). We suggest that rather than calculating wave number relative to disc length, disc *perimeter* is a more meaningful parameter for *P. orbignyi*, as it better represents the length over which the wave travels. This method yields a wave number of 1.65±0.12, congruent with images of swimming stingrays and firmly within the undulatory region of the continuum. Future studies calculating this value should consider the path of wave travel when selecting a method of standardization.

For a fully detailed description of pectoral surface undulation, we offer an extensive table of pectoral fin excursions beyond the results discussed here (S1), as well as a sample dataset giving the motion of surface through time (S2; and animation S3).

Mediolateral fin curvature

In addition to anteroposterior bending associated with the propulsive wave, notable mediolateral curvature of pectoral fin radials occurs during swimming by *Potamotrgon orbignyi* (Figures 1.9, 1.10). Curvature varies across the mediolateral axis, increasing dramatically near the distal margin. Calculated values (Figure 1.9A) underestimate curvature due to the limited resolution available given the number of points digitized on the distal fin, but we observed dramatic distal curvature directly (Figure 1.9B), and as change in the rate of amplitude increase near the distal margin of the fin, where amplitude increases more sharply than in medial regions (Figure 1.6).

Changes in curvature along the length of a fin element, whether the cartilaginous fin radial of an elasmobranch or the bony lepidotrichia of an actinopterygian fish, can result from direct muscle action or inherent structural features. In actinopterygians, the jointed, bilaminar structure of lepidotrichia translates small changes in the length of muscles at the fin base into dramatic fin curvature (Alben et al. 2007; Geerlink and Videler, 1987). This structure-mediated curvature plays a major role in labriform locomotion by bluegill sunfish *Lepomis macrochirus*; by curving into a cupped position the pectoral fins are able to produce net thrust throughout the fin cycle, rather than incurring net drag as the fin abducts (Lauder and Madden, 2007). Skeletal structure also determines flexibility in the pectoral fins of longhorn sculpin *Myoxocephalus octodecimspinosus*, where variations in segmentation and hemitrich cross-section along the length of individual fin rays allow regionalization of fin function by creating local changes in

stiffness (Taft, 2011; Taft et al., 2008). Batoid fin elements lack the bilaminar structure of actinopterygian fin rays and, as seen in blue-spot stingray *Taenuria lymma*, the muscles that control fin adduction/abduction are not confined to the fin base but extend across the full length of the fin radials (Rosenberger and Westneat, 1999). Therefore, muscles may act directly to create distal curvature. Yet, mediolateral variations in the structure of fin elements do occur in batoid pectoral fins, as described by Schaefer and Summers (2005). Among undulating batoids, stingrays and freshwater stingrays (Dasyatidae and Potamotrygonidae) are both found to have reduced cartilage calcification in the distal fin relative to medial positions, reducing fin stiffness near the margin (Schaefer and Summers, 2005). In addition, fin elements bifurcate near the distal margin, further altering fin stiffness (Schaefer and Summers, 2005). Therefore, spanwise curvature in stingray fins is most likely a combination of local muscle action and inherent flexibility determined by fin element structure; the exact contributions of each factor are as yet unknown.

In this study we observe two patterns of distal fin curvature during pectoral fin swimming. In the first case, the lateral edge of the fin bends away from the direction of motion, trailing the main portion of the fin. As the fin moves from wave crest to wave trough, the fin margin is curved concave-up; as the fin moves from trough to crest, the margin is curved concave-down (Figure 1.10A, B). Therefore, curvature changes direction between upstroke and downstroke. This is the same behavior we would expect from a passive flexible fin, with the edge of the fin bending away from the direction of overall fin motion in response to induced fluid pressure. This pattern of curvature dominates in most swimming sequences, as reflected in the nearly equal portions of the wave cycle spent in positive and negative curvature when all data are combined (59±4% of the cycle in negative curvature). However, in approximately one third

of sequences the fin retained negative curvature for over 75% of the wave cycle. These sequences exhibit the second pattern of distal curvature we observe in *P. orbignyi*, where concave-down curvature is retained throughout the wave cycle (Figure 1.10A, C). Neither this study nor any previous research has collected data on the activity of distal fin musculature during swimming. However, in the second pattern of curvature we observe, fins are curved in opposition to fluid loading. It seems highly likely that this phenomenon is driven by the direct action of local muscles, with passive curvature resulting from inherent fin flexibility determined by fin element structure.

The effects of a similar curvature pattern, with the edges of a flexible fin curved into flow, have been studied using a robotic caudal fin (Esposito et al., 2012). In that study, a motion program in which the dorsal and ventral margins of the caudal fin lead the middle of the fin during swimming results in the caudal fin surface cupping into the flow. Measurements of thrust forces generated during the cupping motion were compared to those produced by the same caudal fin moved as a flat plate. Cupping motions of the fin produced consistently higher thrust forces than the flat plate movement, suggesting that the cupping motion enhances streamwise momentum (Esposito et al., 2012).

In stingrays, retaining a concave-down fin shape is also likely to have hydrodynamic significance, as it will affect flow passing beneath and beside the fin. Compared to a flat fin, distal curvature may improve flow control under the fin by reducing the strength of wingtip vortices, a type of induced drag. Wingtip vortices result from pressure differences between the dorsal and ventral surfaces of an airfoil or hydrofoil; vortices form around the tip of the foil as fluid moves from high to low pressure, circulating around the fin or wing (Vogel, 2003). Though wingtip vortices are most often considered for fixed-wing scenarios, as in aircraft and

soaring birds, they also occur at the edge of an undulating fin. In stingrays, the body is held at a positive angle of attack; it acts as a fixed wing, with greater pressure occurring ventrally, and therefore induces wingtip vortex formation. In addition, since most undulating rays typically swim near the substrate, pressure may be increased underneath the fin as it moves from crest to trough and traps fluid between the pectoral disc and the substrate. In aeronautics, various structures are employed to reduce tip vortices or alter their orientation, including the familiar winglets or upswept sections on the wingtips of commercial airliners (Tennekes, 1997). The tightly-curled edge of the stingray fin may have a similar effect; changes in spanwise curvature have been found to affect wingtip circulation during bat flight (Hubel et al., 2010). A curved margin may also help control the direction of flow beneath the fin, keeping the bolus of water accelerated by the propulsive wave aligned towards the posterior. As the propulsive wave propagates around the disc radially, not directly from anterior to posterior, the direction of fluid flow is not always aligned to the direction of thrust. By curling the distal region of the fin downward, stingrays may "cup" the fluid moving under the fin, prevent it from spilling around a flat edge, and reorient spanwise flow toward a more optimal axis.

The variability in curvature pattern is interesting. Concave-down curvature was retained throughout the wave cycle in a significant portion of sequences, but not in all; yet, if a cupped fin margin offers a hydrodynamic advantage to swimming rays, increasing thrust or reducing drag, we would expect it to be ubiquitous. All individuals were capable of swimming with consistent concave-down curvature, and stingrays were no more or less likely to employ this pattern of curvature as swimming speed increased (ANOVA, $p>0.3$), contrary to the expectation that increased locomotor demands would elicit it more often. This variability may indicate that the hydrodynamic benefit of swimming with a curled fin is limited.

Variations with swimming speed

In general, fish can increase thrust by varying the frequency or amplitude of the motion of a propulsive surface, or even the area of the surface itself (Bainbridge, 1958; Webb, 1975; Lauder, 2006). The previous study of stingray *T. lymma* had found significant individual variability in the wave parameters driving increased swimming speed, with velocity appearing frequency-dependent in some stingrays and amplitude-dependent in others (Rosenberger and Westneat, 1999). In contrast, locomotion by undulating stingray *P. orbignyi* is decidedly frequency-driven; the mid-disc frequency of the propulsive wave increases by 50% when swimming speed increases by 65%, a highly significant variation (Figure 1.4B; 2.53±0.16 Hz to 3.80±0.18 Hz, ANOVA, $p<0.0001$). Mid-disc wavespeed increased by the same proportion (Figure 1.4C; 31.00±2.53 cm s^{-1} to 46.02±3.25 cm s^{-1}, ANOVA, $p<0.01$). Mean wavelength, the ratio of wavespeed to frequency, therefore remained constant across speeds (12.5±0.7 cm, ANOVA, $p=0.89$). Contrary to some findings by Rosenberger and Westneat (1999) for *T. lymma*, amplitude does not vary between swimming speeds in *P. orbignyi*, whether considered as maximum amplitude, mid-disc amplitude, or for any point across the disc (Figure 1.4A; all $p>>0.05$)—excepting one point near the posterior margin which is unlikely to play a significant role in propulsion, though it may influence flow separation from the fin. One might conjecture that amplitude remains constant because stingrays have maximized potential excursion at the lower swimming speed, and cannot further expand the range of motion. Our data contradict this idea: potential excursion should correspond to angular displacement, increasing with fin span, yet maximum amplitude occurs posterior to the maximum disc width (0.7 DL vs. 0.5 DL). We conclude that the amplitude of undulations are not maximized at either swimming speed, and could be increased if changes in swimming velocity were amplitude-driven. The lack of

amplitude increase therefore confirms frequency as the driver of increased swimming speed in stingrays, in agreement with the majority of studied fish species (Bainbridge, 1958; Drucker and Jensen, 1996). Increases in the amplitude of propulsive motions, whether a trout's tailbeats or a stingray's undulations, increase projected area and therefore increase drag; a higher swimming speed resulting from increased amplitude would only heighten the drag effect. Frequency-driven increases in velocity do not increase projected area, and are therefore employed by many swimmers as a more efficient means of increasing thrust.

Univariate and multivariate analyses (principal component and discriminant function analyses) concurred that frequency and wavespeed are the main wave parameters influencing swimming speed (Figure 1.11). Mean values of the principal component described by frequency and mid-disc wavespeed differed significantly between swimming speeds (Figure 1.11A; ANOVA, $p<0.01$). The discriminant function analysis correctly identified the swimming speed of 100% of sequences based on frequency and wavespeed data, but was also influenced by mid-disc amplitude and wavelength values despite the lack of significant by-speed differences in the latter two variables when considered independently (Figure 1.11B; ANOVA). Given the flexibility of the stingray pectoral disc, it is not surprising that fin modulations may be subtle. The major changes in waveform that determine velocity (frequency and wavespeed) may be accompanied by minor changes in secondary parameters like amplitude and wavelength.

As stingrays swim faster, the angle between the body and oncoming flow increases slightly but significantly, from 5.18 ± 1.05^{o} to 7.75 ± 0.73^{o} (Fig 4D; ANOVA, $p<0.05$). It is important to note that the magnitude of these values represents the angle between the dorsal surface of the stingray and oncoming flow, as all digitized points were positioned dorsally. This yields higher body angles than would be calculated from the flat ventral surface, as stingray body

depth decreases from head to tail; a sagittal cross-section through the midline would resemble an airfoil, with a flat ventral surface and cambered dorsal surface. However, as the effect of body depth is constant between speeds, the positive correlation between body angle and swimming speed stands. Elasmobranchs are known to use their bodies as lift-generating surfaces; among oscillatory rays (Myliobatidae), pitching of the body can be used to generate thrust (Heine, 1992), and in leopard and bamboo sharks (*Triakis semifasciata* and *Chiloscyllium punctatum*), a positive body angle offsets torques generated by the heterocercal tail (Wilga and Lauder, 2002). In stingrays, a slightly positive body angle will allow their bodies to act as hydrofoils too, generating lift that may counterbalance inherent negative buoyancy or uneven torques produced during locomotion. Yet, if the body surface is used to generate a constant amount of lift we would expect body angle to decrease with speed, not increase, as the amount of lift generated at a given angle of attack increases with flow speed. If the slight change in body angle is robust, stingrays experience increasing lift force as they swim faster, perhaps offsetting a change in torques produced by the pectoral fin.

Our analysis reveals that frequency and wavespeed—the two main drivers of swimming speed in *P. orbignyi*—are accurately represented by mid-disc values, but that major features of pectoral fin undulation can only be described when the fin is considered as a three-dimensional undulating surface. We find several three-dimensional phenomena with significant implications for the hydrodynamics of rajiform locomotion, including active mediolateral fin curvature and an asymptotic pattern of amplitude variation along the pectoral fin, aspects of waveform that cannot be inferred from a two-dimensional analysis. We also note that only a relatively small proportion of the fin undulates with significant amplitude. Incorporating these findings into future models of undulating fins will allow further investigation of their hydrodynamic impacts;

three-dimensional studies of other undulators may reveal convergent locomotor strategies for waveform modulation.

Acknowledgements

We thank E. M. Standen, J. Lim, N. Danos and B. Flammang-Lockyer for helpful conversations during both data-collection and analysis phases of this work, as well as A. Stubbs for assistance during experiments. We are grateful for the biological illustration work of Laszlo Meszoly, and for valuable advice on stingray species from P. Petry, K. Hartel and A. Williston of the Ichthyology Collection at the Harvard University Museum of Comparative Zoology. Funding for this project was provided by NSF EFRI-0938043 to G.V. Lauder, in addition to support from the Harvard University Department of Organismic and Evolutionary Biology, NSF-IGERT Training Grant in Biomechanics, and Robert A. Chapman Memorial Scholarship to E. L. Blevins.

References

Alben, S., Madden, P.G.A. and Lauder, G.V. (2007). The mechanics of active fin-shape control in ray-finned fishes. *J. Roy. Soc. Interface.* **4**, 243–256.

Bainbridge, R. (1958). The speed of swimming of fish as related to size and to the frequency and amplitude of the tail beat. *J. Exp. Biol.* **35**, 109-133.

Breder, C. M. (1926). The locomotion of fishes. *Zoologica* **50**, 159–297.

Clark, R. P. and Smits, A. J. (2006). Thrust production and wake structure of a batoid-inspired oscillating fin. *J. Fluid Mech.* **562**, 415-429.

Compagno, L. J. V. (1999). Endoskeleton. In *Sharks, Skates and Rays: The Biology of Elasmobranch Fishes* (ed. W. C. Hamlett), pp. 69-92. Baltimore, MD: John Hopkins University Press.

Curet, O. M., Patankar, N. A., Lauder, G. V. and MacIver, M. A. (2011). Mechanical properties of a bio-inspired robotic knifefish with an undulatory propulsor. *Bioinspir. Biomim.* **6,** 026004

Daniel, T. L. (1988). Forward flapping flight from flexible fins. *Can. J. Zool*. **66**, 630–638.

Drucker, E. G. and Jensen, J. (1996). Pectoral fin locomotion in the striped surfperch. I. Kinematic effects of swimming speed and body size. *J. Exp. Biol.* **199**, 2235-2242.

Esposito, C., Tangorra, J., Flammang, B. E. and Lauder, G. V. (2012). A robotic fish caudal fin: effects of stiffness and motor program on locomotor performance. *J. Exp. Biol.* **215**, 56-67.

Geerlink, P. J. and Videler, J. J. (1987). The relation between structure and bending properties of teleost fin rays. *Neth. J. Zool.* **37**, 59–80

Gillis, G. B. (1996). Undulatory locomotion in elongate aquatic vertebrates: anguilliform swimming since Sir James Gray. *Am. Zool*. **36**, 656–665.

Gray, J. (1933). Studies in animal locomotion. I. The movement of fish with special reference to the eel. *J. Exp. Biol*. **10**, 88–104.

Harris, J. E. (1936). The role of the fins in the equilibrium of the swimming fish. I. Wind tunnel tests on a model of *Mustelus canis* (Mitchell). *J. Exp. Biol.* **13**, 476-493.

Hedrick, T. L. (2008). Software techniques for two- and three-dimensional kinematic measurements of biological and biomimetic systems. *Bioinspir. Biomim.* **3**, 034001.

Heine, C. E. (1992). Mechanics of flapping fin locomotion in the cownose ray, *Rhinoptera bonasus* (Elasmobranchii: Myliobatidae). PhD thesis, Duke University.

Hubel, T. Y., Riskin, D. K., Swartz, S. M. and Breuer, K. S. (2010). Wake structure and wing kinematics: the flight of the lesser dog-faced fruit bat, *Cynopterus brachyotis. J. Exp. Biol.* **213**, 3427-3440.

Klausewitz, W. (1965). Die Bewegungsweise der Geigenrochen–aus Funktioneller und Stammesgeschichtlicher sicht. *Natur. Museum* **95**, 97–108.

Lauder, G. V. (2006). Locomotion. In *The Physiology of Fishes*, Third Edition, (D. H. Evans and J. B. Claiborne, eds.), pp. 3-46. Boca Raton: CRC Press.

Lauder G. V. and Madden, P. G. (2007). Fish locomotion: kinematics and hydrodynamics of flexible foil-like fins. *Exp. Fluids.* **43**, 641–653.

Lighthill, M. J. (1975). *Mathematical biofluiddynamics*. Philadelphia: Philadelphia Society for Industrial and Applied Mathematics.

Low, K. H. (2006). Locomotion and depth control of robotic fish with modular undulating fins. *Int. J. Autom. Comput.* **2006 (4)**, 348-357.

Macesic, L. J. and Kajiura, S. M. (2010). Comparative punting kinematics and pelvic fin musculature of benthic batoids. *J. Morph.* **271**(10),1219-1228.

Moored, K.W., Dewey, P. A., Leftwich, M. C., Bart-Smith, H. and Smits, A. J. (2011). Bio-inspired propulsion mechanisms based on manta ray locomotion. *Mar. Technol. Soc. J.* **45**, 110-118.

Parson, J., Fish, F. E. and Nicastro, A. J. (2011). Turning performance in batoid rays: Limitations of a rigid body. *J. Exp. Mar. Biol. Ecol.* **402**, 12-18.

Roberts, B. L. (1969). The buoyancy and locomotory movements of electric rays. *J. Mar. Biol. Ass. UK* **49**, 621–640.

Rosenberger, L. J. (2001). Pectoral fin locomotion in Batoid fishes: undulation versus oscillation. *J. Exp. Biol.* **204**, 379-394.

Rosenberger, L. J. and Westneat, M. W. (1999). Functional morphology of undulatory pectoral fin locomotion in the stingray *Taenuria lymma. J. Exp. Biol.* **202**, 3523-3539.

Schaefer, J. T. and Summers, A. P. (2005). Batoid wing skeletal structure: novel morphologies, mechanical implications, and phylogenetic patterns. *J. Morph.* **264**, 298-313.

Standen, E. M. and G. V. Lauder. (2005). Dorsal and anal fin function in bluegill sunfish *Lepomis macrochirus*: three-dimensional kinematics during propulsion and maneuvering. *J. Exp. Biol.* **208**, 2753-2763

Standen, E. M. and Lauder, G. V. (2007). Hydrodynamic function of dorsal and anal fins in brook trout (*Salvelinus fontinalis*). *J. Exp. Biol.* **210**, 325-339.

Taft, N. K. (2011). Functional implications of variation in pectoral fin ray morphology between fishes with different patterns of pectoral fin use. *J. Morph.* **272**, 1144–1152.

Taft, N., Lauder, G. V. and Madden, P.G. (2008). Functional regionalization of the pectoral fin of the benthic longhorn sculpin during station holding and swimming. *J. Zool.* **276**, 159-167.

Taneda, S. and Tomonari, Y. (1974). An experiment on the flow around a waving plate. *J. Phys. Soc. Jpn.* **36**, 1683-1689.

Tennekes, H. (1997). *The Simple Science of Flight.* Cambridge, Massachusetts: MIT press.

Tytell, E. D. and Lauder, G. V. (2004). The hydrodynamics of eel swimming: I. Wake structure. *J. Exp. Biol.* **207**, 1825-1841.

Tytell, E. D., Standen, E. M. and Lauder, G. V. (2008). Escaping flatland: three-dimensional kinematics and hydrodynamics of median fins in fishes. *J. Exp. Biol.* **211**, 187-195.

Vogel, S. (2003). *Comparative Biomechanics: Life's Physical World*. New Jersey: Princeton University Press.

Webb, P. W. (1975). Hydrodynamics and energetics of fish propulsion. *Bull. Fish Res. Bd. Can.* **190**, 1-159.

Webb, P. W. (1994). The biology of fish swimming. In *Mechanics and Physiology of Animal Swimming* (ed. L. Maddock, Q. Bone and J. M. V. Rayner), pp. 45–62. Cambridge: Cambridge University Press.

Webb, P. (2006). Stability and maneuverability. In *Fish Biomechanics*. Volume 23 in *Fish Physiology*, (R. E. Shadwick and G. V. Lauder, eds.), pp. 281-332. San Diego: Academic Press.

Wilga, C. D. and Lauder, G. V. (2002). Function of the heterocercal tail in sharks: quantitative wake dynamics during steady horizontal swimming and vertical maneuvering. *J. Exp. Biol.* **205**, 2365-2374.

Wilga, C. D., Maia, A., Nauwelaerts, S. and Lauder, G. V. (2012) Prey handling using whole body fluid dynamics in batoids. *Zoology.* **115**, 47-57.

Wu, C., Wang, L. and Wu, J. (2007). Suppression of the von Kármán vortex street behind a circular cylinder by a travelling wave generated by a flexible surface. *J. Fluid Mech.* **574**, 365-391.

LIST OF SYMBOLS AND ABBREVIATIONS

DL	disc length
f	frequency
κ	curvature
λ	wavelength
s	three-point curve used to calculate κ
T	unit tangent vector of curve s
U	overall swimming speed
v	wavespeed

Chapter 2

Synchronized Swimming: Coordination of pelvic and pectoral fins during augmented punting by freshwater stingray *Potamotrygon orbignyi*

Abstract

The physical properties of the fluid-solid interface shape the lives of benthic animals, including their means of locomotion. Aquatic walking and similar substrate-dependent forms of underwater propulsion have evolved multiple times in benthic invertebrate and vertebrate taxa, including batoid elasmobranchs. Skates (Rajidae) use the pelvic fins to punt across the substrate, keeping the pectoral fin disc still. Other batoids combine pelvic fin motions with pectoral fin undulation in augmented punting, but the coordination of the two modes has not been described. In this study of an augmented punter, the freshwater stingray *Potamotrygon orbignyi*, we demonstrate the synchrony of pelvic and pectoral fin cycles. The punt begins as the pelvic fins, held in an anterior position, are planted into the substrate and used to push the body forward. Meanwhile, a wave of pectoral fin undulation begins, increasing to maximum height just before the cycle's halfway point, when the pelvic fins reach their furthest posterior extension. The pectoral fin wave subsides as the pelvic fins return to their starting position for subsequent punts. Despite definitive links between pectoral and pelvic fin activity, we find no significant relationship between pectoral fin kinematics (frequency, wave height, and wavespeed) and punt performance. However, slip calculations indicate that pectoral undulation can produce thrust and augment punting. Pelvic fin kinematics (frequency and duty factor) do have significant effects, suggesting that while both sets of fins contribute to thrust generation, the pelvic fins likely play the major role in determining augmented punt performance.

Introduction

Benthic animals live at the boundary of the fluid and solid world, a physical environment fundamentally different than the three-dimensional fluid habitat of pelagic species. The nearby substrate offers opportunities for crypsis and habitat for prey, but benthic species also benefit from the basic physical properties of the solid-fluid interface. Proximity to the substrate allows small fish like darters (Etheostomatinae) to shelter from fast currents in the slower flow of the boundary layer (Carlson and Lauder, 2010), aids prey capture in bamboo sharks (Nauwelaerts et al., 2007) and certain batoids (Wilga et al., 2012), and offers unique opportunities for locomotion. Benthic animals can either swim above the substrate like their pelagic counterparts, or "walk" along it by pushing off the solid surface. Aquatic walking and other, similar forms of substrate-based locomotion have evolved multiple times; evidence from tetrapod ancestors like *Tiktaalik roseae* demonstrates the importance of fin-walking in our own evolutionary history (Shubin et al., 2006). Invertebrates including octopi (Huffard et al, 2005) and even relatively sessile gastropods like abalone (Donovan and Carefoot, 1997) demonstrate an impressive capability for benthic locomotion. This type of transport also occurs in extant vertebrates from seals (Fish, 1988), turtles (Zug, 1971), and salamanders (e.g. Ashley-Ross and Bechtel, 2003; Azizi and Horton, 2004) to coelacanths and lungfish (Fricke and Hissman, 2004; King et al., 2011), epaulette and bamboo sharks (Pridmore, 1994; Goto et al., 1999; Wilga and Lauder, 2001), and many teleosts (e.g. frogfish, Pietch and Grobecker, 1987; flying gurnards, Renous et al., 2000; and batfish, Ward, 2002). The occurrence of substrate-based locomotion across such a diverse array of taxa suggests its utility. Aquatic gaits vary within and between taxa, including both walking and galloping, and may involve one or both sets of paired fins/limbs, used synchronously or asynchronously.

Given the prevalence of substrate-based locomotion among diverse benthic species, it is no surprise to encounter this mode among batoids, as the majority of skate and ray species are benthically associated (McEachran and de Carvalho, 2002). In the water column, batoids swim via oscillations or undulations of the pectoral fin disc (or axial undulation in Rhinobatidae, Pristidae, and Torpediniformes) (Breder, 1926; Rosenberger, 2001; Blevins and Lauder, 2012). In contrast, the pelvic fins are used when batoids move across the substrate. Skates are benthic locomotion specialists, using robust, specialized portions of the pelvic fins (crurae) to walk (alternating fin motion; Lucifora and Vassallo, 2002) or "punt" (synchronous fin motion, Koester and Spirito, 2003). During a punt, skates sweep their pelvic fins anteriorly, plant them against the substrate, and then use them to push the rest of the body forward, keeping the pectoral fin disc completely still ("true punting"; Macesic and Kajiura, 2010). Other benthic batoids lack pelvic fin specializations, but still perform punting behaviors; however, most do not keep the pectoral fin still during punting, but instead combine pectoral fin undulations with pelvic fin motions (Macesic and Kajiura, 2010). This "augmented punting" has been proposed as a way for batoids with relatively less robust and less specialized pelvic fins to generate supplementary thrust during punting (Macesic & Kajiura, 2010). Both modes of punting can provide the fine scale maneuverability required for detecting and capturing benthic prey items. Additionally, it likely produces slight mechanical disturbances in the water column compared to pectoral or axial swimming, thus reducing detection by both the batoid's predator and prey (Koester & Spirito, 2003; Macesic and Kajiura, 2010).

In this study, we examine how pelvic and pectoral fin modes of locomotion—essentially, pelagic and benthic forms of propulsion—are combined during augmented punting by the freshwater stingray *Potamotrygon orbignyi*. We hypothesize that there will be synchrony

between pelvic and pectoral fin cycles, with coordination between fin pairs aligning fin kinematics so that pectoral fin undulation can augment the thrust produced by the pelvic fins. To test this hypothesis, we use major kinematic landmarks to characterize the pectoral and pelvic fin cycles, and then determine whether the kinematic events of the pectoral fin cycle occur at random or predictable times relative to the pelvic fin cycle.

Materials and Methods

Animals

Juvenile freshwater stingrays, *Potamotrygon orbignyi* (Castelnau, 1855), were purchased from a local importer. The five individuals used in our experiments (mean disc length 9.1 cm ± 0.2 SD, mean disc width 8.6 cm ± 0.1 SD) were housed in individual 100 liter aquaria at a constant temperature of 27±1º C, under a 12 h:12 h photoperiod; the bottom of each tank was covered by >2 cm of sandy substrate (grain size 1-3 mm). Stingrays were fed live blackworms (*Lumbriculus variegatus*) six times per week. We chose to work with *P. orbignyi* as we had previously observed augmented punting during benthic locomotion by this species. In addition, their small size makes them well suited to laboratory experiments, and we were able to compare the pectoral fin undulations observed during punting with previous work on the pectoral fin kinematics of pelagic locomotion in this *P. orbignyi* (Blevins and Lauder, 2012). All husbandry and experimental procedures were performed in accordance with Harvard University IACUC protocols (no. 20-03).

Behavioral Observations & Videography

During experiments, individual stingrays were placed into the working section of a variable-speed flow tank (28 cm wide, 28 cm high and 66 cm long), bounded by upstream and downstream baffles. All experiments were performed in still water (0 m/s water flow). The floor of the tank was lined with plastic mesh (0.5 cm grid) to improve pelvic fin traction with minimal visual obstruction, as fins can slip on smooth surfaces like glass and Plexiglas, altering kinematics and thrust production. Stingrays were allowed to locomote freely; if prompting was necessary, sedentary rays were stimulated by lightly touching the tail region with a wooden dowel to provoke a series of punts. Punting was filmed at 125 frames per second by two synchronized high-speed video cameras (FASTCAM 1024 PCI; Photron USA, Inc., San Diego, CA, USA). One camera was positioned laterally to visualize pectoral fin motion, while the second camera captured a ventral view of the pelvic fins via 45º angled mirror positioned below the flow tank. We filmed at least nine punting events per individual, with an event defined as a continuous, steady-state series of punts (6 or more punt cycles). From each event we selected four punts for analysis, always excluding the first and last punt of the event. We analyzed 195 punts overall.

Video Analysis

To test for synchrony between pelvic and pectoral fin motions, we compared the timing of five kinematic events within a punt cycle (Figure 2.1). Pelvic fin motions were described by (A) the start of the pelvic fin punt, when the pelvic fins reached their most anterior position; (B) the end of the pelvic fin thrust phase of the pelvic punt, as the pelvic fins reached their most posterior

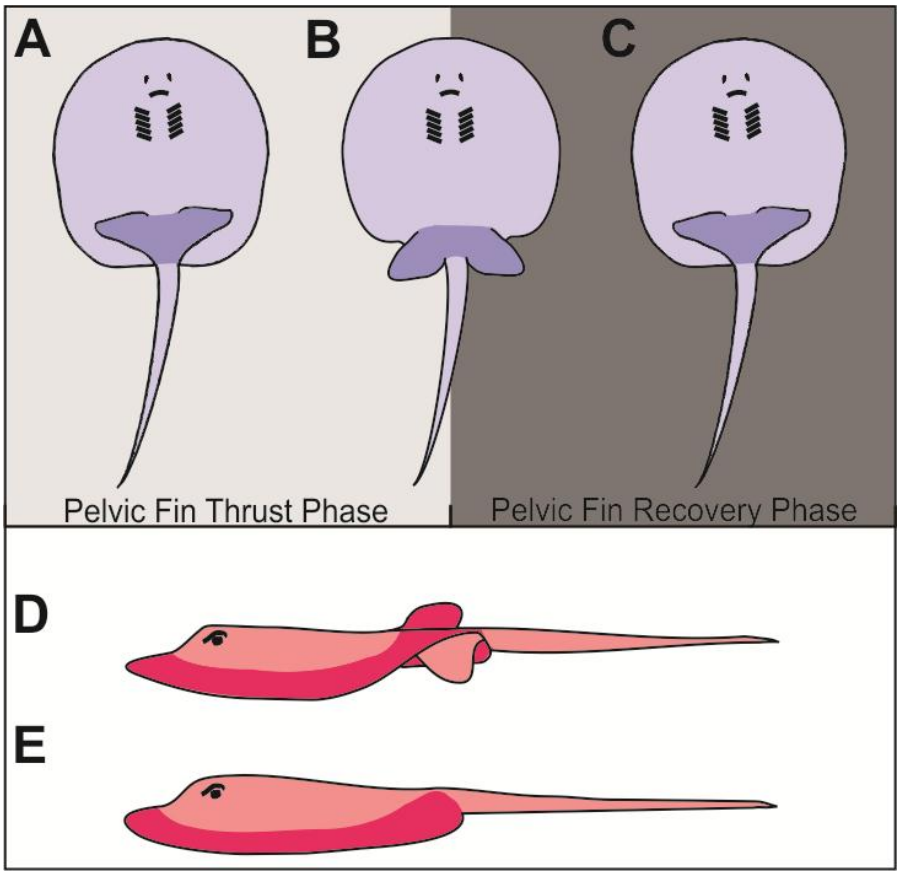

Figure 2.1. Key kinematic events used to characterize pelvic fin (blue) and pectoral fin (red) motions during augmented punting: (A) start of the pelvic fin punt, (B) end of the thrust phase of the pelvic fin punt, (C) end of the pelvic fin punt (identical to the start of the subsequent punt), (D) pectoral wave maximum, and (E) pectoral wave minimum. The pelvic fin cycle is divided into pelvic fin thrust and recovery phases. Deeper colors highlight the fin of interest. See text for further description of kinematic events.

position; and (C) the end of the pelvic punt, when the pelvic fins returned to their anterior position at the end of the pelvic fin recovery phase. Therefore, if no pause existed between punts, the end of one punt (event C) would coincide with the beginning (event A) of the subsequent punt. To characterize pectoral fin motion, we first located the position along the pectoral fin with the greatest dorsoventral excursion during one wave cycle (~0.7 disc lengths), then determined the times of two kinematic events at this position: (D) maximum wave height (crest) and (E) minimum wave height (wave trough or flat fin), representing the end of the pectoral wave, as the pectoral fin subsided back toward the substrate. We measured all event timings by viewing video sequences in either ImageJ (NIH, Bethesda, MD, USA; Abramoff et al., 2004) or Photron Motion Player 1.2.0.0 (Photron, Inc., USA), determining the frame number of each event, and converting frame numbers into time intervals in seconds. Pelvic fin punt frequency (Hz) was calculated as the inverse of the time elapsed between the beginning and end of the pelvic fin punt (events A-C). Pectoral fin wave frequency (Hz) was calculated by doubling the time elapsed between the pectoral wave crest and trough (events D and E) before taking the inverse, as the crest-trough interval represents half of a wave cycle. Pelvic fin duty cycle, the percentage of a punt cycle when the pelvic fin was in contact with the substrate (i.e., producing thrust), was determined as the ratio of the time elapsed during the pelvic fin thrust phase of the punt (events A-B) to the time elapsed during the entire pelvic punt (events A-C).

After we identified the individual video frames corresponding to each kinematic event (5 frames per punt), each frame was extracted for further analysis in ImageJ. We calibrated each image using a within-frame known distance and measured two spatial variables: the magnitude of pectoral wave height and the distance traveled by the ray during the punt. We combined spatial and timing data to determine the stingray's swimming velocity during the punt. For a

subset of ten punts (two punts from each individual, randomly selected) we measured the distance traveled by the stingray during the two distinct pelvic fin phases of the punt—the pelvic fin thrust phase (events A-B) and pelvic fin recovery phase (events B-C)—and calculated separate body velocities for each phase. For the ten-punt subset, we also determined the distance traveled by the pectoral wave during a known time interval centered around the time of maximum wave height, tracking the position of the wave crest as it moved from anterior to posterior along the pectoral fin disc. After correcting for the forward motion of the stingray's body during the same time interval, we used the wave crest data to calculate the wavespeed of pectoral fin undulation. The ratio of body velocity to pectoral wavespeed, called slip, summarizes the motion of the pectoral fin relative to the body. For slip<1, the pectoral fin wave is moving from anterior to posterior faster than the body is moving forward. Under this condition, the pectoral fin accelerates fluid backwards, opposite to the stingray's direction of travel, producing thrust. For slip>1, body velocity is greater than pectoral wavespeed, and the pectoral fin cannot contribute thrust.

All values are presented as mean±1 standard deviation, or mean±1 angular deviation for angular variables (see below). Angular deviation is a measure of dispersion for data with a circular distribution, analogous to the standard deviation of linear variables (Zar, 2010)

Statistical Analysis

To compare event timings among punts, we first standardized each augmented punt to polar coordinates, defining the start of the pelvic fin punt (event A) as 0º and the end of the pelvic fin punt (event C) as 360º. The remaining kinematic events (the end of the pelvic fin thrust phase, pectoral fin wave maximum, and pectoral fin wave minimum) were superimposed on this cycle

to examine timing relationships. After verifying unimodal distributions for all timing variables, we performed Rayleigh's test for uniformity (Zar, 2010) to determine whether the remaining events were randomly distributed throughout the cycle, or clustered non-randomly. The test was performed for each individual and for all stingrays, pooled. All remaining statistical analyses were performed in JMP 9.0.2 (SAS Institute, Cary, NC, USA). We performed a mixed-model two-way analysis of variance (ANOVA) of kinematic event timing to test for differences between the mean times of events, with event type (A, B, D, E) as a fixed factor and individual as a random factor. To prevent errors from angular data (i.e., 360º and 10º are closer than 360º and 330º) we first transformed data for event E (pectoral wave minimum), the only event near this threshold, translating angles between 180º and 360º into negative values (330º becomes -30º, and so forth). Post-hoc Tukey tests were used to specify where significant differences in means occurred. A pairwise multiple correlation analysis was performed to explore timing relationships between kinematic events (B, D, E). Multiple regression was used to examine relationships between punt distance (as a measure of punt performance) and kinematic variables (pelvic fin and pectoral fin frequencies, pectoral wave height, and pelvic fin duty factor). A mixed-model two-way ANOVA was used to test for differences in distance-traveled, duration, and body velocity between the pelvic fin thrust phase (events A-B) and pelvic fin recovery phase (events B-C), with phase as a fixed factor and individual as a random factor. The same procedure was performed to determine the effect of wavespeed on the distance traveled by the stingray during the entire punt, and during each of the two punt phases. Bonferroni correction was applied to p-values to prevent Type I errors from multiple comparisons.

Results

Event timing during the augmented punting cycle

During augmented punting by *P. orbignyi*, pelvic fin punts and pectoral fin undulations occur at regular intervals during the punt cycle. When the start of the augmented punting cycle (event A, pelvic fin punt start) is set at 0º, the end of the pelvic fin thrust phase (event B) occurs at 179±19º (mean±angular deviation), yielding a duty factor of 50±10%; maximum pectoral wave height (event D) occurs at 165±51º, and minimum pectoral wave height (i.e. the end of the pectoral wave; event E) at 18±51º, equivalent to 378±51º (Figure 2.2). A Rayleigh test of circular uniformity confirms that events are not randomly distributed over the cycle ($p<0.001$ for all events, for each individual and for pooled data). All kinematic events occur at significantly different times during the cycle (ANOVA, $p<0.0001$). There is a significant correlation between the time of pectoral wave maximum and the end of the pectoral fin thrust phase (events B and D; Pearson's $r=0.27$, $R^2=0.07$, $p<0.0001$).

Fin kinematics and punt performance

Pelvic fin punting and pectoral fin undulation occur at the same frequency, 1.3±0.3 Hz (mean±standard deviation), an average of 0.8±0.3 seconds per augmented punt cycle, equally divided between the pelvic fin thrust and pelvic fin recovery punt phases (events A-B and B-C, respectively; both 0.4±0.1 s). Stingrays travelled 1.9±0.4 cm per punt, or 0.21±0.09 disc-lengths (DL); more than 80% of punts are 2 cm or less, though the longest punt we observed reached 4.8 cm (0.53 DL). Overall body velocity is 2.4±1.8 cm/s (0.26 DL/s). In the subsample of punts (n=10) where distance-traveled was measured separately for pelvic fin thrust and pelvic fin recovery punt phases, we found no significant differences between phases in distance traveled

Figure 2.2. Polar plot of the phase relationship between pelvic fin motions and pectoral fin undulations during augmented punting by *P. orbignyi*. The radial axis represents one punt cycle, defined by the motion of the pelvic fins. The augmented punt cycle begins when the pelvic fins are at their most anterior position (event A, 0º), and concludes as they return to this position at the end of the punt (event C, 360º). We indicate the timing of other major kinematic events relative to this cycle, giving the mean angle (black square) ± 1 angular deviation (colored bar), the mean vector (colored arrow; longer vectors indicate less angular dispersion), and an illustration of the fin position corresponding to that event. Pelvic fin events are shown in blue, pectoral fin events in red; see text for detailed descriptions of each event. A Rayleigh test of circular uniformity confirms that events are not randomly distributed over the cycle ($p<0.001$ for all events, for each individual and pooled data). The end of the pelvic fin thrust phase (event B) occurs at 179±19º, maximum pectoral wave height (event D) at 165±51º, and minimum pectoral wave height (event E) at 18±51º; all events times are significantly different (ANOVA, $p<0.0001$) with significant correlation between the time of pectoral fin maximum and the end of the pelvic fin thrust phase.

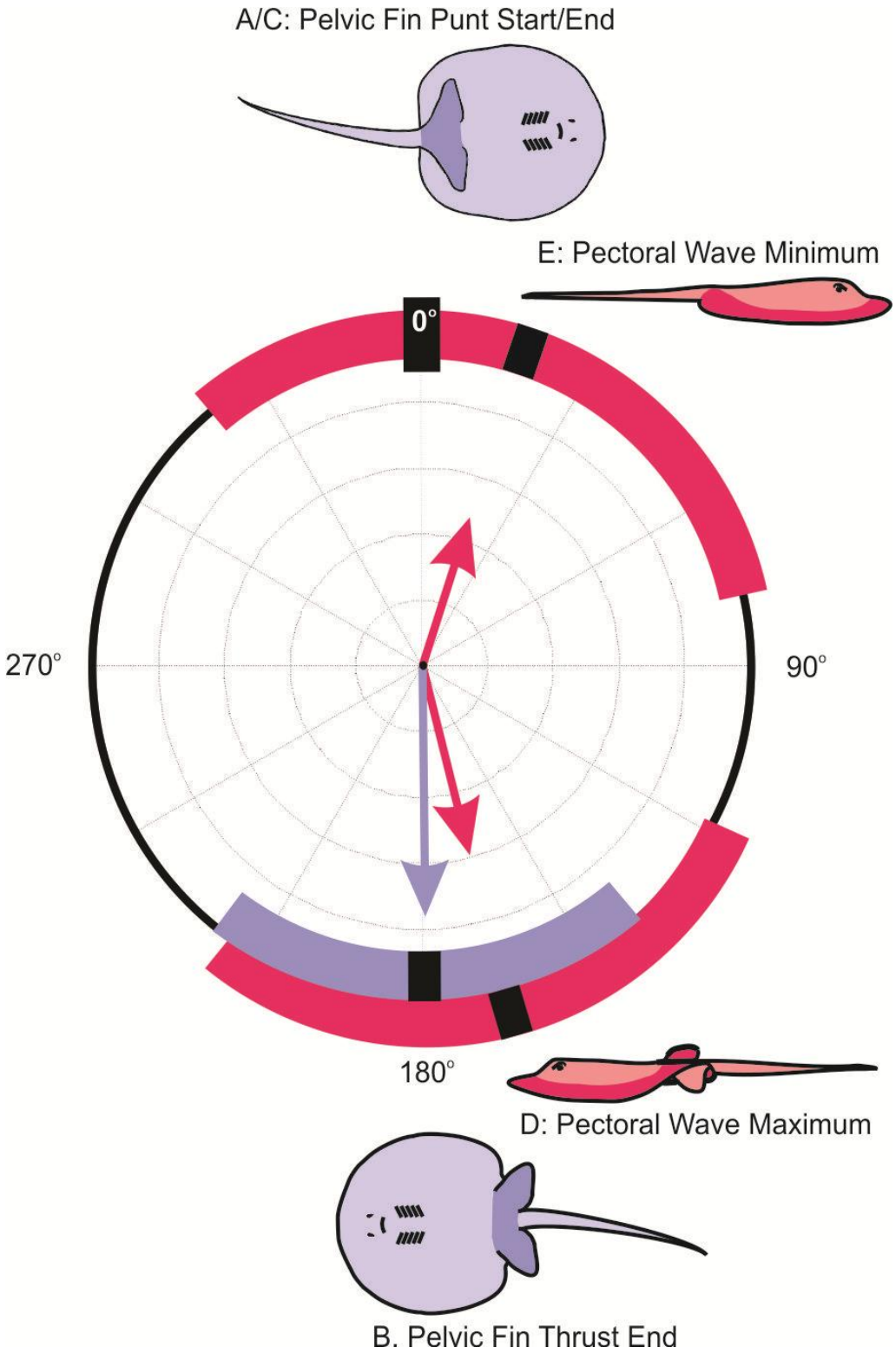

Figure 2.2 (Continued)

(0.7±0.2 cm and 0.6±0.4 cm, respectively) or body velocity (2.2±0.8 cm/s and 1.6±0.7 cm/s, respectively) (ANOVA, $p>0.1$; n.b. total distance-traveled is 1.4±0.3 cm in the subsample, slightly lower than in the dataset overall). Pectoral fin wave height is highly variable, with a mean of 0.9±0.5 cm. A multiple regression of pectoral fin wave height, pectoral fin frequency, pelvic fin duty factor and pelvic fin frequency against punt distance finds significant relationships for pelvic duty factor and frequency only (both $p<0.0001$), though model fit is improved by adding pectoral fin variables (adjusted $R^2=0.33$, vs. 0.25 for pelvic fin variables alone). Relationships between individual kinematic variables and punt distance or punt speed are minimal, indicating that punt performance is not strongly determined by kinematics (Figure 2.3).

Pectoral fin wavespeed, calculated from the ten-punt subsample, averages 4.5±2.0 cm/s, while body velocity calculated for the same interval is 2.8±1.2 cm/s. Calculations based on these averages give a slip of 0.6, but pairwise comparisons of body and wave velocity result in a highly variable mean slip of 0.8±0.6, with six of ten values <1 (Figure 2.4). Slip values less than one indicate that the pectoral fin wave is traveling from anterior to posterior along the fin more rapidly than the stingray, as a whole, is moving forward. Under this condition, pectoral fin undulation will produce thrust, as it accelerates fluid opposite to the stingray's direction of travel. However, increases in pectoral fin wavespeed have no significant relationship with the stingray's body velocity or the distance traveled by the stingray during either punt phase or the entire punt (ANOVA, $p>0.1$).

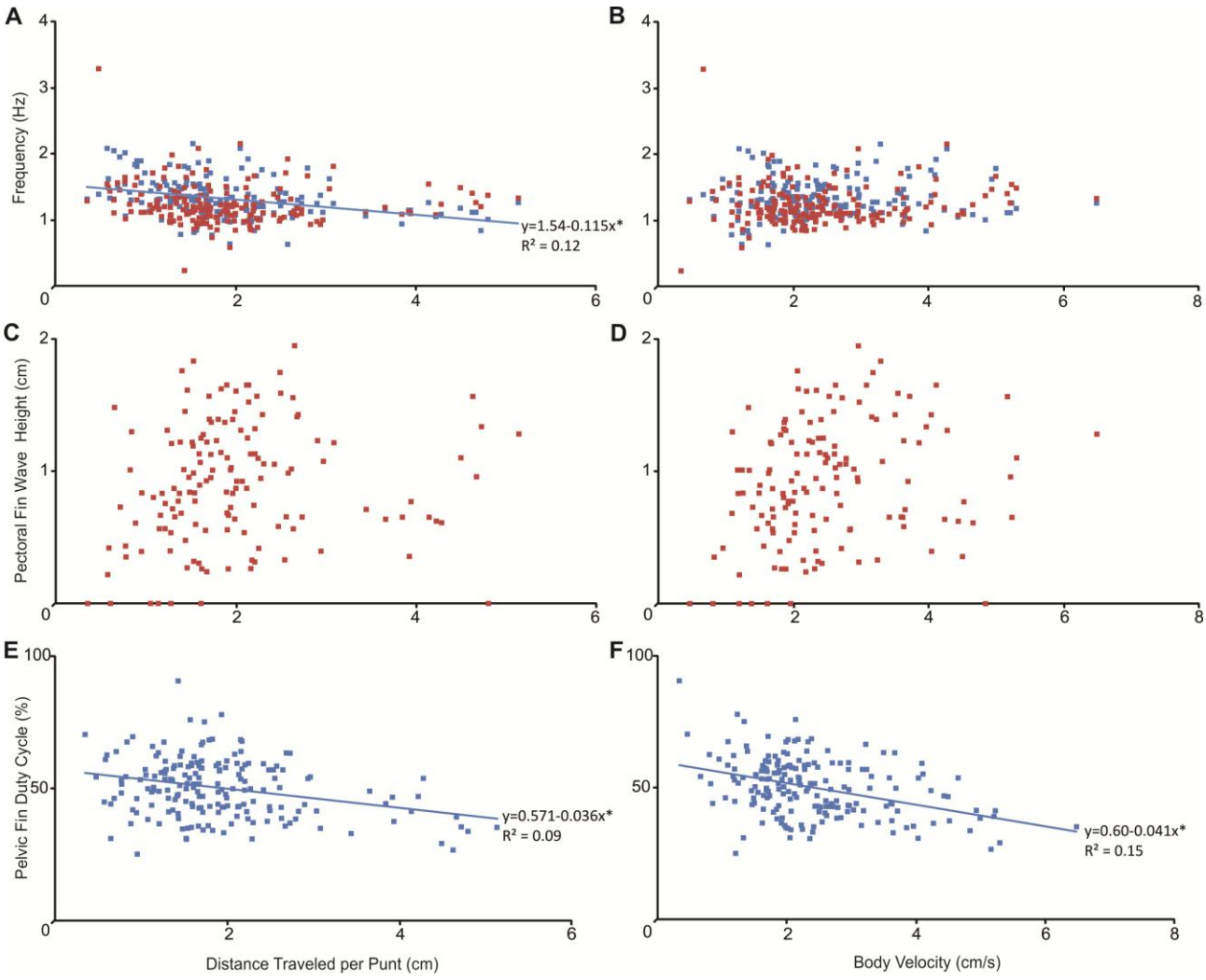

Figure 2.3. Plots of pectoral and pelvic fin kinematics vs. measures of augmented punt performance: pelvic fin frequency (blue) and pectoral fin frequency (red) vs. punt distance (A) and body velocity (B); pectoral fin wave height vs. punt distance (C) and body velocity (D); and pelvic fin duty factor vs. punt distance (E) and body velocity (F). Each point represents one punt. Regression lines, equations, and R^2 values are shown for relationships significantly different from zero ($p<0.001$, indicated by asterisks).

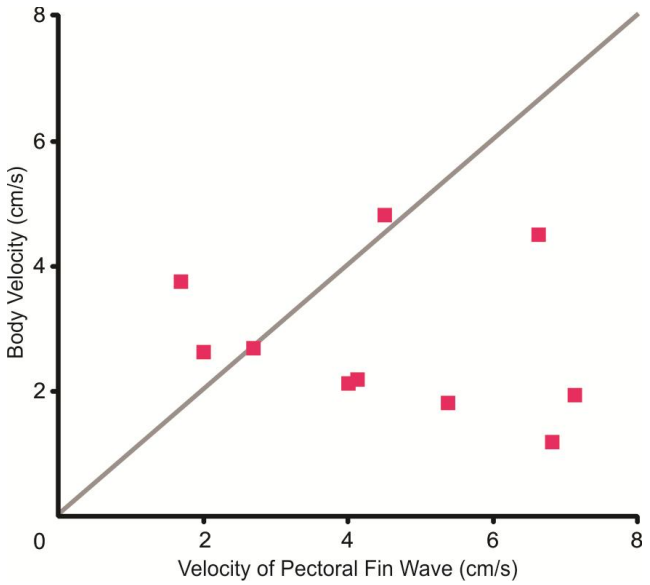

Figure 2.4. Velocity of the pectoral fin wave vs. body velocity during augmented punting by *P. orbignyi*. Each point represents a single punt. A reference line (grey, slope=1) represents a slip of 1. Points above the line have slip values >1; points below the line have slip <1.

Discussion

Pectoral and pelvic fin synchrony

Freshwater stingray *P. orbignyi* is an augmented punter, employing both pelvic and pectoral fins during benthic locomotion. At the start of a punt, the pelvic fins are held in an anterior position, then pressed into the substrate to push the stingray's body forward while a wave of undulation begins along the pectoral disc (Figure 2.2). The pectoral wave reaches its maximum height just before the pelvic fins are fully extended toward the posterior, ending the pelvic fin thrust phase of the punt cycle (Figure 2.2). The pectoral fin wave subsides as the pelvic fins enter the recovery phase, falling to a minimum wave height (representing the end of the pectoral fin wave) just after the pelvic fins return to their anterior starting position (Figure 2.2). Pelvic fin punts and pectoral fin undulations occur at the same frequency (1.3±0.3 Hz), and the cycles are aligned to create two closely-linked pairs of events: (1) the start of the pelvic fin punt and the pectoral fin wave minimum height, and (2) the end of the pelvic fin thrust phase and the pectoral fin wave maximum height. Though each event occurs at a statistically distinct time during the cycle, paired events are separated by less than 5% of a cycle (~40 ms for an average cycle with duration 0.8 s). Therefore, the synchrony of pelvic fin and pectoral fin cycles is clear. The two sets of fins are used in coordination during augmented punting, rather than one fin's cycle occurring randomly with respect to the other.

Studies of other aquatic species demonstrate that fin/limb pairs may be used synchronously or asynchronously during benthic locomotion, depending on taxon and gait. Frogfish use their fins synchronously during galloping, but asynchronously during walking (Pietch & Grobecker, 1987; Edwards, 1989). However, augmented punting combines locomotor modes as well as fin pairs: the pelvic fins push off the substrate, while the pectoral fins undulate.

In the only other study examining a similar combination of "fin walking" and undulatory locomotion, Azizi and Horton (2004) determine that salamander *Siren lacertina* uses both forelimbs and axial undulation to move across a submerged substrate, but found no synchrony between limb motion and body undulation. Augmented punters like *P. orbignyi* may have different patterns of neural control or different hydrodynamic constraints leading to the tight linkage of pelvic and pectoral fin cycles.

Kinematics of augmented punting

Augmented punting is a widespread locomotor mode among benthic batoids (Macesic and Kajiura, 2010), but it will win no prizes for speed. *P. orbignyi* traveled at 0.26 DL/s while punting, comparable to the velocities of other augmented punters (*Urobatis jamaicensis* and *Dasyatis sabina*; Macesic and Kajiura, 2010), slower than "true punters" like skates, which travel at 0.30-0.40 DL/s using the pelvic fins alone (Holst and Bone, 1993; Koester and Spirito, 2003; Macesic and Kajiura, 2010) and much slower than epaulette sharks, which can fin-walk at speeds of 0.64 body lengths/s (BL/s) (Pridmore, 1995). Aquatic walking velocity in salamander *Siren lacertina* ranges from 0.2 to 0.8 BL/s (Azizi and Horton, 2004). On average, the distance traveled per punt by *P. orbignyi* is about half that of other augmented punters (0.21 DL vs. ~0.4 DL), and the longest punt observed here reaches only the mean punt distance for the species studied in Macesic and Kajiura (2010). As overall punt velocity is the same for all studied augmented punters, this indicates that the punt cycle must occur twice as quickly in *P. orbignyi* compared to the other species. Interestingly, the pelvic fins spend more time in contact with the substrate during punting by *P. orbignyi* than by other augmented punters (pelvic fin duty factor

of 50%, rather than <40%); only a true punter, *Raja eglanteria*, approaches the *P. orbignyi* value (Macesic and Kajiura, 2010).

When swimming in the water column, fish increase velocity by increasing the frequency or amplitude of propulsive motions, whether this involves a set of paired fins, the caudal fin, or the entire body (Bainbridge, 1958; Blake, 1983; Lauder, 2006). In substrate-based locomotion there is another option: fish can increase the force used to push off the substrate, or the duration over which that force is applied. Augmented punting is so-named because pectoral fin undulation is thought to augment the thrust produced by the pelvic fin punt (Macesic and Kajiura, 2010). The synchrony between pectoral and pelvic fin cycles seems to support this idea, suggesting that cycles are aligned purposefully. We therefore expect pectoral fin undulation to increase as stingrays punt farther or faster, contributing more thrust via increased wave height or wave frequency. However, in augmented punting by *P. orbignyi* we find no significant relationship between pectoral fin kinematics (frequency, wave height, or wavespeed) and increased punt performance (distance traveled per punt, or body velocity during a punt) (Figure 2.3A-D). Pelvic fin kinematics do influence punt performance: as the pelvic fin thrust phase of the punt cycle (pelvic fin duty cycle) becomes longer punts become longer and faster (Figure 2.3E, F). As pelvic fin frequency decreases, punts also become longer (Figure 2.3A). However, all effects of pelvic fin kinematics (frequency or duty factor) explain a relatively small proportion of the variation in punt performance (distance or speed). A multivariate regression model including all kinematic variables explains only one-third of the variation in punting speed, with the duration of the pelvic fin thrust as one of the largest predictors of body velocity and punt distance (Figure 2.3E-F). The remaining explanation, then, is that punt performance (in terms of

both distance and velocity) is largely determined by the amount of force applied by the pelvic fins during their duty cycle.

While pectoral fin undulation does not drive variations in punt performance, slip calculations reveal that the pectoral fins produce some thrust during the majority of augmented punts in *P. orbignyi* (Figure 2.4). Slip is highly variable during augmented punting, and for punts with slip values greater than one the pectoral fin is not producing thrust. However, both the majority and the mean of slip values are less than one, indicating that the wavespeed of pectoral undulation exceeds the forward velocity of the body. Under this condition the pectoral fin must produce thrust, as the pectoral wave will accelerate fluid in the direction opposite to the stingray's direction of travel. It is less clear whether the *net* thrust contributed by the pectoral fin outweighs the increased drag induced by undulation, as any wave traveling along the pectoral fin will increase the surface area of the body held into the flow. Skates are thought to be particularly efficient punters in part because they minimize drag by maintaining a flat pectoral fin disc (Koester and Spirito, 2003); for overall punt performance to benefit from "augmentation," pectoral fin undulations must offset the additional drag they create and produce net thrust.

An alternative explanation for pectoral fin motion during augmented punting is that undulation occurs not to produce thrust, but to prevent pectoral disc from interfering with pelvic fin motions. The pectoral fin disc overlaps the pelvic fins to a greater extent in augmented punters than in true punters (Macesic and Kajiura, 2010), so perhaps the pectoral fin must be lifted to allow the pelvic fins to move back and forth beneath the disc. Timing data seems to support this idea, as the pectoral fin is lifted highest while the pelvic fins slip back under the disc during their return to an anterior position (Figure 2.2). However, pectoral fin control is exceedingly fine in *P. orbignyi*, allowing localized, small-scale alterations in fin shape (Blevins

and Lauder, 2012), and the pelvic fins are only a few millimeters thick; the pectoral wave heights we measure are far greater than would be required to allow the thin pelvic fins to slip under the disc (~1 cm), and the pectoral wave often starts further forward on the fin that would be necessary to admit the pelvic fins. This suggests that pectoral fin undulation does not occur just to allow the pelvic fins to move under the pectoral disc. Further, we observed several punting sequences with a pectoral fin wave height of 0 cm, demonstrating that pectoral undulation is not necessary to allow pelvic fin motion, or for stingrays to lift off of the substrate (Figure 2.3C-D).

From the variability in slip and fin kinematics, we suggest that augmented punting is a transitional gait. Stingrays moved slowly during the ad libitum punting studied here, with pelvic and pectoral fins completing one punt cycle, then settling back into starting positions before beginning another. For the pectoral fin disc, this resulted in a discrete series of waves interspersed by pauses rather than the continuous undulation seen during pectoral fin swimming (Rosenberger, 2001; Blevins and Lauder, 2012). Just as pelvic fin thrust duration is a significant factor in punt performance, the duration of pectoral fin undulation throughout a punt cycle may have more influence on punt performance than wave frequency or wave height. In addition, our measurement of pectoral fin kinematics accounts for the motion of the pectoral fin margin only. This allows us to pinpoint the timing of wave crests, as required for our investigation of pelvic and pectoral fin synchrony, but does not consider mediolateral (or anteroposterior) variations in fin motion. Blevins and Lauder (2012) demonstrate that three-dimensional wave properties have significant influence on stingray locomotion.

Furthermore, the apparent lack of contribution to thrust generation from the pectoral fin could be related to the age of the batoid. It is possible that although the synchronous motor pattern is present early on, as demonstrated in these juvenile rays, the pectoral fins are not fully

exploited for maximum thrust production until the ray reaches adult size. The added mass may require the pectoral fins to be more engaged to achieve effective locomotion. Future studies should focus on how the kinematic patterns of augmented punting change throughout ontogeny in these batoids.

During augmented punting by benthic batoid *P. orbignyi*, pelvic and pectoral fin motions are synchronous. Pelvic fin punting, a substrate-based form of locomotion, is combined with pectoral fin undulations similar to those used in pelagic swimming, merging benthic and aquatic modes of propulsion, perhaps during behaviors such as prey detection and predator avoidance. Pectoral fins contribute thrust during augmented punting, but increases in the kinematic variables studied here (frequency, wave height, and wavespeed) do not increase punt distance or velocity. Augmented punting performance is largely determined by pelvic fin action, though a large proportion (2/3) of the variation in punt distance is not accounted for by kinematics and is attributed to the force of pelvic fin punting (not measured here). We expect that with greater "motivation" (i.e. higher velocity during foraging or more purposeful benthic locomotion), pectoral undulation during augmented punting would become increasingly continuous, eventually transitioning to full pectoral fin swimming. Future investigations of this transition—the velocity at which it occurs, the shifts in pelvic fin force production and overall hydrodynamics—can further address the combination of aquatic and benthic modes of propulsion by batoids and other benthic animals.

Acknowledgements

We thank Dr. Steven Kajiura, Dr. George Lauder, the Florida Atlantic University Elasmobranch Lab and the Lauder Lab for support during the experiment and analysis phases of this study, with special appreciation for work by undergraduate assistants Victoria Paulis and Alyson Myers, and constructive discussions with Jeanette Lim and Dr. Manny Azizi.

References

Abramoff, M.D., Magalhaes, P.J. and Ram, S.J. (2004). Image Processing with ImageJ. *Biophotonics International*. **11**(7) 36-42.

Ashley-Ross, M.A. and Bechtel, B.F. (2003). Kinematics of the transition between aquatic and terrestrial locomotion in the newt *Taricha torosa*. *J. Exp. Biol.* **207**, 461–474.

Azizi, E. and Horton, J. M. (2004). Patterns of axial and appendicular movements during walking in the salamander *Siren lacertina*. *J. Zool.* **107**, 111-120.

Bainbridge, R. (1958). The speed of swimming of fish as related to size and to the frequency and amplitude of the tail beat. *J. Exp. Biol.* **35**, 109-133.

Blake, R.W. (1983). *Fish locomotion.* Cambridge, UK: Cambridge University Press.

Blevins, E. and Lauder, G. V. (2012). Rajiform locomotion: three-dimensional kinematics of the pectoral fin surface during swimming by freshwater stingray *Potamotrygon orbignyi*. *J. Exp. Biol.* **215**, 3231-3241.

Breder, C. M. (1926). The locomotion of fishes. *Zoologica.* **50**, 159–297.

Carlson, R.L. and Lauder, G.V. (2010). Living on the bottom: the kinematics of benthic station-holding in darter fishes (Percidae: Etheostomatinae). *J. Morph.* **271**, 25-35.

Donovan, D.A. and Carefoot, T.H. (1997). Locomotion in the abalone *Haliotis kamschatkana*: pedal morphology and cost of transport. *J. Exp. Bio.* **200**, 1145-1153.

Edwards, J. L. (1989). Two perspectives on the evolution of the tetrapod limb. *Am. Zool.* **29**, 235-254.

Fish, F.E., Innes, S. and Ronald, K. (1988). Kinematics and estimated thrust production of swimming harp and ringed seals. *J. Exp. Biol.* **137**, 157–173.

Fricke, H. and Hissman, K. (2004). Locomotion, fin coordination and body form of the living coelacanth *Latimeria chalumnae*. *Env. Biol. Fish.* **34**, 329-356.

Goto, T., Nishida, K. and Nakaya, K. (1999). Internal morphology and function of paired fins in the epaulette shark, *Hemiscyllium ocellatum*. *Ichthyol. Res.* **46**, 281–287.

Huffard, C.L., Boneka, F. and Full, R.J. (2005). Underwater bipedal locomotion by octopuses in disguise. *Science.* 307, 1927.

King, H.M., Shubin, N.H., Coates, M.I. and Hale, M.E. (2011). Behavioral evidence for the evolution of walking and bounding before terrestriality in sarcopterygian fishes. *Proc. Nat. Acad. Sci. USA.* **52**, 21146-21151.

Koester, D. M. and Spirito, C. P. (2003). Punting: An unusual mode of locomotion in the Little Skate, *Leucoraja erinacea* (Chondrichthyes: Rajidae). *Copeia.* **3**, 553-561.

Lauder, G. V. (2006). Locomotion. In: *The Physiology of Fishes, Third Edition* (eds. D.H. Evans and J.B. Claiborne), pp. 3-46. Boca Raton, FL: CRC Press.

Lucifora, L.O. and Vassallo A.I. (2002). Walking in skates (Chondrichthyes. Rajidae): Anatomy, behaviour and analogies to tetrapod locomotion. *Biol. J. Linn. Soc.* **77**, 35–41.

Macesic, L. J. and Kajiura, S. M. (2010). Comparative punting kinematics and pelvic fin musculature of benthic batoids. *J. Morph.* **271**, 1219-1228.

McEachran J.D. and de Carvalho, M.R. (2002). Batoid fishes. In: *FAO Species Identification Guide for Fishery Purposes, the Living Marine Resources of the Western Central Atlantic, Vol. 3.* (ed. K.E. Carpenter), pp. 508–589. Rome: FAO.

Nauwelaerts, S., Wilga, C.D., Sanford C.P. and Lauder, **G.V. (**2007). Substrate passively improves suction feeding in benthic sharks. *J. R. Soc. Interface.* **2**, 341-345.

Pietch, T.W., Grobecker, D.B. (1987). *Frogfishes of the World.* Stanford University Press, Stanford, CA.

Pridmore, P.A. (1994). Submerged walking in the epaulette shark *Hemiscyllium ocellatum* (Hemiscyllidae) and its implications for locomotion in rhipidistian fishes and early tetrapods. *Zool—Anal. Complex Sy.* **98**, 278–297.

Renous, S., Gasc, J.P., Bels, V.L. and Davenport, J. (2000). Six-legged walking by a bottom-dwelling fish. *J. Mar. Biol. Assoc. UK.* **80**, 757–758.

Rosenberger, L. J. (2001). Pectoral fin locomotion in Batoid fishes: undulation versus oscillation. *J. Exp. Biol.* **204**, 379-394.

Shubin, N.H., Daeschler, E.B., and Jenkins, F.A. (2006). The pectoral fin of *Tiktaalik roseae* and the origin of the tetrapod limb. *Nature.* **440**, 764-771.

Ward, A.B. (2002). Kinematics of the pectoral fins in batfishes (Ogcocephalidae) during aquatic walking. *Integr. and Comp. Biol.* **6**, 1331.

Wilga, C.D. and Lauder, G.V. (2001). Functional morphology of the pectoral fins in bamboo sharks, *Chiloscyllium plagiosum*: Benthic vs. pelagic station-holding. *J. Morphol.* **249**,195–209.

Wilga, C.D., Maia, A., Nawelaerts, S. and Lauder, G. (2012). Prey handling using whole-body fluid dynamics in batoids. *Zoology.* **115**, 47-57.

Zar, J.H. (2010). *Biostatistical Analysis 5th Edition.* Upper Saddle River, NJ: Prentice-Hall.

Zug, G.R. (1971). Buoyancy, locomotion, morphology of the pelvic girdle and hindlimb, and systematics of cryptodiran turtles. *Misc. Publ. Mus. Zool. Univ. Michigan.* **142**, 1–98.

Chapter 3

Swimming near the substrate: a simple robotic model of stingray locomotion

Abstract

Studies of aquatic locomotion typically assume that organisms move through unbounded fluid. However, benthic fishes swim close to the substrate and will experience significant ground effects, which will be greatest for fishes with wide spans such as benthic batoids and flatfishes. Ground effects on fixed-wing flight are well understood, but these models are insufficient to describe the dynamic interactions between substrates and undulating, oscillating fish. Live fish alter their swimming behavior in ground effect, complicating comparisons of near-ground and freestream swimming performance. In this study, a simple, stingray-inspired physical model offers insights into ground effects on undulatory swimmers, contrasting the self-propelled swimming speed, power requirements, and hydrodynamics of stingray-like undulating fins swimming with fixed kinematics near and far from a solid boundary. Contrary to findings for gliding birds and other fixed-wing fliers, ground effect does not necessarily enhance the performance of model undulating fins. Under most kinematic conditions, fins do not swim faster in ground effect, power requirements increase, and the cost of transport can increase by up to 25%. The influence of ground effect varies with kinematics, suggesting that benthic fish might modulate their swimming behavior to minimize locomotor penalties and incur benefits from swimming near a substrate.

Introduction

Benthic fish are specialized for life at the boundary between fluid and solid environments. Many species use the substrate for a direct boost to propulsion: various forms of fin-walking are seen across benthic taxa from lungfish (King et al., 2011), to skates and rays (Lucifora and Vassallo, 2002; Koester, 2003; Macesic and Kajiura, 2010), sharks (Pridmore, 1994; Goto et al., 1999; Wilga and Lauder, 2001), and many teleosts (e.g. frogfish, Pietch and Grobecker, 1987; flying gurnards, Renous et al., 2000; and batfish, Ward, 2002). However, even without direct contact, locomotion is influenced—and can be enhanced—by a nearby substrate, as ground effects alter fluid flow in the narrow gap between substrate and fish (Blake, 1979; Webb, 1981, 1993, and 2002; Nowroozi et al., 2009).

Ground effects are most commonly considered for rigid, static structures, in many computational and experimental studies of fixed-wing airfoils. In general, ground effects are greatest on broad structures moving close to the ground, as the magnitude of ground effect depends on the ratio of gap (the distance between the structure and the ground) to span (the width of the structure parallel to the ground) (Reid, 1932). Ground effects decrease rapidly as the gap/span ratio increases, becoming negligible at a ratio of 3 (Reid, 1932; Blake, 1979 and 1983). The consequences of moving near the ground vary substantially with foil shape (e.g. planform, camber, angle of attack) and distance from the substrate (Zerihan and Zhang, 2000; Zhang et al., 2004; Ahmed and Sharma, 2005). However, human designs such as wing-in-ground aircraft (built for flight very near the ground; Rozhdestvendky, 2006) and biological fixed-wing fliers can both experience significant gains in locomotor performance due to ground effect. The presence of a nearby substrate reduces flight costs in gliding birds (Baudinette and

Schmidt-Nielsen, 1974; Withers and Timko, 1977; Hainsworth, 1988) and increases glide distance in flying fish (Park and Choi, 2010).

Performance benefits from locomotion in ground effect are significant for engineers and organisms alike, with the potential for large reductions in cost of transport (15%) and power requirements (35%) (Rayner, 1991). However, fixed-wing models are insufficient to describe the ground effects experienced by most organisms, or in biomimetic designs. Very few models consider ground effects on moving foils (Tanida, 2001; Argentina et al., 2007; Molina and Zhang, 2011), yet in the vast majority of cases, animal locomotion is dynamic—wings, fins, and bodies flex and flap over time. When an animal moves near the ground (a substrate, wall, etc.), these locomotor motions continuously alter the animal's distance from the substrate and its effective shape. The pressure and flow structure between the animal and the substrate will fluctuate as well, creating a dynamic ground effect that varies during locomotion.

Fish swim by oscillating and undulating the body and fins, and are therefore subject to dynamic ground effects when swimming near a solid boundary. Most fish (e.g. trout, bluegill sunfish) are laterally compressed and swim "upright;" due to their very narrow ventral span, they are unlikely to experience significant ground effects from swimming near the substrate (high gap/span ratio; Webb, 2002). However, these fish can experience wall effects (analogous to ground effects) when swimming near the solid side wall of a channel; the gap/span ratio will decrease as the broad lateral surface of the body and caudal fin approaches the wall, with significant effects at gap/span <1 (Webb, 1993). In contrast, many benthic fish species are compressed in the same plane as the substrate— the most notable and extreme examples are the flatfishes (Pleuronectiformes) and stingrays (here referring to benthic, undulatory members of Batoidea). These fishes undulate in close proximity to the substrate with a low gap/span ratio,

and are likely to experience significant ground effect. Undulatory locomotion, whether by a stingray, eel, or flatfish, produces strong lateral jets (Webb, 2002; Tytell and Lauder, 2004), with great potential to alter the pressure and flow between fish and wall or ground. Plaice alter their kinematics as they swim closer to the substrate, suggesting a response to ground effect (Webb, 2002). However, studies of live fish do not allow the kinematic manipulations or force measurements required for a detailed investigation of ground effects on undulatory swimming performance.

In this study, a simple physical model based on freshwater stingray *Potamotrygon orbignyi* (Castelnau, 1855) is used to examine the effects of a nearby substrate on undulatory swimmers. Rather than creating a complex biomimetic stingray, the aim of this investigation is to approximate the flow conditions experienced by stingray-like swimmers using a simple robotic system in which motion parameters can be easily altered, input forces measured, and consistent kinematics maintained during swimming near and far from a solid boundary (in and out of ground effect). The dimensions and motion parameters of the model fin were selected to correspond with stingray kinematics determined in previous work on pectoral fin locomotion by *P. orbignyi* (Blevins and Lauder, 2012); fin width, length, and the range of undulation frequency, amplitude, wavespeed and swimming speed encompass values determined for live stingrays (Figure 3.1). Therefore, three main indicators of fluid regime and flow structure, Reynolds number (~10,000), Strouhal number (~0.2), and slip (wavespeed/swimming speed, ~0.6) are similar for model fins and stingrays. Self-propelled swimming speeds, costs-of-transport, and hydrodynamics are determined for undulating fins swimming in and out of ground effect. Comparisons are made between identical fins swimming with identical kinematics in one of two positions, either in the center of a recirculating flow tank ("center position") or near the side wall

of the tank ("wall position"). As model fins swim parallel to the tank wall, with the undulatory wave occurring perpendicular to the wall (Figure 3.2), this situation is analogous to a stingray undulating near the substrate: in the wall position, fins swim in ground effect (gap/span <1, Table 3.1). Two fin structures (described in detail below) are tested under various combinations of frequency (1 and 2 Hz) and undulation amplitude (1-2 cm). This experimental study of ground effects on an undulating model offers insight into the likely consequences of swimming near the substrate for stingrays and other benthic undulators.

Methods

A simple model system was used to investigate the influence of ground effect on undulatory swimmers: a flexible fin (30 Shore A Neoprene, 15 x 7.5 x 0.3 cm) connected to a robotic apparatus controlling the heave and pitch of the fin through time. (For a detailed description of the control apparatus, see Lauder et al., 2007; Lauder et al., 2011a, b). The heave and pitch motors driving the fin are controlled by a custom Labview program, and sit on a carriage suspended over a recirculating flow tank on low-friction air bearings, allowing the entire apparatus to move upstream or downstream as the fin moves within the tank. The model fin was designed as a simplified representation of the pectoral fin of freshwater stingray *Potamotrygon orbignyi* (Castelnau, 1855), as the swimming kinematics of this species have been studied in detail (Blevins and Lauder, 2012). The length and width of the model fin approximate the dimensions of the pectoral fin of stingrays studied in Blevins and Lauder (2012; mean pectoral fin length ~13 cm, mean pectoral fin width ~6 cm). The heave, pitch and frequency values used to animate the model fin were also based on stingray data (Table 3.1, Figure 3.1), and created a traveling wave that passed from anterior to posterior along the fin during swimming.

Figure 3.1. (A) Amplitude variation across the surface of the pectoral fin of freshwater stingray *Potamotrygon orbignyi* during steady swimming, with warmer colors indicating greater amplitude (from Blevins and Lauder 2012). Amplitude values represent ½ of the maximum excursion occurring at each point during one wave cycle. (B) Traces of the distal edge of the stingray pectoral fin (posterior quadrant) during locomotion near the substrate, at 25%, 50%, 75% and 100% of a wave cycle (compare to midline traces of the model fin in Figure 3.3). Anterior is at left. Pectoral fin amplitude is slightly greater than shown in (A), where stingrays were swimming steadily in midwater. (C) Hydrodynamic analysis of flow around the undulating stingray pectoral fin (highlighted in white) during locomotion near the substrate, illustrating vortex compression between fin and ground. Yellow vector arrows represent flow speed and direction relative to freestream flow, with vorticity indicated by red (positive) and blue (negative) shading. For clarity, only ¼ of vectors are shown. Vectors were not computed for masked areas (bright blue) outside the laser light sheet and overlapping the ground.

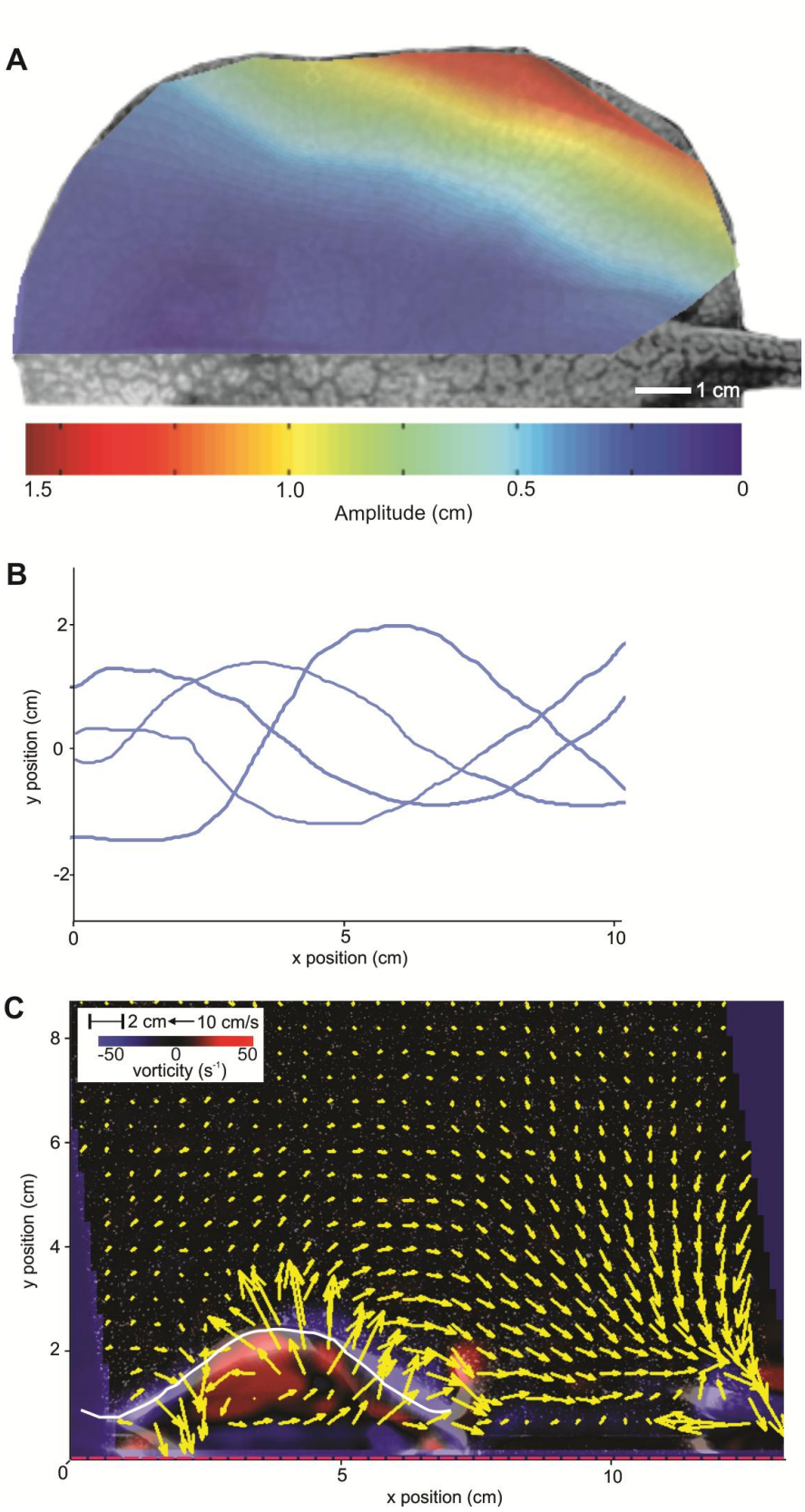

Figure 3.1 (Continued)

Swimming performance was determined for two fins, one connected to the control apparatus by one attachment (single attachment fin) and the other by two attachments (double attachment fins); the two fin designs allowed us to explore different waveforms (Figure 3.2, 3.3). Both fins were attached to the motors via a metal shaft clamping the fin's leading edge; the double-attachment fin was also actuated by a second shaft, positioned two-thirds of the way along the fin. This second attachment produced a traveling wave with higher amplitude than the wave produced on the single-attachment fin, by constraining the motion of the posterior portion of the double-attachment fin, more closely approximating stingray kinematics. The swimming performance of single-attachment fins was determined at heave values of +/- 1 cm and +/- 2cm, at frequencies of 1 Hz and 2 Hz (Table 3.1). The double-attachment fin was also tested at 1 Hz and 2 Hz, with a leading edge heave of +/- 1 cm and posterior heave of +/- 2cm (Table 3.1). For both fins, all heave motions were accompanied by a +/- 20 degree pitch, to turn the leading edge of the fin toward the direction of heave motion, producing a more fluid, fish-like undulation. To create a smooth traveling wave along the double-attachment fin, a phase offset of 180 degrees separated the heave and pitch of the anterior and posterior attachments.

The swimming performance of each combination of fin, frequency, and heave was compared between fins swimming in two positions: (1) the center of the recirculating flow tank ("center position") and (2) near the side wall of the tank ("wall position"). As the tank wall is perpendicular to the direction of undulation (Figure 3.2), fins swimming near the wall experience the same ground effect as stingrays, flatfish, and similar undulatory swimmers moving near a solid substrate; "wall effect" and "ground effect" are interchangeable here. Fins swimming in the center of the tank were always more than 9 cm from the tank wall, yielding a gap/span ratio

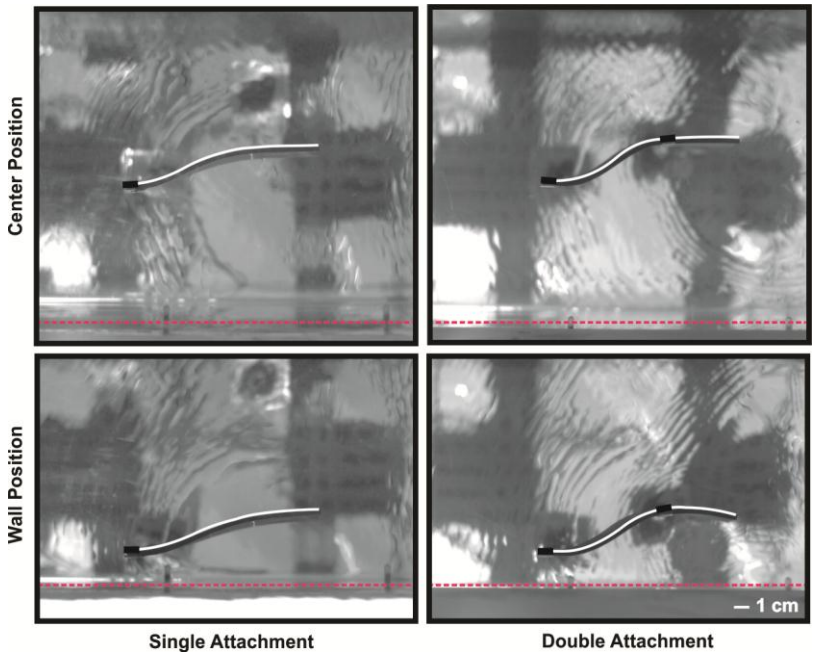

Figure 3.2. Ventral-view images of the single-attachment model fin (left column) and double-attachment model fin (right column) swimming at self-propelled speeds in the center of the recirculating flow tank (upper row; "center" position) and near the tank wall (lower row; "ground" position). Flow travels from left to right. Fins are actuated at 2 Hz and +/- 1 cm anterior heave (for the double-attachment fin, posterior heave = +/- 2cm). Fin outlines are traced in white, with black bars indicating points of attachment to the robotic controller located above the tank. Dashed red lines highlight the position of the tank wall.

of ≥1.5 (negligible ground effect; Table 3.1). When swimming in the wall position, the posterior margin of the fin approached within 1 cm of the tank wall (0.9 cm); anterior portions of the fin undulated with slightly lower amplitude, and reached a minimum of 1.5 cm from the tank wall. The exact distance values given are for the single-attachment fin, swimming at 1 Hz and +/- 2 cm heave, but are representative of all conditions (Figure 3.3). Fins in the wall position swam with a gap/span ratio of ≤0.5 (within ground effect; Table 3.1).

Fins' swimming performance was quantified using three metrics: self-propelled swimming speed (SPS), total work, and cost of transport. The SPS of each fin was determined by matching the flow speed of the recirculating tank to the thrust produced by the moving fin, following the procedures described in previous work with the same robotic apparatus (Lauder et al., 2007; Lauder et al., 2011a, b). In brief, linear encoders on the robotic carriage precisely track the position of the fin while the flow speed of the recirculating tank is varied. If the fin swims faster than the flow speed, it moves upstream; if it swims more slowly, it is pushed downstream. When the fin maintains an equilibrium position, thrust and drag are balanced during each cycle of motion. Rotary encoders on the recirculating tank determine the flow speed at which the fin maintains its equilibrium position; this speed is defined as the SPS of the fin under the tested swimming conditions (frequency, heave, and distance-from-ground). The mean SPS for each swimming condition was determined as the average of multiple trials (n=15 for single-attachment fin, n=10 for double-attachment fin).

After self-propelled speeds were determined for each swimming condition, force data were collected for single-attachment fins swimming at SPS. An ATI Nano-17 six-axis force/torque sensor (ATI Inc., Apex, North Carolina) was attached to the leading-edge shaft, simultaneously collecting 3 force and 3 torque measurements in an XYZ coordinate plane.

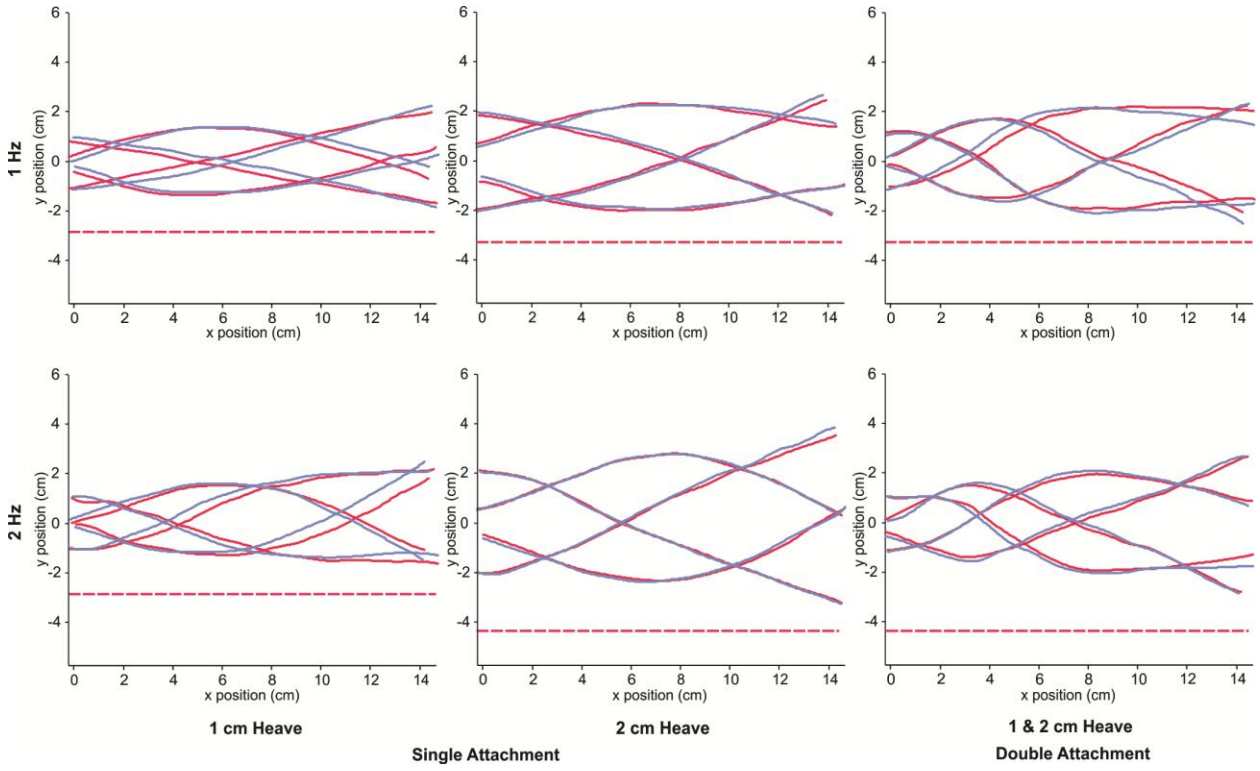

Figure 3.3. Midline traces through time for single- and double-attachment fins swimming at center (blue) and ground (red) positions. Flow travels from left to right. For each condition, traces are shown for 25%, 50%, 75% and 100% of one heave cycle. Dashed red lines indicate the position of the ground for fins swimming in the ground position. For center swimming positions, the ground lies below the horizontal axis.

Fin Type (Attachment No.)	Kinematics (Frequency, Amplitude)	Gap/Span[a]		Wavespeed (c) (cm/s)	
		Center	Wall	Center	Wall
Single	1 Hz, 1 cm	1.5	0.4	7.8	7.0
Single	1 Hz, 2 cm	1.6	0.4	14.8	16.4
Single	2 Hz, 1 cm	1.5	0.4	21.7	18.5
Single	2 Hz, 2 cm	1.7	0.6	25.0	26.5
Double	1 Hz, 1 & 2 cm	1.5	0.4	14.4	18.1
Double	2 Hz, 1 & 2cm	1.7	0.5	55.6	61.4
Stingray[b]	2.5 Hz, 1.4 cm	~1.0	--	31.0	--
Stingray[c]	3.8 Hz, 1.4 cm	~1.0	--	46.0	--

[a] As the ratio of gap (distance between structure and wall) to span (width of structure parallel to wall) decreases, the influence of ground effect increases, with significant effects occurring when gap/span < 1 (Webb 1993).

[b,c] from Blevins and Lauder (in press) for freshwater stingray *Potamotrygon orbignyi* swimming at (a) 20 cm/s and (b) 33 cm/s.

Table 3.1. Gap/span ratios and wavespeeds of undulating model fins swimming near and far from a solid wall, under all tested kinematic conditions (n=15 for single-attachment fin conditions, n=10 for double-attachment fin conditions). Values from stingrays swimming in midwater are given for comparison.

Sensor tolerance did not permit force data to be collected from the double-attachment fin. A Labview trigger pulse synchronized the data collection (500 Hz) of the fin's heave position, force and torque magnitudes, and video frames from a ventral high-speed camera (FASTCAM 1024 PCI, Photron USA, Inc., San Diego, CA, USA). We used the X axis (upstream/downstream) forces, Y axis (lateral) forces, and Z axis (vertical) torques in combination with distances determined from fin position data to calculate the fin's total work per cycle (mJ/cycle) in LabChart 7 (ADInstruments, Inc., Colorado Springs, Colorado), determining a mean total work for each swimming condition (n=7). The frequency and SPS for each condition were used to convert total work into cost of transport (mJ/m). For each performance variable (SPS, total work, and cost of transport) a nested analysis of variance (ANOVA) with post-hoc Tukey tests was performed to determine differences between center and ground swimming positions, and among swimming kinematics. Values are presented as mean +/- 1 standard error.

Video footage from the ventral-view camera mentioned above was used to perform a kinematic analysis of single- and double-attachment fin motion under each swimming condition, for fins swimming at self-propelled speeds. Video of the single-attachment fin was collected synchronously with force data. All videos were viewed in Photron Motion Player 1.2.0.0 (Photron, Inc., USA), and midline positions were tracked through time using a custom program in MATLAB version 7.10 (Mathworks, Natick, MA, USA). The phase velocity of the undulatory wave (c) was calculated for each swimming condition by measuring the distance traveled by the wave crest during a known time interval. To calculate c/U, an important parameter for predicting flow patterns around a waving structure (Shen et al., 2003), c was divided by SPS (identical to U, flow velocity). Paired t-tests were used to determine significant

differences in wavespeed between center and wall positions. Gap/span ratios were calculated for all swimming conditions; as the influence of ground effect decreases as gap/span increases (Reid, 1932; Rayner 1991), this verified that fins in "wall" and "center" positions were swimming in and out of significant ground effect regions, respectively. For undulating fins, the gap/span ratio varies during swimming as fins move toward and away from the wall. Span remains constant, as the width of the fin (7.5 cm) is the same for all conditions. To account for the variation in gap as the fin moves, an average gap was calculated by adapting the method of Webb (1993), by locating the point on the fin that approaches the wall most closely (here, the posterior margin of the fin) and determining its minimum and maximum distance from the wall during one motion cycle. The mean of these two values represented an average gap, and was divided by the constant fin span to calculate the gap/span ratio for fins swimming at center and wall positions under each kinematic condition.

Digital particle image velocimetry (DPIV) was used to visualize fluid flow around the fin. The recirculating tank was seeded with reflective particles (50 microns), which were filmed by the ventral camera as they passed through a laser sheet generated by a continuous 10 W Coherent argon-ion laser. The laser sheet was positioned at ½ fin height, and captured flow motion along the fin, in its wake, and between the fin and the tank wall (i.e., between fin and ground). During DPIV sequences, the fin was positioned slightly further from the tank wall than in experiments used to determine SPS and collect force data. In the near-wall position, the posterior margin of the single-attachment fin at 1 Hz and +/- 2 cm heave amplitude approached within 2 cm of the tank wall, and anterior portions came within 2.5 cm, a 1 cm increase compared to the positions used in our other experiments. Lastly, we filmed DPIV sequences with no fin present in the tank, to determine the flow profile of the boundary layer near the tank

wall. DPIV analyses were performed in DaVis 7.2 (LaVision Inc., Goettingen, Germany) to quantify velocity vectors and vorticity. In particular, the mean strength of leading-edge vortices (n=15 vectors) was compared for fins swimming in center and wall positions using a Student's test, as was the average magnitude and angle of flow between the fin and wall (n=36 vectors). Values are presented as mean +/- 1 standard error.

Results

Kinematics of self-propelling fins

The shape of fins during swimming varied with frequency, heave amplitude, and between single- and double-attachment fins, but showed very little change between center and wall positions (Figure 3.3). Gap/span ratios were approximately 0.5 for fins swimming near the wall, and ≥1.5 for fins swimming in the center of the tank (Table 3.1). For all single-attachment conditions, approximately 0.5 waves were present on the fin at one time. Wave number was slightly higher for double-attachment fins (0.6-0.8), as was fin curvature. Under all conditions, amplitude increased by roughly one centimeter from anterior to posterior along the fin—a 50% increase for fins swimming with a +/- 1 cm heave, and a 25% increase for fins with +/- 2 cm heave. However, amplitude reached a maximum at a more anterior position on double-attachment fins than on single-attachment fins with the same anterior heave (+/- 1 cm). This is due to the prescribed motion of the posterior attachment point (+/- 2 cm heave) on the double-attachment fin.

Under all conditions, a traveling wave moved down the fin during swimming at self-propelled speeds. Wavespeed *c* increased with frequency and heave amplitude (Table 3.1), but did not differ significantly between center and wall positions (paired t-test, $p>0.1$). Average slip

was 0.6, yielding a *c/U* ratio of 1.7. This indicates relatively little flow separation from the undulating fin (Shen et al., 2003). Wavespeed and *c*/*U* values for the model fin were generally similar to those found for pectoral fin undulation during swimming by stingray *P. orbignyi* (Table 3.1; Blevins and Lauder, 2012).

Swimming performance

For most kinematics, swimming near the wall had no significant effect on the self-propelled swimming speed (SPS) of single- or double-attachment fins (Figure 3.4; nested ANOVA, Tukey post-hoc, $p>0.05$). Only the single-attachment fin swimming at 1 Hz with a 2 cm heave showed a significant change in SPS near the wall, swimming 13 +/- 1% (mean +/- 1 standard error) faster than in the center of the tank (Tukey post-hoc, $p<0.0001$), though there was a general trend toward increased SPS near the wall for single-attachment fins. For double-attachment fins, there was a slight trend toward decreased swimming speed near the wall. Predictably, SPS increased with both frequency and heave amplitude across kinematic groups (nested ANOVA, $p<0.0001$, Tukey post-hoc, $p<0.0001$).

For the single-attachment fin, total work increased significantly when fins swam near the wall, under all kinematic conditions (Figure 3.5; nested ANOVA, Tukey post-hoc, $p<0.02$). The magnitude of the effect increased slightly across kinematic groups, ranging from 1.9 +/- 0.2 mJ/cycle (mean +/- 1 standard error) under the 1 Hz 1 cm condition to 3.8 +/- 0.3 mJ/cycle for fins swimming at 2 Hz 2 cm. Therefore, relative effect size—the percent change in total work between center and wall positions for a given set of kinematics—was greatest for fins moving at lower frequencies and heave amplitudes. For fins swimming at 1 Hz, total work increased near

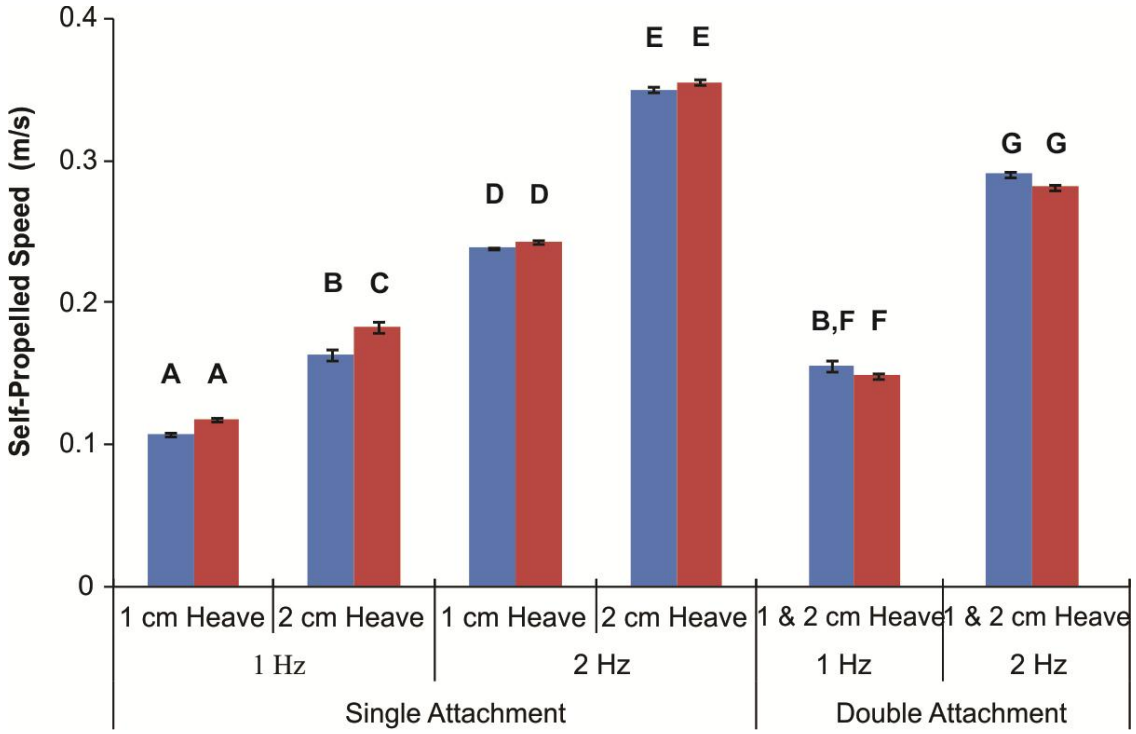

Figure 3.4. The self-propelled speed (m/s) of single- and double-attachment fins swimming at center (blue) and ground (red) positions, at the given frequencies and heave amplitudes. Error bars represent +/- 1 standard error. Levels indicated by different letters are significantly different (nested ANOVA with Tukey post-hoc, $p<0.01$).

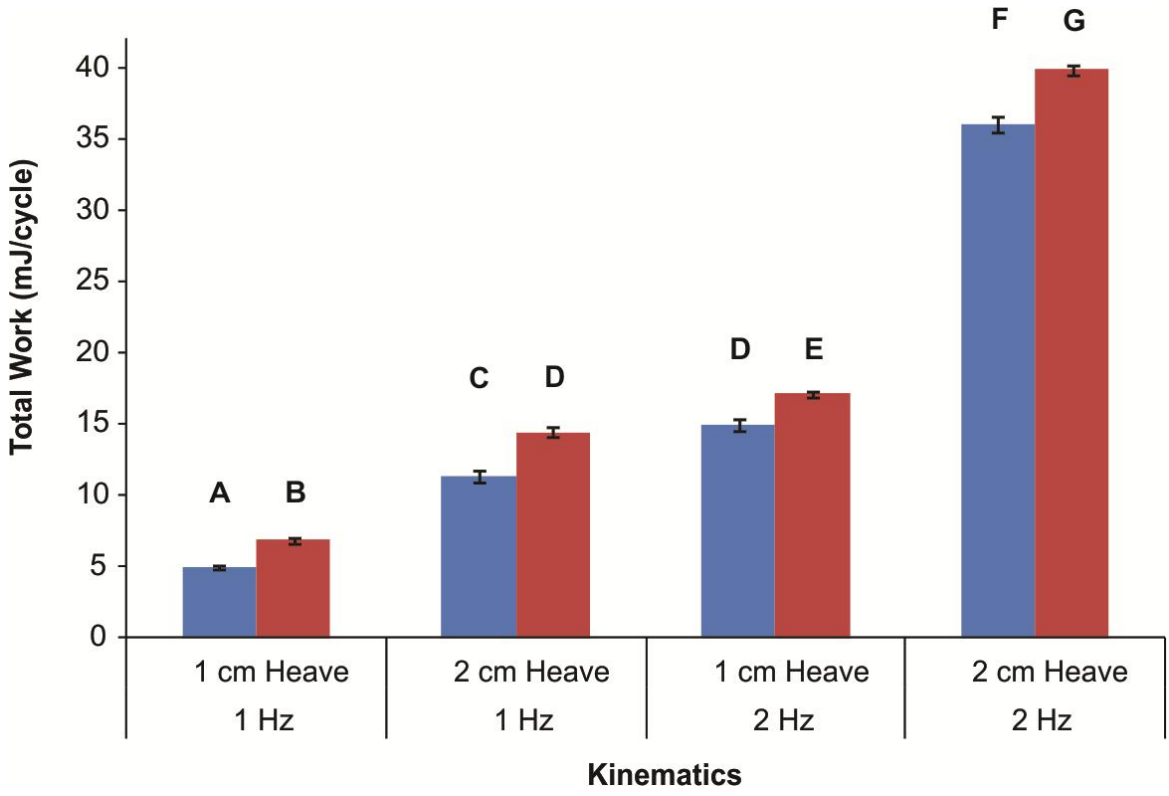

Figure 3.5. Total work per cycle (mJ/cycle) for each single-attachment fin condition, at center (blue) and ground (red) positions at the given frequencies and heave amplitudes. Error bars represent +/- 1 standard error. Levels indicate by different letters are significantly different (nested ANOVA with Tukey post-hoc, $p<0.0001$ for kinematic comparisons, $p<0.02$ for position comparisons).

the wall by 39 +/- 5% for a 1 cm heave amplitude and 28 +/- 2% with a 2 cm amplitude. Fins swimming at 2 Hz experienced a 15 +/- 4% and 11 +/- 1% increase in total work near the wall for 1 cm and 2 cm heave amplitudes, respectively. Total work also increased with frequency and heave amplitude, across kinematic groups (nested ANOVA, Tukey post-hoc, $p<0.0001$).

Cost of transport increased when fins swam near the wall (Figure 3.6). Fins with identical swimming kinematics had significantly higher costs of transport near the wall than in the center of the tank (nested ANOVA, Tukey post-hoc, $p<0.04$), for all kinematic conditions except the 1 Hz, 2 cm condition (Tukey post-hoc, $p>0.05$). For this condition, the increase in total work for near-wall swimming was counterbalanced by increased SPS near the wall, reducing the effect on cost of transport. The magnitude of the near-wall increase in cost of transport increased across kinematic groups from 12.0 +/- 1.7 mJ/m (mean +/- 1 standard error) under the 1 Hz 1 cm condition to 18.3 +/- 1.7 mJ/m in the 2 Hz 2 cm condition. Therefore, similar to the results for total work, relative effect size decreased as swimming frequency and heave amplitude increased: near the wall, cost of transport increased by 27 +/- 5% for the 1 Hz 1 cm condition, 14 +/- 2% for 1 Hz 2 cm (not significant), 13 +/- 4% for 2 Hz 1 cm, and 9 +/- 1% for 2 Hz 2 cm. Cost of transport also increased across kinematic groups with frequency and heave amplitude (nested ANOVA, Tukey post-hoc, $p<0.0001$).

Hydrodynamics

Particle image velocimetry reveals differences in flow patterns around fins swimming in the center of the tank and near the tank wall (Figure 3.7). Hydrodynamic data are presented for fins swimming at 1 Hz 2 cm, as these kinematics produce the largest position-dependent change in self-propelled speed, and show increases in total work and cost-of-transport similar to other

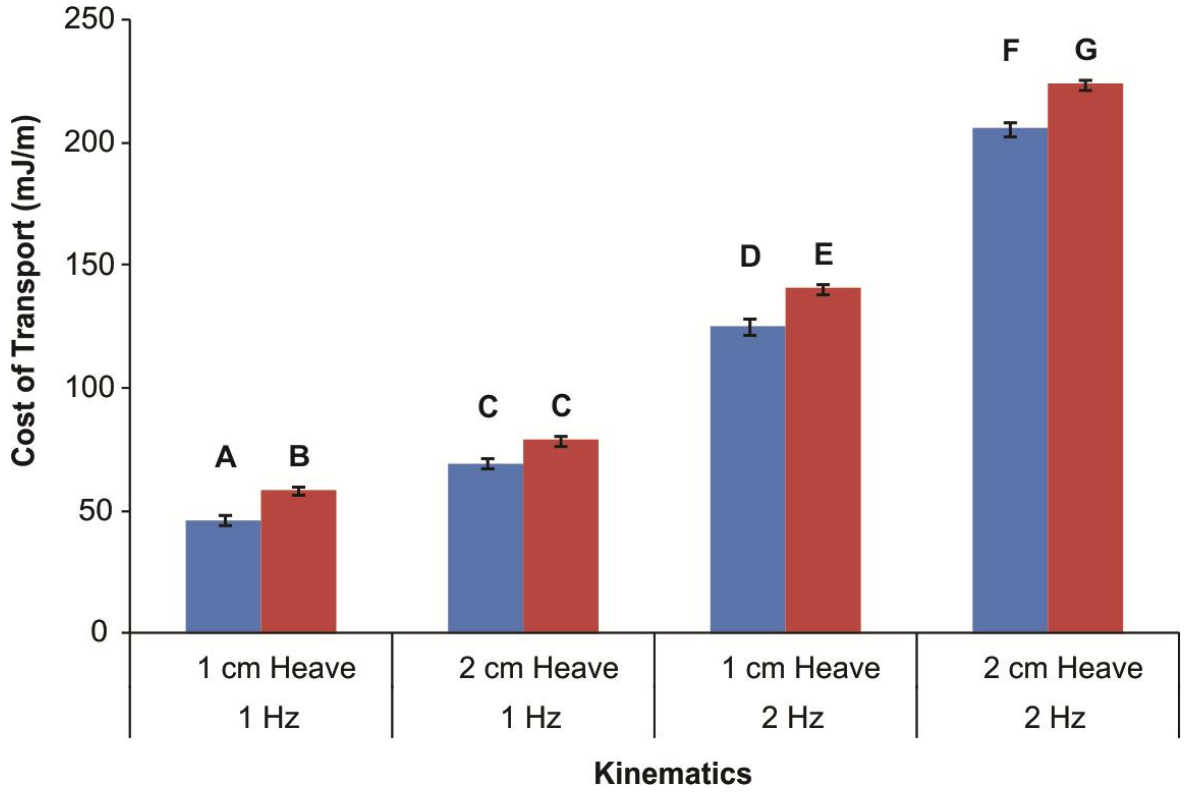

Figure 3.6. Cost of transport (mJ/m) for each single-attachment fin condition, at center (blue) and ground (red) positions at the given frequencies and heave amplitudes. Cost of transport is calculated from total work using swimming frequency and self-propelled speed. Error bars represent +/- 1 standard error. Levels indicated by different letters are significantly different (nested ANOVA with Tukey post-hoc, $p<0.0001$ for kinematic comparisons, $p<0.04$ for position comparisons).

Figure 3.7. Hydrodynamic analysis of flow around fins swimming in center (A) and ground (B) positions in a recirculating flow tank, with comparison of wake profiles between the two positions (C). From top to bottom, images illustrate flow at 25% intervals through one motion cycle (125 ms between images), beginning when the leading edge of the fin is closest to the ground (dashed red line). Fins (highlighted in white) are swimming at 1 Hz, +/- 2 cm heave amplitude, at their self-propelled speeds. Yellow vector arrows represent flow speed and direction relative to freestream flow, with vorticity indicated by red (positive) and blue (negative) shading. For clarity, only ¼ of vectors are shown. Vectors were not computed for masked areas (bright blue) behind the fin and overlapping the ground; masked areas and ground positions appear slightly different between (A) and (B) due to the different camera positions required to film fins in the center of the tank and near the ground. Flow profiles (C) show the downstream component of velocity vectors at a transect across the fin's wake, 2 cm downstream of the trailing edge of the fin (parallel to the y-axis in A and B). Profiles were determined for fins swimming in center (blue) and ground (red) positions, and are shown relative to a reference line at zero (grey dashed line); timesteps correspond to (A) and (B).

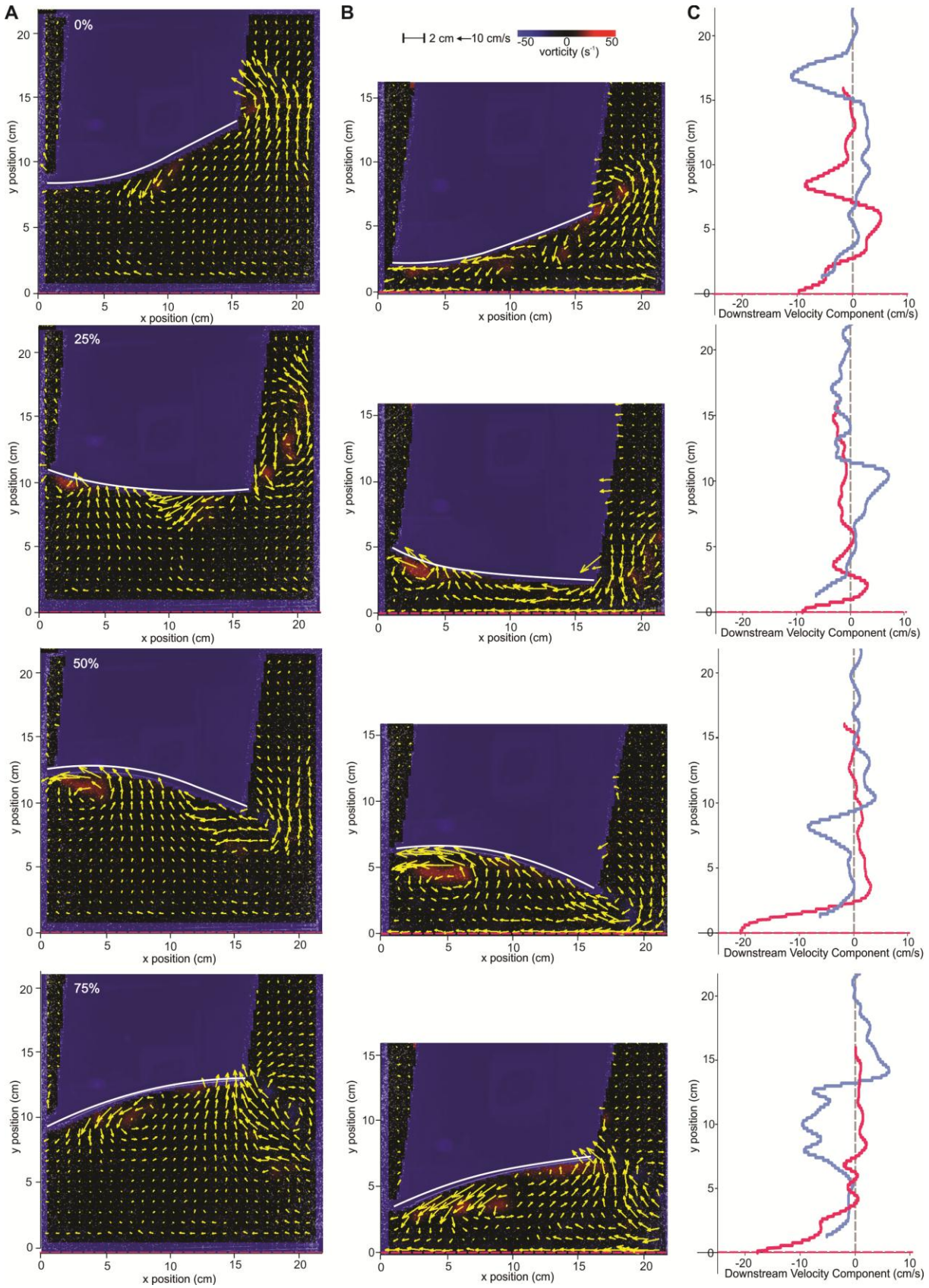

Figure 3.7 (Continued)

kinematic conditions; the 1 Hz 2 cm condition therefore offers the best insight into the hydrodynamics of ground effect. For fins near and far from the wall, flow is dominated by a strong leading-edge vortex, which detaches from the leading edge and propagates along the length of the fin until it is shed. As fins undulate toward and away from the wall, leading-edge vortices develop on alternate sides of the fin. Vortices occurring on the side of the fin closer to the wall were analyzed to investigate alterations in flow due to ground effects. For fins swimming near the wall and in the center of the tank, these vortices reached maximum rotational strength (vorticity) at 50% of the fin cycle, as the leading edge of the fin reached its maximum heave distance from the wall and began to return towards the wall (Figure 3.7A,B). Maximum vortex strength was significantly higher for fins swimming near the wall, with maximum rotation values of 41.4 +/- 2.6 s^{-1} near the wall versus 32.4 +/- 3.2 s^{-1} in the center of the tank (Student's t-test, $p<0.05$). The second key difference in the hydrodynamics of fins swimming near and far from the wall involves the direction of fluid jets shed from the fin. As the leading edge of the fin begins to move away from the wall, the posterior portion of the fin continues towards the wall, making its closest approach (25% cycle, Figure 3.7A,B). At this point in the cycle, fins shed a jet of fluid; for fins swimming near the wall, this jet enters the narrow gap between fin and wall. The magnitude of the jet was not significantly different between center and wall swimming positions (16.1 +/- 1 cm and 15.6 +/- 1 cm, respectively, $p>0.05$). However, when fins swim near the wall, the jet is oriented almost directly upstream (5.6 +/- 0.1 degrees from the horizontal), while fins swimming in the center of the tank produce a more laterally oriented jet (33.6 +/- 0.1 degrees) (Student's t-test, $p<0.05$).

Wake profiles of streamwise velocity also reveal differences in wake structure for fins swimming in center and near-wall positions, throughout the motion cycle (Figure 3.7C). During

the second half of the cycle, as fins' leading edge moved toward the wall, the wake profile of fins swimming far from the wall shows large regions of negative flow (-10 cm/s) relative to freestream velocity. At the same time, wake profiles of fins swimming near the wall show relative velocities near zero, except for a region of negative velocity adjacent to the wall, within the boundary layer measured for our recirculating tank. As the fin approaches the wall, the boundary layer thins as it is disrupted by orthogonal, fin-related flows.

Discussion

Undulating fins swimming near a solid boundary experience a fundamentally different fluid regime than when swimming in effectively unbounded fluid. Ground effect decreases non-monotonically with distance from the substrate, falling to zero at a gap/span ratio of 3 (for fixed, non-undulating propulsors; Reid, 1932; Blake, 1979 and 1983) but substantially reduced even at a ratio of 1 (<10% effect, Webb, 1993). In this study, fins swimming near the wall swam with a gap/span ratio of approximately 0.5, well within ground-effect range (Table 3.1). In contrast, fins far from the wall swam with a gap/span ratio greater than 1.5, indicating negligible ground effect. Therefore, comparisons of swimming performance between the two positions will demonstrate the consequences of undulating near a solid boundary.

Our model system allows consistent kinematic inputs (frequency and heave amplitude) for fins swimming in and out of ground effect, in contrast to experiments conducted with live animals, which change their behavior when swimming close to a solid boundary (Webb, 1993 and 2002). The motion of fins' leading edge is proscribed (and, for double attachment fins, so is the motion of the second attachment point at 2/3 fin-length), but proximity to the wall could still skew overall kinematics by altering the motion of the passive portion of the fin, changing the

amplitude of its posterior edge, the symmetry of fin excursions, etc. However, kinematic analyses reveal no substantial alterations in fins' midline motion due to ground effect, under any kinematic condition; fin motion is the same near and far from the wall (Figure 3.3). The stiffness of the model fin may overcome more subtle influences of ground effect on fin shape. The *in vivo* stiffness of swimming fish is unknown (McHenry et al., 1995; Lauder et al., 2011a), but if a sparsely actuated, flexible foil resists passive deformations due to ground effect, it seems likely that the kinematic changes observed in fish swimming in ground effect are due to active modulation, not passive effects.

Fins undulating near the wall have significantly different swimming performance compared to identical fins swimming at identical frequencies and heave amplitudes far from the wall. Contrary to the findings for models of fixed-wing foils (Baudinette and Schmidt-Nielsen, 1974; Withers and Timko, 1977; Hainsworth, 1988; Blake, 1979; Park and Choi, 2010) and heaving foils (Tanida, 2001; Molina and Zhang, 2011), the undulating fins tested here did not experience performance gains from ground effect. For most kinematic conditions, fins did not swim significantly faster near the wall (Figure 3.4), and in all cases more power was required per cycle (Figure 3.5). Therefore, swimming near the wall incurred a higher cost of transport (Figure 3.6). Ground effect "penalties" varied with kinematics, ranging from 9-25%, but increases in cost of transport on this scale are meaningful for both organisms and artificial devices.

However, small changes in kinematics can alter performance outcomes. A statistically-significant increase in self-propelled swimming speed near the wall occurred for only one kinematic condition (single-attachment, 1 Hz +/- 2 cm heave condition; Figure 3.4). Total work also increased in this position (Figure 3.5), but the combination yielded the same cost of transport for fins near and far from the wall, rather than the increased cost of transport seen near

the wall under all other conditions (Figure 3.6). So for certain kinematics, an undulating fin can swim at higher velocities in ground effect without losing efficiency relative to its cost-of-transport out of ground effect. Overall trends in self-propelled speed near and far from the wall also vary with kinematics (Figure 3.4). Single-attachment fins swimming at 1 Hz swam ~10% faster near the wall, for both 1 and 2 cm heave values. In contrast, the trend for single-attachment fins swimming at 2 Hz was negligible, with differences an order of magnitude below those found for 1 Hz, and swimming speed *decreased* (by ~4%) for double attachment fins swimming near the wall, at both frequencies. Though the effects here are slight, we see that the same fin can experience different—and even opposite—ground effects, depending on kinematics. This suggests that the kinematic changes observed in fish swimming in ground effect (reduced tailbeat frequency and amplitude; Webb, 1993 and 2002) may be a mechanism for transforming potential locomotor penalties into performance benefits. Stingrays have extremely fine control of pectoral fin conformation (Blevins and Lauder, 2012), with the potential for precise kinematic tuning to exploit ground effect.

Kinematics influence ground effect because they determine the effective shape of a moving foil. Small changes in ground effect outcomes are seen over the range of frequencies and amplitudes tested here, but the overall ground effects on any of the undulating fins in this study differ from what fixed foils experience, because the effective shape of moving foils constantly changes through time. Shape (e.g. camber, angle of attack) makes a profound difference in the influence of ground effect on fixed-wing foils, in combination with their distance from the substrate. Under some conditions, ground effects on fixed-wing foils increase lift and reduce drag (e.g. Ahmed and Sharma, 2005). In other cases drag is reduced but lift is unchanged (e.g. Withers and Timko, 1977; Zhang et al., 2004), or lift may even become negative

and accompanied by increased drag (Zerihan and Zhang, 2000). Drag effects are determined by the interaction of shed vortices with the substrate, which can alter wake structure, while lift outcomes depend on the pressure changes induced between the foil and the ground. If local pressure decreases, downforce (negative lift) increases due to suction forces (Vogel, 1994; Zerihan and Zhang, 2000). Race cars use this type of ground effect to keep fast-moving vehicles engaged with the road (Jones and Smith, 2003; Katz, 2006). In the lift-enhancing case, flow is compressed between the foil and the ground; local pressure is increased, and so is lift (Vogel, 1994; Ahmed and Sharma, 2005). Fish-like undulating foils will transition between positive and negative lift states, as effective camber, angle of attack, and direction of motion change during the heave cycle. In addition, ground effects depend not only on the current shape of the foil, but its previous conformation. Molina and Zhang (2011) note hysteresis in the forces experienced by a heaving foil in ground effect; undulating fins are subject to the same effect, as the flows shaped by the foil at one point in time determine the forces acting upon the foil at later points in time.

A description of flow around undulating fins in ground effect is presented here (Figure 3.7) in order to help explain the increased cost of transport observed for undulating fins near the wall. By comparing the hydrodynamics of identical fins with consistent kinematics swimming in freestream and near-wall positions, differences due to the influence of the ground can be detected. As the leading edge of the fin moves away from the wall during the first half of the motion cycle, flow around fins both near and far from the wall is dominated by a strong leading edge vortex, developed on the side of the fin closer to the wall (Figure 3.7A,B). Vortices create areas of low pressure, inducing suction; due to the fin's orientation as the leading edge vortex forms, a component of the suction force vector aligns with the fin's direction of travel, and the

fin is "pulled" forward (Wolfgang et al, 1999). Fins undulating near the wall develop stronger ground-side leading edge vortices than freestream fins (41.4 +/- 2.6 s^{-1} versus 32.4 +/- 3.2 s^{-1}, $p<0.05$). Therefore, fins swimming near the wall will also experience stronger suction forces.

As the fin's leading edge moves away from the wall during the first half of the motion cycle, the posterior portion of the fin continues toward the wall (Figure 3.7A,B), shedding a jet of fluid. For fins swimming in ground effect, the presence of the nearby wall alters the orientation of this jet to face almost directly upstream (5.6 +/- 0.1 degrees from the horizontal), significantly different from the more lateral jet shed by fins swimming far from the wall (33.6 +/- 0.1 degrees from the horizontal; $p<0.05$). The magnitude of fluid flow does not differ significantly between these two states ($p>0.05$). Therefore, fins swimming in ground effect may experience a locomotor benefit from the "cushion" of fluid moving between fin and wall, along the same vector as the fin's direction of travel—this effect may be responsible for the increase in self-propelled speed determined for this swimming condition.

Flow compression due to the nearby wall also occurs during the second half of fins' motion cycle, as the leading edge of the fin moves toward the wall (Figure 3.7B,C), similar to predictions by Argentina et al. (2007). In particular, the leading-edge vortex developed on the side of the fin closer to the wall during the first half of the cycle is compressed as the fin moves back toward the wall. In the freestream case there can be no compression. In air, fluid compression effects could potentially allow a thin, undulating foil to fly, hovering over a solid substrate on a high-pressure fluid cushion (Argentina et al., 2007). Neither the model fin tested here nor live stingrays depend on this effect to suspend themselves in the water column, as they are well capable of swimming far from the substrate. However, just as reduced pressure due to the leading edge vortex can act to pull the fin forward, increased pressure between the wall and

the posterior portion of the fin due to flow compression may increase lift. Lift effects depend on the fin's effective angle of attack, as it changes direction and begins to move away from the wall. The increased power requirements (and cost of transport) for swimming near the wall may occur as fins must overcome fluid forces to continue moving toward the wall despite high-pressure areas of flow compression beneath the fin, or away from the wall despite low-pressure regions between fin and ground.

Locomotion near a solid boundary inevitably involves the boundary layer, the velocity gradient that surrounds solid objects in moving fluid, with flow velocity decreasing to zero at the boundary (Vogel, 1994). A relatively undisturbed boundary layer is present when fins are at their maximum distance from the wall, but as fins approach the wall the boundary layer is disturbed and virtually disappears (Figure 3.7C). Therefore, performance effects are not simply due to swimming in a low-flow region, but result from changes in fluid pressure and direction induced by fin motion.

In this paper a simple model system is used to offer an experimental analysis of ground effects on undulating swimmers, and reveals that locomotion near the substrate can have significant impacts on swimming performance. The dynamic ground effects experienced by undulating fins differ from fixed-wing ground effects, as fins' effective shape and distance from the substrate changes through time. Rather than the performance gains observed for fixed-wing systems in ground effect (Baudinette and Schmidt-Nielsen, 1974; Withers and Timko, 1977; Hainsworth, 1988; Rozhdestvendky, 2006; Park and Choi, 2010), the undulating fins examined here generally incur costs from moving close to a solid boundary. However, ground effect outcomes depend on swimming kinematics. The waveforms produced by undulating model fins (Figure 3.3) correspond well to the pectoral fin waveforms used by freshwater stingray

Potamotrygon orbignyi (Figure 3.1B). Similar flow patterns are observed for model fins and stingray fins undulating near the substrate, with vortices trapped and compressed beneath the fin (Figure 3.1C, 3.7A,B). However, the broad, flexible fins of stingrays allow fine control of fin conformation during locomotion (Schaefer and Summers, 2005; Blevins and Lauder, 2012). Small alterations in three-dimensional fin shape may allow these benthic swimmers to modulate near-substrate flow and avoid the costs of undulating in ground effect experienced by model fins. The kinematic changes seen in plaice during near-ground locomotion may serve the same purpose (Webb, 2002). Otherwise, while the presence of a nearby substrate can enhance crypsis or foraging, benthic undulatory swimmers may incur substantial costs to swimming performance by swimming near the ground. Robotic models provide an excellent platform for further investigations of dynamic ground effects on moving fins, wings, and limbs, to better understand the locomotor environment of benthic animals and inform the design of biomimetic systems.

Acknowledgements

We thank Erik Anderson, Vernon Baker, Ryan Shelton and Chuck Witt for their work on the design and control of the robotic apparatus and associated programs. We are particularly grateful for the support and advice of Jeanette Lim, Brooke Flammang-Lockyer, and other members of the Lauder Lab. This research was supported by NSF grant EFRI-0938043 to George V. Lauder, and support from the Harvard University Department of Organismic and Evolutionary Biology.

References

Ahmed, M.R. and Sharma, S.D. (2005). An investigation on the aerodynamics of a symmetrical airfoil in ground effect. *Exp. Therm. Fluid. Sci*. **29**, 633-647

Argentina, M., Skotheim, J. and Mahadevan, L. (2007). Settling and swimming of flexible fluid-lubricated foils. *Phys. Rev. Lett.* **99**, 224503

Baudinette R.V. and Schmidt-Nielsen, K. (1974). Energy cost of gliding flight in herring gulls. *Nature* **248** 83-84.

Blake, R.W. (1979). The energetics of hovering in the mandarin fish (*Synchropus picturatus*). *J. Exp. Biol.* **82,** 25–33.

Blake, R.W. (1983). Mechanics of gliding birds with special reference to the influence of ground effect. *J. Biomech.* **16**, 649–654.

Blevins, E. and Lauder, G.V. (2012). Rajiform locomotion: three-dimensional kinematics of the pectoral fin surface during swimming by freshwater stingray *Potamotrygon orbignyi*. *J Exp Biol.* **215**, 3231-3241.

Carlson, R.L. and Lauder, G.V. (2011). Escaping the flow: boundary layer use by the darter *Etheostoma tetrazonum* (Percidae) during benthic station holding. *J. Exp. Biol.* **214,** 1181-1193.

Goto, T., Nishida, K. and Nakaya, K. (1999). Internal morphology and function of paired fins in the epaulette shark, *Hemiscyllium ocellatum*. *Ichthyol. Res*. **46,** 281–287.

Hainsworth, F.R. (1988). Induced drag savings from ground effect and formation flight in brown pelicans. *J. Exp. Biol.* **135,** 431-444.

Jones, M.A. and Smith, F.T. (2003). Fluid motion for car undertrays in ground effect. *J. Eng. Math.* **45,** 309-334.

Katz, J. (2006). Aerodynamics of race cars. *Annu. Rev. Fluid Mech.* **38,** 27-63.

King, H.M., Shubin, N.H., Coates, M.I. and Hale, M.E. (2011). Behavioral evidence for the evolution of walking and bounding before terrestriality in sarcopterygian fishes. *Proc. Nat. Acad. Sci. USA* **52**, 21146-21151.

Koester, D.M. and Spirito, C.P (2003). Punting: An unusual mode of locomotion in the Little Skate, *Leucoraja erinacea* (Chondrichthyes: Rajidae). *Copeia* **3**, 553-561.

Lauder, G.V., Anderson , E.J., Tangorra, J., and Madden, P.G.A. (2007). Fish biorobotics: kinematics and hydrodynamics of self-propulsion. *J. Exp. Biol.* **210**, 2767-2780.

Lauder, G., Tangorra, J., Lim, J., Shelton, R., Witt, C., and Anderson, E.J. (2011a). Robotic models for studying undulatory locomotion in fishes. *Marine Tech. Soc J.* **45**, 41-55

Lauder, G.V., Madden, P.G.A, Tangorra, J., Anderson, E. and Baker, T.V. (2011b) Bioinspiration from fish for smart material design and function. *Smart Mater. Struct.* **20** doi:10.1088/0964-1726/20/9/094014

Lucifora, L.O., Vassallo, A.I. (2002). Walking in skates (Chondrichthyes. Rajidae): anatomy, behaviour and analogies to tetrapod locomotion. *Biol. J. Linn. Soc.* **77**, 35–41.

McHenry, M.J., Pell, C.A. and Long, J.A. (1995). Mechanical control of swimming speed: stiffness and axial wave form in undulating fish models. *J. Exp. Biol.* **198**, 2293-2305.

Molina, J. and Zhang, X. (2011). Aerodynamics of a heaving airfoil in ground effect. *AIAA J.* **49**, 1168-1179.

Nowroozi, B.N., Strother, J.A. and Horton, J.M. (2009). Whole-body lift and ground effect during pectoral fin locomotion in the northern spearnose poacher (*Agonopsis vulsa*). *Zoology* **112**, 393-402.

Park, H. and Choi, H. (2010). Aerodynamic characteristics of flying fish in gliding flight. *J. Exp. Biol.* **213**, 3269-3279.

Pietch, T.W. and Grobecker, D.B. (1987). *Frogfishes of the World.* Stanford, CA: Stanford University Press.

Pridmore, P.A. (1994). Submerged walking in the epaulette shark *Hemiscyllium ocellatum* (Hemiscyllidae) and its implications for locomotion in rhipidistian fishes and early tetrapods. *Zool—Anal. Complex Sy.* **98**, 278–297.

Rayner, J.M.V. (1991). On the aerodynamics of animal flight. *Phil. Trans. R. Soc. B.* **334**, 119–128.

Reid, E.G. (1932) *Applied Wing Theory.* New York, NY: McGraw-Hill.

Renous, S., Gasc, J.P., Bels, V.L. and Davenport, J. (2000). Six-legged walking by a bottom-dwelling fish. *J. Mar. Biol. Assoc. UK* **80**, 757–758.

Rozhdestvendky, K. (2006). Wing-in-ground effect vehicles. *Prog. Aerosp. Sci.* **42** (3), 211-283.

Schaefer, J.T. and Summers, A.P. (2005). Batoid wing skeletal structure: novel morphologies, mechanical implications, and phylogenetic patterns. *J. Morph.* **264**, 298-313.

Shen, L., Zhang, X., Yue, D.K.P. and Triantafyllou, M.S. (2003). Turbulent flow over a flexible wall undergoing a streamwise travelling wave motion. *J. Fluid. Mech.* **484**, 197-221.

Tanida, Y. (2001). Ground effect in flight (birds, fishes, and high-speed vehicle). *JSME Int. J. Ser. B* **44**, 481-486.

Tytell, E.D. and Lauder, G.V. (2004). The hydrodynamics of eel swimming I. Wake structure. *J. Exp. Biol.* **207**, 1825-1841.

Vogel, S. (1994). *Life in Moving Fluids: The Physical Biology of Flow*. Princeton, NJ: Princeton University Press.

Ward, A.B. (2002). Kinematics of the pectoral fins in batfishes (Ogcocephalidae) during aquatic walking. *Integr. and Comp. Biol.* **6,** 1331.

Webb, P.W. (1981). The effect of the bottom on the fast start of a flatfish, *Citharichthys stigmaeus*. *Fish. Bull. US* **79**, 271–276.

Webb, P.W. (1993). The effect of solid and porous channel walls on steady swimming of steelhead trout *Oncorhynchus mykiss. J. Exp. Biol.* **178**, 97–108.

Webb, P.W. (2002). Kinematics of plaice, *Pleuronectes platessa*, and cod, *Gadus morhua*, swimming near the bottom. *J. Exp. Biol.* **205**, 2125-2134.

Wilga, C.D. and Lauder, G.V. (2001). Functional morphology of the pectoral fins in bamboo sharks, *Chiloscyllium plagiosum*: benthic vs. pelagic station-holding. *J. Morphol.* **249**, 195–209.

Withers, P.C. and Timko, P.L. (1977). The significance of ground effect to the aerodynamic cost of flight and energetics of the black skimmer (*Rhyncops nigra). J. Exp. Biol.* **70**, 13-26.

Wolfgang, M.J., Anderson, J.M., Grosenbaugh, M.A., Yue, D.K.P. and Triantafyllou, M.S. (1999). Near-body flow dynamics in swimming fish. *J. Exp. Biol.* **202**, 2303-2327.

Zerihan, J. and Zhang, J. (2000). Aerodynamics of a single element wing in ground effect. *J. Aircraft.* **37**, 1058-1064.

Zerihan, J. and Zhang, J. (2003). Off-surface measurements of a wing in ground effect. *J. Aircraft.* **40**, 716-725.

Zhang, X., Senior, A. and Ruhrmann, A. (2004). Vortices behind a bluff body with an upswept aft section in ground effect. *Int. J. Heat Fluid Flow* **25**, 1-9.

Chapter 4

Pectoral fin morphology of freshwater stingray *Potamotrygon orbignyi*

Abstract

To achieve the characteristic undulations of rajiform locomotion, the pectoral fins of batoid fishes must be flexible and well-controlled, to generate, accommodate, and adjust the propulsive wave. Yet, batoids lack the mechanical linkages that provide control in the pectoral fins of actinopterygian fishes; they evolved from shark-like ancestors, but have dramatically diverged in fin use and structure. This study examines the pectoral fin morphology of freshwater stingray *Potamotrygon orbignyi*, connecting structure and function in the fin of an undulatory rajiform swimmer. The morphology of skeletal and muscular fin elements differs across fin chord and span, creating regional variations in fin structure that correlate with the swimming kinematics of *P. orbignyi*. Anterior regions of the pectoral fin, which form a stable leading edge during swimming, are structurally stiffened by a more robust fin skeleton, with the potential for active stiffening from a pennate arrangement of muscle fibers. Structure predisposes mid-disc and posterior regions of the fin to greater flexibility; these same regions show the greatest amplitudes during undulation. The locations of particular morphological landmarks—the branching of fin rays, and the insertion of superficial muscles—correspond to increases in undulatory amplitude. Comparisons with the fins of a representative actinopterygian fish (bluegill sunfish *Lepomis macrochirus*) and shark (dogfish *Squalus acanthias*), reveal structural convergence between stingrays and actinopterygians in fin ray branching and segmentation. The repetition of fin elements during the evolution of batoid pectoral fins created the potential for this convergence, as well as for regional specialization within the batoid pectoral fin, and unique structural features connecting pectoral fin morphology and undulatory performance.

Introduction

The pectoral fins of batoids are far different in structure and function than the fins of their closest relatives, the sharks. In sharks, swimming is driven by axial undulations (Breder, 1926; Lauder, 2006); the pectoral fins contribute to stability against lateral roll and can generate positive and negative lift forces during ascents and descents (Wilga and Lauder, 2002), but are not relied upon to generate thrust. Yet in batoids, pelagic locomotion is driven by the undulation and oscillation of expanded pectoral fins (Breder, 1926; Rosenberger, 2001; Blevins and Lauder, 2012). There are a few exceptions: among batoids, Rhinobatidae, Pristidae, and Torpediniformes swim via axial undulation (Breder, 1926; Rosenberger, 2001), and many benthic species use their pelvic fins to punt along the nearby substrate (Lucifora and Vassallo, 2002; Koester and Spirito, 2003; Macesic and Kajiura, 2010; Macesic et al., in revision), augmenting pectoral fin locomotion. However, the eponymous rajiform locomotion (Breder, 1926) is the rule, with species ranging along a continuum from pectoral fin oscillation (<1 wavelength present on the fin at one time) to undulation (>1 wave present on the fin; Rosenberger, 2001). Batoids swimming via undulation require flexibility and fine control of the pectoral fins to generate the propulsive wave, and subtly alter waveforms and fin conformation for maneuvering (Figure 4.1; Blevins and Lauder, 2012). For this swimming mode to evolve, morphological changes in pectoral fin structure had to occur in tandem with changes in locomotor behavior.

Textbooks describe chondrichthyan fins as composed of unsegmented, unbranching collagenous elements called ceratotrichia, which connect to larger, underlying fin radials (Compagno, 1999). In batoids, extensions of basal cartilages (propterygium and metapterygium) expand the pectoral fins anteriorly and posteriorly to form a pectoral disc, ceratotrichia are

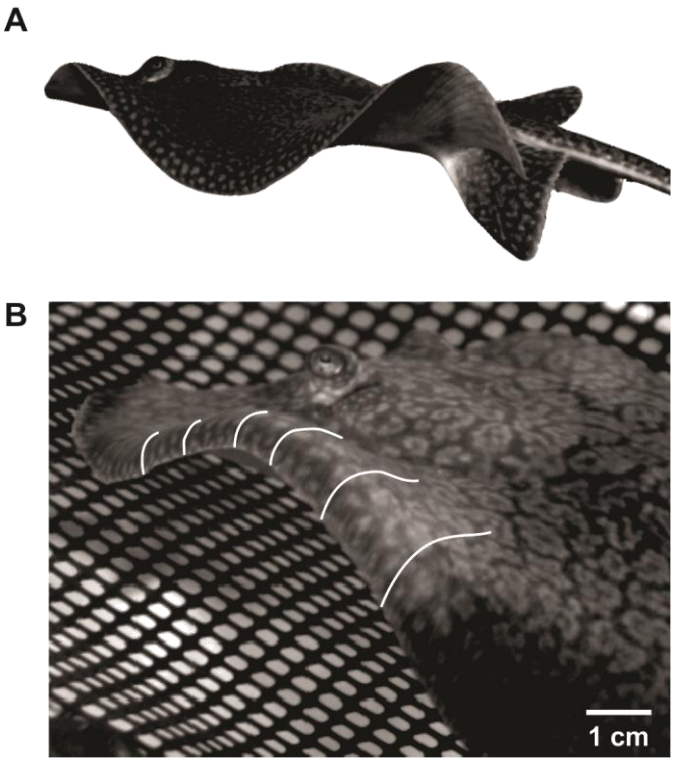

Figure 4.1. Fin conformations of freshwater stingray *Potamotrygon orbignyi* during locomotion by undulatory swimming. (A) Posterolateral view of stingray swimming at 1.5 disc-lengths per second; >1 wave is present on the fin, indicating undulatory locomotion. (B) Concave-down "cupping" of the distal fin margin during locomotion, against the pressure of fluid flow. Fin curvature is highlighted by white lines. Anterior is at left in (A) and (B).

extremely reduced or lost, and fins are instead supported by a proliferation of radial cartilages (Figure 4.2, Compagno, 1999). Radials are positioned end-to-end, forming fin rays that extend distally to the fin margin; the overall number of fin rays is dramatically increased relative to sharks, or when compared to actinopterygian fishes (Figure 4.2C, 4.3). Pectoral fin musculature is also expanded in batoids. Rather than the dorsal and ventral pterygoideus muscles present in sharks, which run from the pectoral girdle to insert partway along the proximal radials (Liem and Summers, 1999), deep (profundus) and shallow (superficialis) muscle layers run parallel to fin rays on dorsal and ventral sides of the fin, and extend across most or all of the fin span (Calvert, 1983).

At evolutionary timescales, repeated elements often serve as a substrate for specialization. Semi-redundancy allows elements to evolve in different directions: some may be coopted for a dramatically different function (i.e. dorsal-fin derived fishing lures in anglerfishes), while in other cases a more subtle adaptation occurs. In the pectoral fins of benthic sculpin, particular fin rays show variations in stiffness associated with the different functions of fin regions involved in swimming or station-holding on the substrate (Taft et al., 2008; Taft, 2011). Batoid pectoral fins are comprised of repeated elements along both span (radials) and chord (fin rays, muscles). Therefore, batoid fins may exhibit local morphological specializations related to fin function.

In this study, I examine morphological variation within the pectoral fin of freshwater stingray *Potamotrygon orbignyi* (Castelnau, 1855). Prior research across species has described batoid fin characteristics associated with particular swimming modes (undulatory or oscillatory; Schaefer and Summers, 2005), but the structure of batoid fins suggests the potential for within-fin specialization. The pectoral fins of *P. orbignyi* are expected to show morphological changes

Figure 4.2. Dorsal view images of *P. orbignyi* right pectoral fin: (A) the intact pectoral fin. Colored boxes indicate the location of fin rays representing anterior (red), mid-disc (light blue) and posterior (purple) portions of the fin. (B) The pectoral fin, dissected to show subdermal arrangement of fin structures, with dorsal muscles (DM), blood vessels (BV), and lateral line canals (LL) all radiating out from the axial skeleton, following the fin skeleton. (C) Radiograph of *P. orbignyi* in dorsal view, revealing arrangement of radial cartilages (R). Fin rays insert on one of three basal cartilages, the propterygium (PR), mesopterygium (MS), or metapterygium (MT). Anterior is at top in (A) and (B), at left in (C).

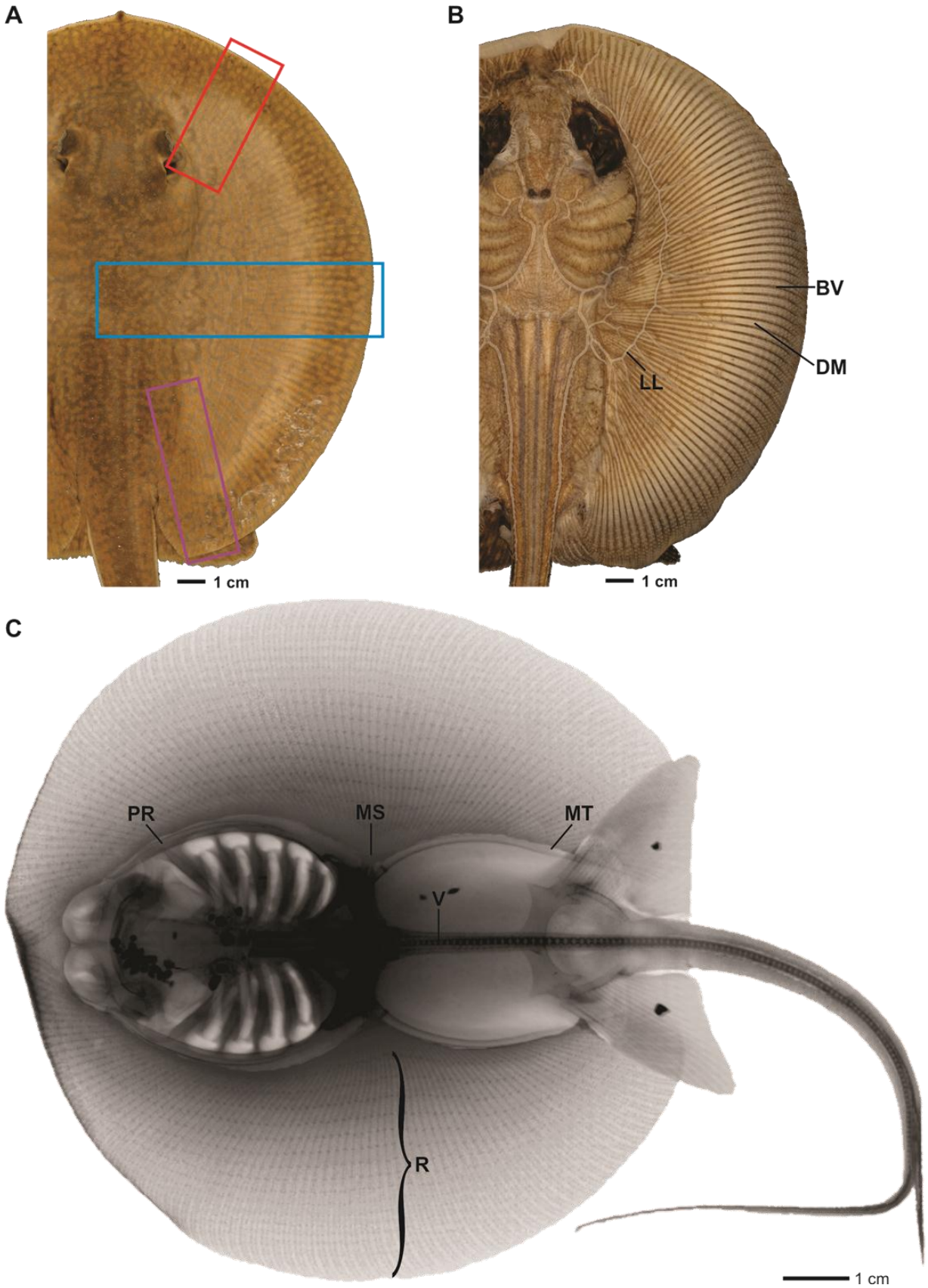

Figure 4.2 (Continued)

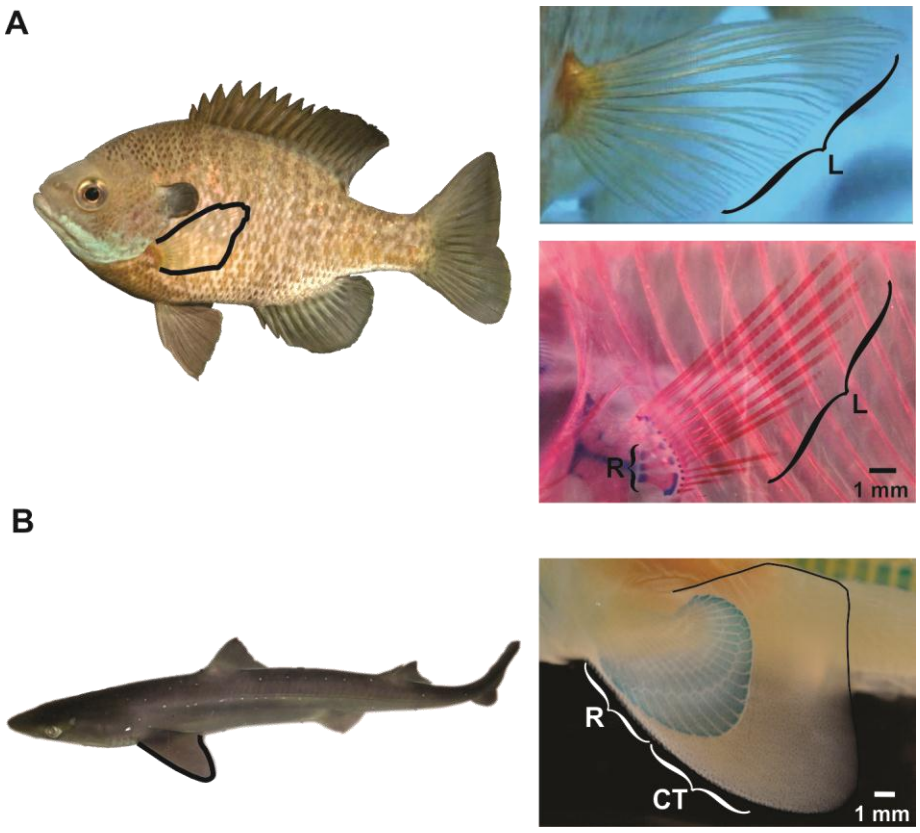

Figure 4.3. (A) Lateral view image of bluegill sunfish *Lepomis macrochirus*, with pectoral fin outlined in black. Pectoral fin close-ups at right show the fin in a live, swimming fish (top), depicting an intact fin with bifurcating lepidotrichia (L); and a cleared and stained specimen (bottom) with fin ray segmentation visible within lepidotrichia. (B) Lateral view image of dogfish shark *Squalus acanthias*, with pectoral fin highlighted in black. At right, a ventral view close-up of the pectoral fin of a cleared and stained specimen. The fin is supported proximally by radials ® and distally by ceratotrichia (CT). Live animal photographs of *L. macrochirus* and *S. acanthias* courtesy of B. Flammang-Lockyer, A. Maia, and G.V. Lauder.

across fin chord and span, correlating to the demands for fin flexibility and control imposed by undulatory locomotion in this species (Blevins and Lauder, 2012). Whole-disc images and histological cross-sections were examined to determine the morphology of skeletal and muscular elements in anterior, mid-disc, and posterior regions of the pectoral fin; findings for *P. orbignyi* were contrasted with data from a representative actinopterygian fish (bluegill sunfish *Lepomis macrochirus,* Rafinesque, 1819) and shark (*Squalus acanthias,* Linnaeus, 1758).

Materials & Methods

Specimens

Juvenile freshwater stingrays, *Potamotrygon orbignyi* (Castelnau, 1855), were obtained from the author's personal collection (n=10). The animals had been previously purchased from a local importer and maintained in captivity at Harvard University, MA, USA for periods of time from two weeks to two years. Post-mortem, stingrays were either frozen or fixed in 10% formalin. Stingrays had a mean disc length (DL) of 132.5±7.1 mm, and a mean disc width (DW) of 122.8±6.3 mm. For comparative purposes, representative actinopterygian and shark species were also examined: bluegill sunfish *Lepomis macrochirus* (Rafinesque, 1819; n=2), from the personal collections of K. Feilich and G.V. Lauder, and dogfish shark *Squalus acanthias* (Linnaeus, 1758; n=2), from the personal collections of B. Flammang-Lockyer and G.V. Lauder. Specimen details and procedures are given in Table 4.1.

Radiography

Digital radiographs of *P. orbignyi* in dorsal view (n=10) and *L. macrochirus* in lateral view (n=1) were taken with a digital x-ray machine at the Digital Imaging Facility of the Harvard Museum

Species	Provenance	Procedures
P. orbignyi	E. Blevins, personal coll.	radiography, gross dissection, histology
P. orbignyi	E. Blevins, personal coll.	radiography, gross dissection, histology
P. orbignyi	E. Blevins, personal coll.	radiography, photography
P. orbignyi	E. Blevins, personal coll.	radiography
P. orbignyi	E. Blevins, personal coll.	radiography
P. orbignyi	E. Blevins, personal coll.	radiography
P. orbignyi	E. Blevins, personal coll.	radiography
P. orbignyi	E. Blevins, personal coll.	radiography
P. orbignyi	E. Blevins, personal coll.	radiography
P. orbignyi	E. Blevins, personal coll.	radiography
L. macrochirus	K. Feilich, personal coll.	radiography
L. macrochirus	G.V. Lauder, personal coll.	cleared and stained
S. acanthias	B. Flammang-Lockyer, personal coll.	radiography
S. acanthias	G.V. Lauder, personal coll.	cleared and stained

Table 4.1. Description of specimens, where they were obtained, and procedures in which they were used.

of Comparative Zoology. Voltage and exposure settings were adjusted to yield the best contrast between hard and soft tissues in each image. Image contrast was further adjusted in Corel Photo-Paint 15.2.0.686 (Corel, Ottawa, Canada) so that pectoral fin rays could be resolved in both thicker proximal and thinner distal portions of the fin.

Histology and Photomicrography

To quantify variations in the cross-sectional area of pectoral fin elements across fin span and chord, and include soft tissues not visible in radiographs, I examined sagittal histology sections of the pectoral fin of *P. orbignyi* (Table 1; n=2). Tissue samples containing three fin rays and surrounding tissues were removed from stingray pectoral fins at anterior, mid-disc (50% fin chord length), and posterior locations along the fin (Figure 4.2A). For comparative purposes, tissue samples were also taken from the pectoral fins of a representative actinopterygian (*Lepomis macrochirus,* n=1) and shark (*Squalus acanthias*, n=1) at 50% chord length (Figure. 4.3A,B). All tissue samples included the full length of the fin rays, from their origination on the pectoral girdle to the distal margin of the fin.

Tissue samples from frozen specimens (*P. orbignyi* and *S. acanthias*, n=1 each) were thawed and fixed in Bouin's fluid (Presnell and Schreibman, 1997) for 24 hours; specimens previously fixed in 10% formalin (*P. orbignyi* and *L. macrochirus*, n=1 each) were re-fixed in Bouin's for the same time period. All tissue samples were then decalcified overnight (Cal-Ex, Thermo Fisher Scientific, Waltham, MA, USA) and embedded in paraffin for microtome sectioning. Sections (8 µm) were taken at 10% intervals along the length of the fin ray (n=10 sections per tissue sample), perpendicular to the long axis of the fin ray. Sections were stained with Mallory's trichrome (Mallory, 1901; Presnell and Schreibman, 1997) and photographed

under dissecting and compound microscopes (Leica MZFLIII and DMRE, respectively; Leica Microsystems, Wetzlar, Germany) with a digital camera (Regitia 200R Fast 1394, QImaging, Surrey, BC, Canada) using Volocity 6.1.1 image-capture software (PerkinElmer, Waltham, MA, USA).

After tissue samples were removed from one pectoral fin (*P. orbignyi*, n=2; *L. macrochirus* and *S. acanthias*, n=1), the remaining intact fin was examined via gross dissection. Photographs were taken with a Nikon D5000 digital, calibrated with an in-frame scale reference. Specimens were photographed while in 70% ethanol to reduce glare.

Morphometrics

General morphology of the pectoral fin skeleton was determined from the radiographs of *P. orbignyi* and *L. macrochirus*, and additional images of cleared and stained specimens of *L. macrochirus* and *S. acanthias.* Cleared and stained specimens had been previously processed using a standard technique that allows visualization of all mineralized tissues (Dingerkus and Uhler, 1977). These specimens were photographed in glycerol (to reduce glare) using the same microscope and camera systems described above. All images were imported into ImageJ (NIH, Bethesda, MD, USA; Abramoff et al., 2004) and calibrated using an in-frame scale reference; multiple measurements were then taken to describe fin and fin-ray structure. For stingrays, measurements were made for fin rays from three fin regions, corresponding to histological tissue sample sites: anterior (~10^{th} fin ray from snout tip), mid-disc (50% chord length), and posterior (~20^{th} fin ray from tail). For each fin ray, I determined the angle between the fin ray and the body midline, the total length of the fin ray, the number of fin-ray branchings (bifurcations), the length of the pre- and post-branching portions of the fin ray, the total number of segments (fin

radials) in the fin ray, and the number of segments pre- and post- branching. Within each fin ray, I measured the length of individual segments at three positions along the span: proximal (2nd radial from the pterygium), intermediate (second radial after branching), and distal (the distal-most radial visible in radiographs).

Similar morphological measurements were made for mid-fin (50% chord length) fin rays in *L. macrochirus* and *S. acanthias*, modified to accommodate the fin structure of each species. In *L. macrochirus*, I measured the total length of the fin ray, the number of fin-ray branchings, the pre- and post-branching lengths, and the length of proximal, intermediate, and distal segments. Segment numbers were calculated by dividing total and pre/post-branching lengths by segment lengths. Total fin ray length was also determined for *S. acanthias*, but rather than pre- and post-branching lengths I measured the portion of the fin ray comprised of radial cartilages versus ceratotrichia (Figure 4.3B). The total number of pectoral fin rays was determined for each individual from all three species. For *S. acanthias*, fin ray number was defined as the number of radial cartilages in the most distal row.

Histological sections were used to study pectoral fin soft tissue morphology and the cross-sectional arrangement of pectoral fin elements. Section images were imported into ImageJ and calibrated using a reference image. To minimize distortions from the sectioning process, only sections from the center of paraffin tissue blocks were measured; fin rays near the lateral edges of a section were excluded from analysis. In each stingray fin section, I measured the following variables for three radials per section: the height and width of the radial cartilage, the height and width of the associated dorsal profundus muscle bundle and ventral profundus muscle bundle; the thickness of the dorsal and ventral superficialis muscle layers; and the distance between neighboring fin rays (i.e., the spacing between elements). I also noted the changes in

radial shape and structure (e.g. calcification patterns) near branching points. For *L. macrochirus* sections, the height and width of each lepidotrich was measured (treated as a cylinder described by the paired hemitrichia), as well as the distance between neighboring fin rays. The fine, flexible fin membrane of *L. macrochirus* often curled during tissue embedding, so the distance between fin rays was measured along the membrane path rather than in a straight line. As no muscles are present in actinopterygian fins, none were measured. In *S. acanthias* sections, I determined the height and width of radial cartilages and ceratotrichia, and the distance between these elements. For all structures (fin rays and muscles) where both height and width were measured, cross-sectional areas and aspect ratios were calculated. Aspect ratio (height/width) gives a general descriptor of shape. An object with an aspect ratio of 1 is a perfect circle or square; as the ratio of height to width increases, objects are taller and narrower. A lower aspect ratio indicates a shorter, wider object. Cross-sectional area describes the size of a fin element, and is relevant for considerations of muscle power and fin flexibility. Both fin rays and muscles were roughly ellipsoid in cross-section, so their areas were calculated as $A=\pi(\frac{1}{2}h)(\frac{1}{2}w)$, where h is the height and w the width of the element.

Statistical Analysis

A mixed-model two-factor analysis of variance (ANOVA) was performed to test effects of anterior-posterior position and individual on the morphological variables determined from stingray radiographs. Post-hoc Tukey tests were used to isolate whether significant differences occurred between anterior, mid-disc, or posterior pectoral fin rays. A second mixed-model two-factor ANOVA analyzed spanwise differences in the length of fin radial cartilages (stingray fin segments); anterior, mid-disc, and posterior fin rays were pooled in this analysis, as the first

ANOVA revealed that radial length did not generally differ with anterior-posterior position. A third ANOVA (Model I) was used to analyze data from histological cross-sections of stingray fins, testing for differences due to anterior-posterior position and spanwise position.

Data from the pectoral fins of *L. macrochirus* and *S. acanthias* are provided for comparison with *P. orbignyi*, but are not included in the previous statistical analyses, which focused on the morphological variation within the stingray fin. Instead, a separate Model I ANOVA was performed, testing the effects of fin ray type (Stingray Anterior, Stingray Mid-Disc, Stingray Posterior, *L. macrochirus*, or *S. acanthias*) and spanwise position on the variables relevant to all species: fin ray height, width, aspect ratio, and cross-sectional area, and the distance between fin rays. For *S. acanthias*, fin ray measurements were made on fin radials in the proximal portion of the fin, and ceratotrichia (largest visible) in the distal portion of the fin. Bonferroni corrections were applied to all p-values to prevent Type I errors from multiple comparisons.

To examine multivariate differences between stingray anterior, mid-disc, and posterior fin rays, a principal components analysis (PCA) was performed on three variables: the total number of radials in a fin ray, the percentage of radials in a fin ray before the branching point, and the percentage of fin ray length before the branching point. All variables related to non-standardized fin ray length were excluded from the PCA, to determine whether anterior, mid-disc, and posterior fin rays could be distinguished by segmentation and branching patterns along. All three variables were major elements of the first two principal component axes, and were retained in a discriminant function analysis (DFA). A second PCA was performed on eight variables from anterior, mid-disc, and posterior histological sections: the cross-sectional area of fin rays, and dorsal and ventral profundus muscles; the thickness of dorsal and ventral

superficialis muscles; the aspect ratio of fin rays, and dorsal and ventral profundus muscles. This analysis was performed by spanwise section position, rather than for pooled section data.

All analyses were performed in JMP 9.0.2 (SAS Institute, Cary, NC, USA). Values are reported as mean ± standard error of measurement. Where n=1 for comparison species *L. macrochirus* and *S. acanthias*, the mean value is given alone.

Results

General pectoral fin skeletal structure

The pectoral fins of *P. orbignyi* are supported by a skeleton comprised of roughly 100 fin rays, emanating radially from the basal cartilages, compared to the 13 pectoral fin rays of *L. macrochirus* (Figure 4.2, 4.3). In the stingray, anterior rays originate on the propterygium, posterior rays from the metapterygium, and for a small region around mid-disc, from the small mesopterygium (Calvert, 1983; Compagno, 1999). Fin ray morphology changes gradually with anterior-posterior position; the anterior, mid-disc, and posterior fin rays discussed here represent the range of morphologies present in a single fin, rather than three discrete and uniform fin ray types.

The angle between fin rays and midline differed significantly between anterior, mid-disc, and posterior regions of the fin (Figure 4.4; ANOVA, Tukey post-hoc, $p<0.0001$). At mid-disc, fin rays were perpendicular to the midline (90 ± 2^{o}); anteriorly, 5 ± 1^{o} from the midline, and posteriorly 31 ± 2^{o} from the midline. Blood vessels, lateral line canals and pectoral fin muscles followed the radial arrangement of fin rays (Figure 4.2). Fin ray lengths also differed significantly between regions; mid-disc fin rays were longest at 45.2±2.4 mm, while anterior fin rays were 26.5±1.4 mm long, and posterior fin rays 34.8±2.3 mm long (ANOVA, Tukey post-

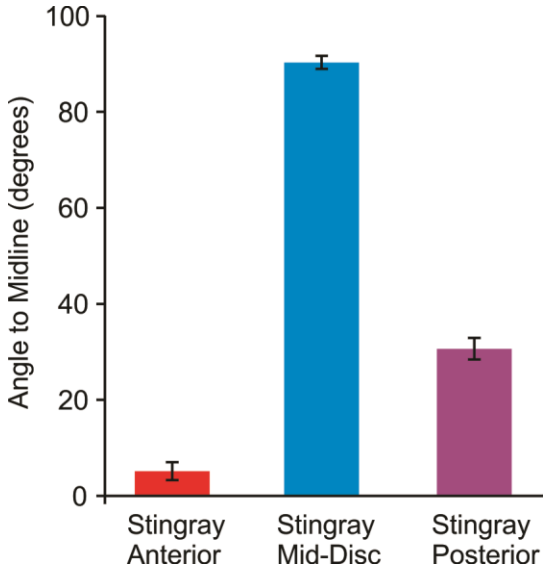

Figure 4.4. Mean angle between fin ray and midline in *P. orbignyi*, for anterior (red), mid-disc (light blue) and posterior (purple) fin rays. Error bars represent ±1 s.e.m., and n=10 for each fin region. All levels are significantly different ($p<0.0001$).

hoc, $p<0.0001$). The fin rays of *L. macrochirus* (radiograph specimen) and *S. acanthias* (cleared and stained specimen) were 27.8 mm and 22.5 mm long, respectively.

Fin ray branching

In all regions of the pectoral fin, stingray fin rays branched once. All branching occurred near the middle of the fin ray (50% fin ray length), but with significant variation between all three fin regions: anterior branch points occurred at 67±1% fin ray length, mid-disc branching at 59±1% fin ray length, and posterior branching at 48±2% (Figure 4.5A; ANOVA, post-hoc Tukey test, $p<0.0001$). The fin rays of *L. macrochirus* branched once, at 52% fin ray length (Figure 4.5A); a second branching occurs at more than 90% fin ray length, and was not captured in histology sections. (N.B. The delicate distal potions of the fin ray were missing from the cleared and stained specimen of *L. macrochirus* shown in Figure 4.3, due to tissue preparation and handling. However, fin rays were intact in specimens examined by radiography and in histology sections.) In *S. acanthias* fin elements did not branch, but the fin consists of two distinct areas: a proximal portion supported by radial cartilages, and a distal portion supported by fine ceratotrichia (Figure 4.3B). This change in structure occurred at 51% fin ray length (Figure 4.5A).

Fin ray segmentation

The fin rays of stingrays are segmented (Figure 4.2). Each fin ray is comprised of radial cartilages, with the number of radials per fin ray differing significantly between anterior, mid-disc and posterior locations: anterior fin rays had 12.5±0.3 radials, mid-disc fin rays had 22.1±0.6 radials, and posterior fin rays had 16.7±.4 radials (Figure 4.5B; ANOVA, post-hoc Tukey test, $p<0.0001$). In *P. orbignyi*, the joints between radials were aligned, forming

Figure 4.5. Branching and segmentation structure within fin rays, for anterior (red), mid-disc (light blue), and posterior (purple) fin rays in *P. orbignyi*, and mid-fin fin rays for *L. macrochirus* (grey blue) and *S. acanthias* (grey). For *P. orbignyi*, error bars represent ±1 s.e.m.; values for other species are presented for comparison only. (A) Total length of fin rays, subdivided into pre-branching (lower, dark color) and post-branching (upper, light color) lengths. Standardized branching lengths (as percentages of total fin length) are presented in the text, with significant differences in branching locations between all three stingray fin regions. (B) Number of segments per fin ray, subdivided into pre-branching (lower, dark color) and post-branching (upper, light color) portions of the fin ray. (C) Length of individual fin radials (or, for *L. macrochirus*, fin segments) at proximal, intermediate, and distal spanwise positions within fin rays. See text for details of fin radial locations. Pectoral fins are of comparable lengths across species (26.5±1.4 mm, 45.2±2.4 mm, and 34.8±2.3 mm for stingray anterior, mid-disc, and posterior rays, respectively, 27.8 mm for *L. macrochirus* and 22.5 mm for *S. acanthias*). N=30 for *P. orbignyi*, n=1 for *L. macrochirus* and *S. acanthias.* All error bars represent ±1 s.e.m.

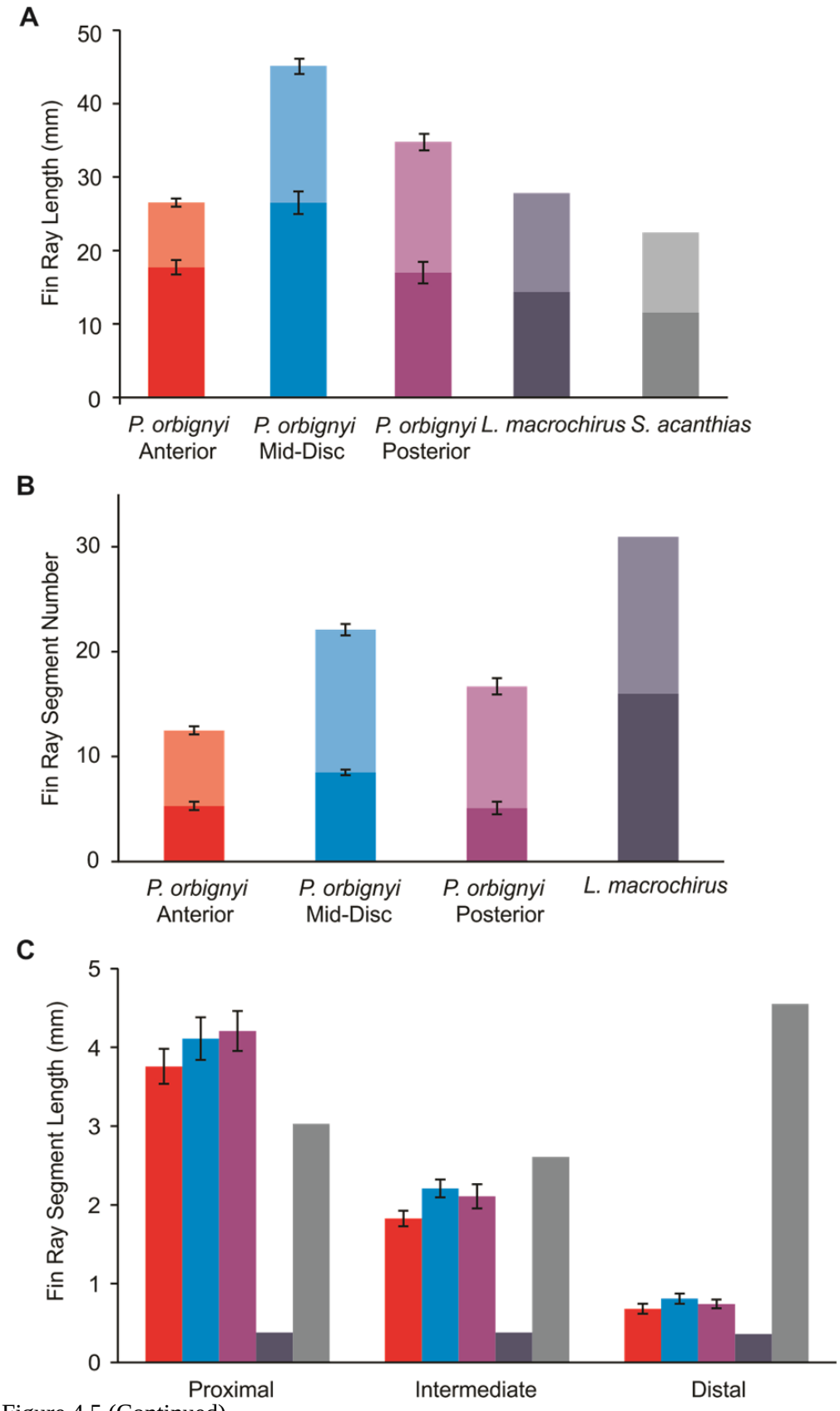

Figure 4.5 (Continued)

concentric semi-circles, rather than offset in the staggered pattern of certain other batoid species (Schaefer and Summers, 2005). Radials were not evenly distributed between pre- and post-branching sections of the fin ray. Fin ray branching occurred at more than 50% fin ray length for all fin regions, but only 37±3% of radials occurred in the pre-branching portion of the fin. The proportion of pre- and post-branching levels was the same for anterior, mid-disc, and posterior fin rays (ANOVA, NS). A higher proportion of radials occurred in the post-branching half of the fin because of a significant spanwise decrease in radial length (Figure 4.5C; ANOVA, post-hoc Tukey test, $p<0.01$.). Proximal radials, very close to the pterygium, had a length of 4.0±0.2 mm, while intermediate radials measured just after the fin ray branching point were 2.0±.1 mm long, and distal radials close to the distal tip of the fin ray were 0.7±.1 mm long. Proximal, intermediate, and distal radial lengths did not differ significantly between anterior, mid-disc, and posterior fin rays, except that anterior fin rays had significantly shorter intermediate radials (ANOVA, post-hoc Tukey test, $p<0.0001$).

The fin rays of *L. macrochirus* are also segmented, with a constant segment length of 0.4±0.2 mm across proximal, intermediate, and distal portions of the fin (Figure 4.5C). In *S. acanthias,* the distal half of the fin is composed of unsegmented ceratotrichia. Proximally, *S. acanthias* fin radials were similar in length to the proximal radials in *P. orbignyi* (~3 mm), but in *S. acanthias* radial length increased from proximal to distal: radials in the outer row were longer than those in more proximal rows (Figure 4.3B, 4.5C). As the specimens from all species used for this analysis had similar pectoral fin lengths, the results remain the same if segment lengths are standardized to total fin ray length.

Pectoral fin musculature

Four major muscle layers were present in stingray pectoral fins, in addition to small interradial muscles not quantified in this study. Broad sheets of dorsal and ventral superficialis musculature extended from the pterygia partway across the fin span, with fibers running parallel to the long axis of the fin ray. Medial to this muscle layer, the deeper dorsal and ventral profundus muscles are more tightly bundled, and run almost the entire length of the fin ray, with fibers oriented at an oblique angle to the fin ray (Figure 4.6).

Histological cross-sections

In all species, sagittal cross-sections taken parallel to the long axis of a fin ray revealed circular or ellipsoid skeletal elements centered along the fins dorsoventral axis (Figure 4.7). In *P. orbignyi*, fin rays were flanked by dorsal and ventral musculature across the entire fin span (Figure 4.6, 4.7A,B,C). In *L. macrochirus*, the two semicircular hemitrichia making up each lepidotrich were centered in a thin fin membrane, with no muscles present in the fin (Figure 4.3A, 4.7D). In *S. acanthias*, the most proximal sections revealed fin musculature surrounding the radial cartilages; more distally, the muscle layers were replaced by dorsal and ventral layers of ceratotrichia, which continued the full length of the fin span (Figure 4.7E). Distal to the end of the radial cartilages, the ceratotrichia formed a loosely-organized bilayer.

In cross-sectional shape, the proximal fin radials of *P. orbignyi* were relatively oblong or ellipsoid, with an average aspect ratio (height/width) of 0.76±0.02; moving distally along the fin span, aspect ratio decreased further as fin rays become more dorsoventrally compressed, down to an average ratio of 0.33±0.02 for the distal fin (Figure 4.8). As fin rays approached the branching point, the "cores" of radials begin to diverge prior to full bifurcation, becoming

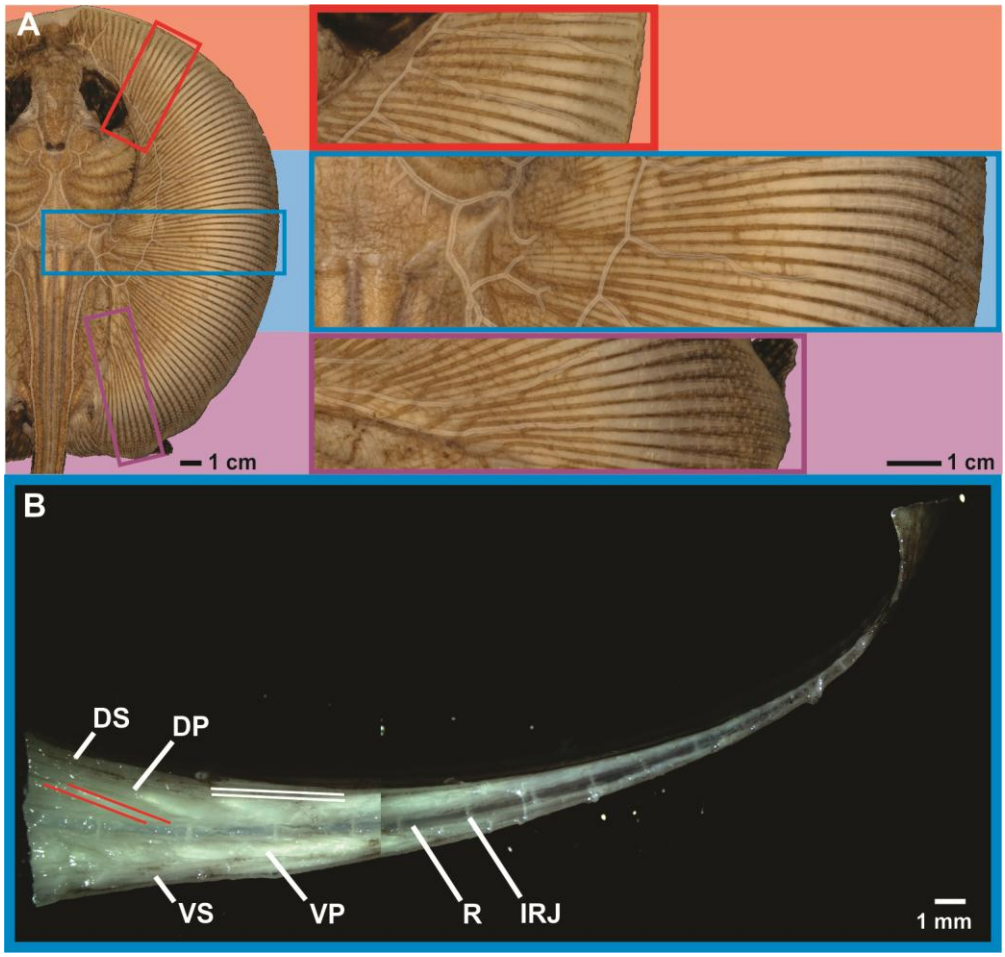

Figure 4.6. Pectoral fin musculature in *P. orbignyi.* (A) Right pectoral fin in dorsal view, with closeups at right of anterior (red), mid-disc (light blue), and posterior (purple) sections of the fin examined in histological sections. Muscle bundles are visible between dark blood vessels, particularly in distal regions of the fin. (B) Transverse section from the mid-disc region of the fin, with dorsal profundus (DP), ventral profundus (VP), dorsal superficialis (DS) and ventral superficialis muscles flanking the segmented fin ray, which is composed of radials (R) separated by interradial joints (IRJ). Dorsal muscle fiber angles are highlighted by white (DP) and red (DS) lines. Proximal is at left, dorsal at top.

Figure 4.7. Sagittal cross-sections of fin rays from (A) *P. orbignyi* anterior (red outline), (B) *P. orbignyi* mid-disc (light blue outline), and (C) *P. orbignyi* posterior (purple line), illustrating fin radials (R), dorsal and ventral profundus muscles (DP and VP), and dorsal and ventral superficialis muscles (DS and VS), shown at 20% intervals of fin ray length. (D) *L. macrochirus* (blue-grey outline) proximal pectoral fin section (10% fin ray length) with lunate hemitrichia (H). (E) *S. acanthias* (grey outline) pectoral fin sections at 40%, 60%, and 80% of fin ray length, showing radials and ceratotrichia (CT). Chains of catenated calcification are visible as red dots at the dorsal and ventral edges of radials. Sequences begin with the most proximal sections at the left, and are oriented with dorsal at the top. All images are shown at the same scale.

Figure 4.7 (Continued)

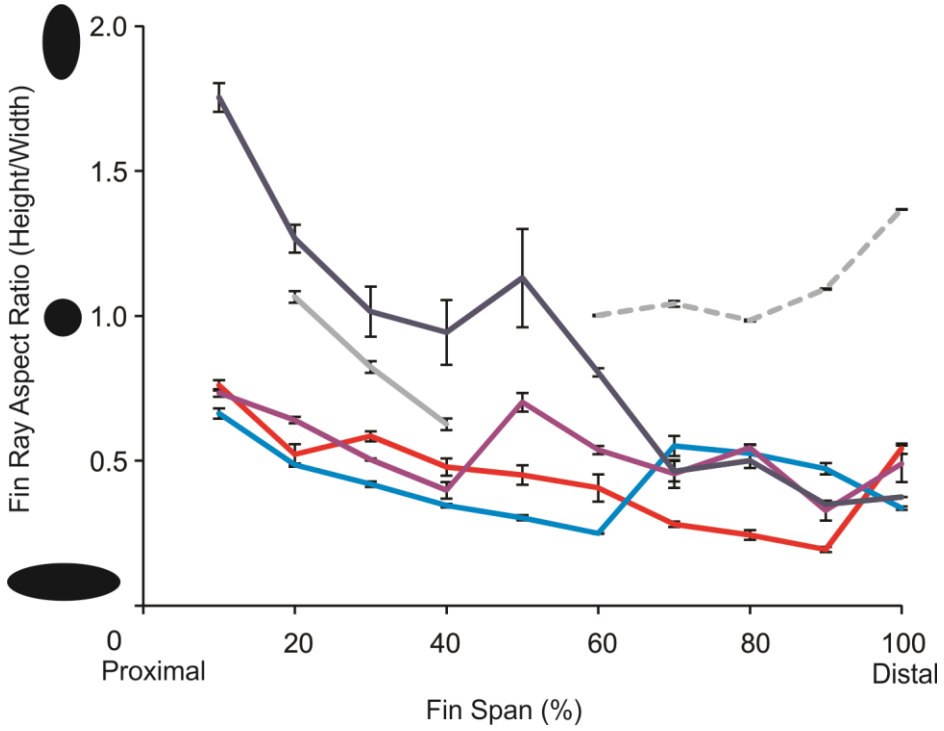

Figure 4.8. Aspect ratio (height/width) of pectoral fin rays from anterior (red), mid-disc (light blue), and posterior (purple) fin rays in *P. orbignyi*, and mid-fin fin rays for *L. macrochirus* (grey blue) and *S. acanthias* (grey: solid line indicates basal radials, dashed line indicates ceratotrichia), at 10% intervals along pectoral fin span. Representative ellipses along the y-axis illustrate the shapes described by high and low aspect ratios. N=6 per spanwise interval for *P. orbignyi*, for each anterior-posterior region. N=3 for other species. Error bars are ±1 s.e.m.

"barbell-shaped," thicker at the ends than in the center. Pre-branching divergence also occurred in the chains of catenated calcification running through the radials (Figure 4.7A,B,C; Schaefer and Summers, 2005). Post-branching, aspect ratio increased as the newly-diverged radials became less compressed. Spanwise changes in fin radial aspect ratio were significant (ANOVA, $p<0.001$), but aspect ratios did not differ significantly between anterior, mid-disc, and posterior fin rays (ANOVA, NS). The fin rays of *L. macrochirus* and *S. acanthias* maintained significantly higher aspect ratios than observed in *P. orbignyi* at all points along the fin span (ANOVA, post-hoc Tukey test, $p< 0.001$). *L. macrochirus* exhibited the greatest change in aspect ratio across the fin span, from a proximal ratio of 1.7±0.1 to a distal ratio of 0.38±0.0. In *S. acanthias*, the proximal radials and distal ceratotrichia were both nearly circular, with aspect ratios near 1.

The overall thickness of the pectoral fin of *P. orbignyi* decreased from proximal to distal, and so did the size of radials (Figure 4.9) and muscles (Figure 4.10). However, patterns of size change differed between anterior, mid-disc, and posterior fin rays. The cross-sectional area (CSA) of fin radials differed significantly based on both anterior-posterior and spanwise position (ANOVA, $p<0.0001$ for all comparisons). At all points along the span, anterior fin radials had a larger CSA than mid-disc or posterior fin radials at the same spanwise position; mid-disc and posterior CSA of fin radials were not significantly different from each other (Figure 4.9; post-hoc Tukey test). Among species, the CSA of *L. macrochirus* fin rays was not significantly different from stingray mid-disc and posterior stingrays, nor was the CSA of *S. acanthias* ceratotrichia (ANOVA, post-hoc Tukey test, NS). The fin radials of *S. acanthias*, however, had a far higher CSA than any other fin elements (ANOVA, post-hoc Tukey test, $p<0.0001$). Interestingly, the difference between proximal and distal fin ray CSA was very similar for

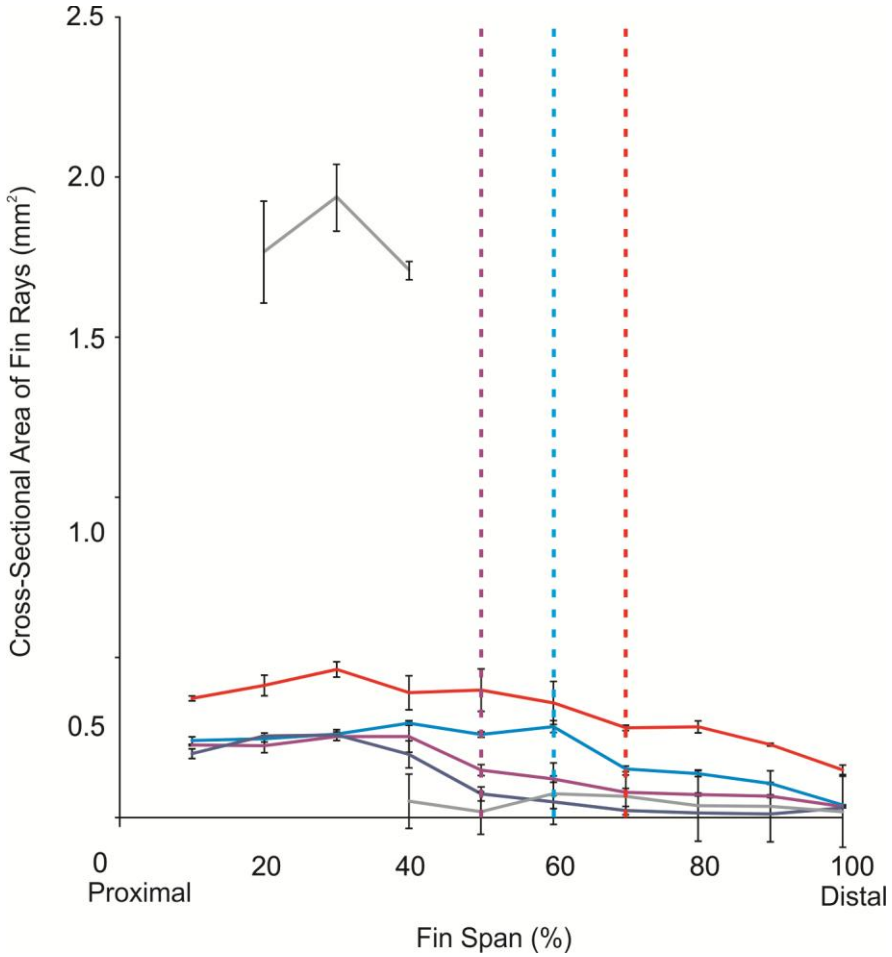

Figure 4.9. Cross-sectional area of fin rays from anterior (red), mid-disc (light blue), and posterior (purple) fin rays in *P. orbignyi*, and mid-fin fin rays for *L. macrochirus* (grey blue) and *S. acanthias* (grey), at 10% intervals along pectoral fin span. Vertical dashed lines highlight the first post-branching datapoint for each *P. orbignyi* fin ray (corresponding colors). N=6 per spanwise interval for *P. orbignyi*, for each anterior-posterior region. N=3 for other species. Error bars represent ±1 s.e.m.

Figure 4.10. Thickness of muscle layers in the pectoral fin of *P. orbignyi*, in (A) anterior, (B) mid-disc, and (C) posterior fin rays. Each graph shows the thickness (height) of profundus (black) and superficialis (green) muscles, from both dorsal (solid lines) and ventral (dashed lines) sides of the fin. Thickness is used to compare muscle size as cross-sectional area could not be obtained for superficialis muscles. A thickness of zero indicates that the muscle is no longer visible in histology sections, and has inserted onto the pectoral fin skeleton. N=6 per spanwise interval for *P. orbignyi*, for each anterior-posterior region. N=3 for other species. Error bars represent ±1 s.e.m.

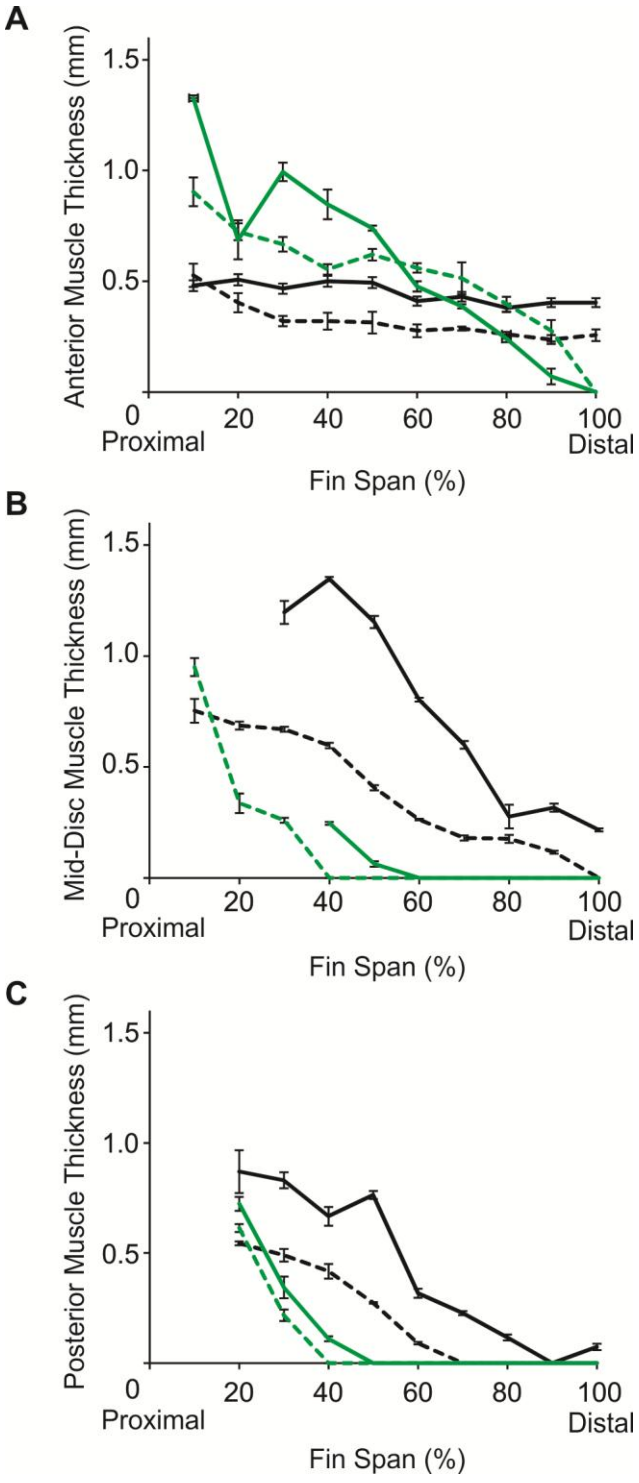

Figure 4.10 (Continued)

stingrays and *L. macrochirus*: 0.2 mm^2 for stingrays and 0.17 mm^2 for *L. macrochirus.* The change in CSA did represent a higher percentage of maximum fin ray CSA for *L. macrochirus* than *P. orbignyi* (85% versus 72%, respectively).

In stingray pectoral fins, the CSA of dorsal and ventral profundus muscle bundles also decreased with fin span (ANOVA, post-hoc Tukey test, $p<0.0001$). At all points across the span, the dorsal profundus was larger (higher CSA) in anterior fin rays than in mid-disc or posterior fin rays (ANOVA, post-hoc Tukey test, $p<0.001$). Ventral profundus CSA differed significantly between all anterior-posterior positions, greatest in anterior fin rays and smallest in posterior fin rays. For all anterior-posterior regions and all positions along the fin span, the dorsal profundus was larger than the ventral (Figure 4.7A,B,C). Superficialis muscles were not as neatly encapsulated as the profundus; since a superficialis width could not be measured, the thickness (height) of profundus and superficialis muscles was used to compare their sizes and presence along the fin span (Figure 4.10). Dorsal profundus muscles ran across the entire span in all anterior-posterior fin regions, but in mid-disc and posterior regions both superficialis muscles and the ventral profundus inserted (dropped to a thickness of 0) around 50% span. Like profundus muscles and fin rays, superficialis muscles decreased in thickness along the fin span (ANOVA, post-hoc Tukey test, $p<0.0001$). All muscles were larger and extended further distally in anterior fin rays than in mid-disc and posterior rays (ANOVA, post-hoc Tukey test, $p<0.0001$). Profundus muscles were taller than superficialis muscles (and larger in general; see Figure 4.7A,B,C), and dorsal muscles (profundus and superficialis) were consistently larger than their ventral counterparts.

The distance between fin rays varied significantly with species, with the greatest distances occurring in *L. macrochirus* (ANOVA, post-hoc Tukey test, $p<0.0001$). In *L.*

macrochirus, fin rays were up to 1 mm apart, compared to less than 0.3 mm in *P. orbignyi* and approximately 0 mm in *S. acanthias.* Within species, pre- and post-branching distances between fin rays were not significantly different across fin span (ANOVA, NS).

Multivariate analyses

In the PCA investigating differences in fin ray branching and segmentation patterns between anterior, mid-disc, and posterior fin rays, a combination of the first two principal components showed significant separation of groups by anterior-posterior position. All three variables (total number of radials in a fin ray and the proportions of fin ray length and fin radials occurring before branching) loaded high on PCA axes; the major contributors to principal component 1 (PC1) were the percentage of fin ray length and fin radials occurring before the branching point of the fin ray, explaining 59% of variation. Total radial number loaded highest on PC2, which explained 29% of variation. The DFA based on PC1 and PC2 identified 97% of sequences correctly (one misclassification). The PCA examining morphological differences at each spanwise interval (10% of fin span) separated anterior, mid-disc, and posterior groups based on all eight included variables, but with the greatest influence from the area and aspect ratios of fin radials and dorsal muscles.

Discussion

The pectoral fin structure of freshwater stingray *P. orbignyi* varies along both anteroposterior (chordwise) and mediodistal (spanwise) axes. These variations have significant implications for undulatory locomotion, as the shape and size of fin skeletal elements and musculature, and their arrangement within the pectoral disc, predisposes the fin toward certain lines of action. Previous

comparative research described a correlation between pectoral fin morphology and batoid swimming mode across species, with lower levels of calcification and aligned interradial joints present in undulators more so than oscillators (Schaefer and Summers, 2005). Here, I investigate the morphological characteristics that underlie the known kinematics of undulatory locomotion in *P. orbignyi* (Blevins and Lauder, 2012), to explore more specific correlations between fin structure and function. For comparison, pectoral fins of bluegill sunfish *L. macrochirus* and dogfish shark *S. acanthias* were also examined, to provide actinopterygian and shark outgroup examples of alternative fin structures.

Compared to their shark relatives, or actinopterygian fishes, batoids are notable for their expanded pectoral fins and proliferation of fin rays. The pectoral fins of *P. orbignyi* is comprised of approximately 100 fin rays, compared to 13 in *L. macrochirus* (Figure 4.2, 4.3A). The distal potion of the *S. acanthias* pectoral fin is supported by dozens of ceratotrichia, but the proximal portion of the fin skeleton is limited to approximately 20 radials (Figure 4.3B; outer radial row).

Chordwise variation across the pectoral fin

The pectoral fin disc of *P. orbignyi* is nearly circular. Fin rays are present throughout the disc, radiating from the central pectoral and pelvic girdles, which are in turn fused with the axial skeleton (Figure 4.2C). As a result of this overall fin geometry, both the total length of fin rays and their angle to the body midline varies based on anterior-posterior position: anterior and posterior fin rays are at a shallow angle to the body midline compared to the perpendicular insertion of mid-disc fin rays, and are significantly shorter than their mid-disc counterparts (Figure 4.4, 4.5A). All fin rays branch (bifurcate) once, but branching occurs more distally in

anterior fin rays than in mid-disc or posterior regions (67±1% fin ray length versus 59±1% at mid-disc and 48±2% posteriorly). Anterior fin rays are also composed of fewer fin radials than mid-disc and posterior fin rays (and therefore have fewer interradial joints; Figure 4.5B), but this is due to the shorter overall length of anterior fin rays, rather than a regional difference in radial length. For a given spanwise position, the length of individual radials is constant in all fin rays (Figure 4.5C). However, fin radials are thicker (higher cross-sectional area) in anterior fin rays than in corresponding spanwise positions in mid-disc and posterior fin rays (Figure 4.7A,B,C, 4.9). Multivariate analyses (PCA and DFA) of whole fin rays separated anterior, mid-disc and posterior fin rays based on total number of radials and differences in the proportion of radials and fin ray length proximal to fin ray branching. Within spanwise sections, anterior, mid-disc, and posterior fin rays were differentiated (PCA) by a combination of radial and dorsal muscle cross-sectional areas and aspect ratios.

The reduced number of interradial joints, shorter total length, greater fin radial width, and distally-shifted branching of anterior fin rays combine to impose structural limits on the flexibility of these fin rays, compared to those in other regions of the fin. Some bending may occur in the largely uncalcified fin radials, but the majority of fin bending should occur at interradial joints. Due to the constant length of fin radials, the ratio of bending per unit of total fin ray length remains the same across the pectoral disc, but in absolute terms the shorter total length and fewer joints in anterior fin rays reduces their bending potential. Assuming equal material properties, the more robust anterior fin radials will stiffen the anterior portion of the fin more than their slender counterparts stiffen other fin regions, as a higher cross-sectional area (for the same aspect ratio) yields a higher second moment of area, i.e. more resistance to bending (Figure 4.8, 4.9). In all fin rays, the cross-sectional area of fin radials decreases after branching

(Figure 4.9), so the distally-shifted location of fin ray branching observed in anterior fin rays will also maintain a higher second moment of area relative to other regions of the fin (Figure 4.9). (The distance between fin rays is the same before and after branching, so smaller post-branching radials are no more tightly packed than pre-branching radials).

Structural stiffening of the anterior region of the pectoral fin is compatible with undulatory locomotion in *P. orbignyi*. Though the entire fin may appear to undulate (Figure 4.1A) during swimming, in actuality the anterior region of the pectoral disc remains still, creating a stable leading edge (Figure 4.11; Blevins and Lauder, 2012). Minimizing the motion of the leading edge of the fin has hydrodynamic benefits to drag reduction, by reducing the area of the body projected into oncoming fluid flow. Passive stiffening of the anterior pectoral fin would reduce the energy requirements of actively maintaining a stable leading edge, helping to counteract opposing forces from oncoming fluid flow or the undulations of the remainder of the fin. There is also greater potential for active stiffening in the anterior pectoral fin than in other regions, due to the larger size of both profundus (deep) and superficialis (shallow) muscle layers, and the persistence of both layers further along the fin span than in mid-disc or posterior portions of the disc (Figure 4.10). In particular, the fiber angles of dorsal and ventral profundus muscles (Figure 4.6B) are such that simultaneous activation of dorsal and ventral muscles would stiffen the fin. Previous work on muscle activation during undulatory swimming by blue-spot stingray *Taenuria lymma* found alternate activation of dorsal and ventral muscles (unclear whether profundus or superficialis), but activity patterns were not recorded for the anterior portion of the pectoral fin (Rosenberger and Westneat, 1999). Additional investigation of muscle activation patterns could reveal whether active stiffening complements passive structural stiffening in the

Figure 4.11. Dorsal view radiograph of *P. orbignyi*, with overlay depicting the amplitude of the pectoral fin during undulatory swimming at 1.5-2.5 DLs^{-1} (Blevins and Lauder, 2012). Lines indicate the position of basal cartilages (solid black), fin ray branching points (dashed black), and the insertion of the dorsal superficialis muscle (dashed green). Amplitude is defined as ½ of the maximum excursion at a given location during one cycle of the propulsive wave employed in undulatory locomotion. Warmer colors represent greater amplitude magnitudes.

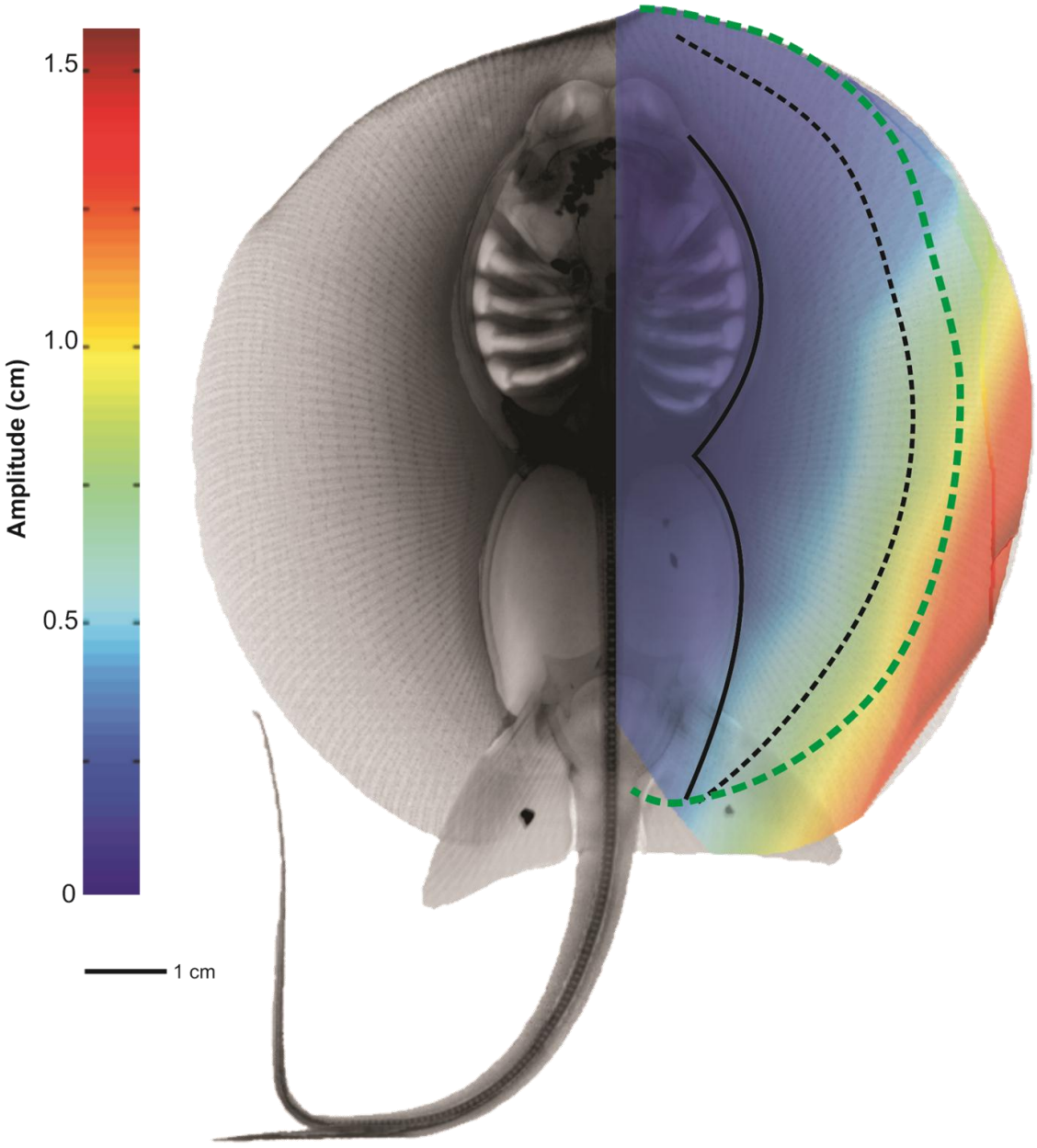

Figure 4.11 (Continued)

anterior pectoral fin of undulating batoids. The fiber angles of the profundus layer are relatively similar among batoid species, but superficialis fiber angles vary widely: the very shallow fiber angles seen in *P. orbignyi* occur in angel shark *Squatina squatina* and an axial-swimming batoid, guitarfish *Rhinobatus lentiginosus,* but much larger angles occur in stingrays *T. lymma* and *Dasyatis sabina,* and in butterfly ray *Gymnura micrura* (Calvert, 1983; Rosenberger and Westneat, 1999). In the latter species, the opposing orientation of superficialis and profundus muscle fibers form pennate arrangements dorsal and ventral to the fin ray. It is surprising that fiber orientation in derived stingray *P. orbignyi* would resemble that of axially-undulating batoids rather than other pectoral-fin undulators. However, both superficialis orientations present the possibility of active fin stiffening with simultaneous activation of dorsal and ventral muscles.

If the anterior portion of the pectoral fin is held still in order to maintain a stable leading edge, it is excluded from locomotor movements. However, this would not significantly affect thrust production during swimming, as contributions from the anterior fin are by fin geometry. During stingray swimming, waves of undulation travel orthogonally to fin radials, passing around the perimeter of the disc. Anterior fin rays are at a shallow angle to the midline, so an anterior wave would travel almost laterally, and would not be well-aligned for to accelerate fluid toward the posterior and generate thrust. In addition to locomotion considerations, a stiffened anterior pectoral fin could also benefit other behaviors: stingrays use the anterior region of the disc to exhume buried prey, and to suspend sand during foraging and burying (Wilga et al., 2012; pers. obs.).

The structural features that result in increased stiffness in the anterior pectoral fin of *P. orbignyi* are reversed in mid-disc and posterior regions of the fin, which therefore have greater

potential bending. Fin rays are longest at mid-disc, but even posterior fin rays are longer than anterior fin rays; the pectoral disc is roughly circular, but the pelvic girdle is more slender than the pectoral girdle, so posterior rays are longer than their anterior counterparts (Figure 4.2C). Longer fin rays contain more radials and therefore more interradial joints. Due to spanwise changes in radial length, and a more proximal location of fin ray branching, anterior and posterior fin rays have a higher proportion of radials in the distal, post-branching portion of the fin (Figure 4.5), concentrating fin flexibility in the outer part of the pectoral disc. These morphological changes correspond to the regions of the pectoral fin disc which undulate with the highest amplitude during locomotion (Figure 4.11). In these same regions, the direction of the propulsive wave corresponds most closely to the direction of thrust (Figure 4.2C). Around mid-disc, the wave will travel directly opposite to the stingray's direction of travel. Posteriorly, fluid will be accelerated diagonally toward the posterior and the body midline; as the paired pectoral fins undulate simultaneously during steady swimming, diagonal jets of fluid shed by posterior portions of the fin may influence each other and redirect posteriorly into the wake. Hydrodynamic studies of stingrays are challenging, but could test such hypotheses about fluid flow beneath the undulating fin. Robotic or computer models could also contrast the fluid dynamics and performance of fins swimming by radial undulation (as in stingrays) or orthogonal undulation, with the propulsive wave travelling parallel to the body midline.

Spanwise variation within fin rays

Morphological variations between anterior, mid-disc, and posterior regions of stingray pectoral fins suggest correlations between pectoral structure and the fin function observed during undulatory locomotion. Fin structure also varies with span, within individual fin rays. All

elements—radials, muscles, and the fin as a whole—decrease in cross-sectional area from proximal to distal (Figure 4.6B, 4.7, 4.9, 4.10). In all areas of the disc, the distal, post-branching portion of the fin ray contains more, shorter radials, compared to the fewer, longer radials in the pre-branching portion (Figure 4.5); therefore, the more interradial joints are present distally, allowing more bending. In *P. orbignyi*, the interradial joints of neighboring fin rays are aligned throughout the fin, not staggered. This is consistent with previous findings for potamotrygonids, and contrasts the staggered joint arrangement in the distal fin of some dasyatid stingrays, thought to reinforce the portion of the fin experiencing the greatest stresses during locomotion (Schafer and Summers, 2005).

Like fin ray cross-sectional area, pectoral fin muscle size is also reduced in distal regions of the *P. orbignyi* pectoral fin. Dorsal and ventral profundus muscles extend across fin span (except for ventral posterior muscles, which insert around 70% fin span), but decrease in size as they approach the fin tip (Figure 4.10). Superficialis muscles only extend across full fin span in anterior portions of the fin; in mid-disc and posterior regions they insert around 50% fin ray length (Figure 4.10). The spanwise reduction in muscle size (and fin thickness overall) decreases the mass of the distal fin, somewhat reducing the energy requirements of sweeping the fin through the water, in the region that travels through the largest arc during locomotion (Figure 4.11)

The general structural trend creating a more flexible distal fin corresponds to the spanwise amplitude increase observed in stingray pectoral fin swimming. Particular morphological changes are closely associated with distinct increases in fin bending: dorsal superficialis insertion and the location of fin ray branching occur near to notable amplitude changes (Figure 4.11). Fin motion is quite limited proximal to fin ray branching, in part due to

fusions in the axial skeleton (Compagno, 1999) that prevent axial undulation in dorsoventral or lateral directions, and in part because of the stable leading edge maintained in the anterior regions of the fin. As the pectoral wave begins posterior to this region, and increases in amplitude as it approaches mid-disc (Blevins and Lauder, 2012), amplitude maxima at all spanwise positions occur relatively posterior on the disc—and correspond closely to structural changes influencing fin flexibility.

Throughout the fin, dorsal muscles (profundus and superficialis) are larger than their ventral counterparts. Ventral muscles power the downstroke of the fin—in undulatory terms, wave motion from crest to trough—which has been hypothesized as the "power stroke" in both undulatory (Rosenberger and Westneat, 1999) and oscillatory (Heine, 1992) batoids. Freshwater stingrays may differ in possessing larger dorsal than ventral muscles, or the greater strength implied by their larger cross-sectional area may be employed in behaviors other than locomotion. For example, *un*-burying from beneath the sand, when the pectoral disc is held flat against the substrate, may require substantial dorsal muscle strength. However, the motion of the undulatory wave is quite symmetrical during swimming, both in speed and amplitude (Blevins and Lauder, 2012). Further research may determine whether a "power stroke" exists in undulating batoids, and whether the size of dorsal muscles reflects their contribution to pectoral fin swimming.

The distal cupping observed during some instances of swimming by *P. orbignyi* (Figure 4.1B; Blevins and Lauder, 2012) is permitted by the spanwise structural changes that result in increased flexibility in the distal fin. However, it is not completely clear what mechanism controls the extreme curvatures. At mid-disc, ventral superficialis muscles insert well before the fin margin, and cannot directly create curvature; cupping may be controlled by ventral profundus muscles, tendons, or possibly small interradial muscles not quantified here.

Comparisons between species

The pectoral fins of *P. orbignyi* and *L. macrochirus* evolved separately, are comprised of different skeletal materials (lightly calcified cartilage versus bone), and are employed differently during locomotion (Compagno, 1999; Lauder, 2006), but structural similarities—i.e. fin ray segmentation and branching—represent a convergence of form allowing the flexibility and precise deformation of the pectoral fins vital to both rajiform and labriform swimming modes. In contrast, although batoid pectoral fins evolved from shark-like precursors (Compagno, 1999), their pectoral fins have diverged markedly.

The pectoral fins of *P. orbignyi* and *L. macrochirus* both branch once near mid-span (59±1% fin ray length for mid-disc stingray fin rays, 52% fin ray length for *L. macrochirus*; Figure 4.5A)—some fin rays in *L. macrochirus* branch a second time near the fin tip, but this was not quantified in the present study. In both species, the distance between fin rays remained the same before and after branching, maintaining uniform support across fin chord. In *S. acanthias*, the proximal half (51%) of the fin was supported several rows of unbranching radials, while the distal half is comprised by unsegmented, unbranching ceratotrichia (Figure 4.3B, 4.5A). The pectoral fin rays of *P. orbignyi* and *L. macrochirus* are both segmented, but the far-shorter segments in *L. macrochirus* result in a much higher number of segments per fin in *L. macrochirus* than *P. orbignyi*, for fins of comparable total length (Figure 4.5B,C). However *P. orbignyi* fin segments (radials) decrease in length with fin span, while *L. macrochirus* segments are of constant length (Figure 4.5C), so *P. orbignyi* possesses a higher percentage of segments in the distal fin, implying a greater spanwise change fin flexibility due to increased distal segmentation than in *L. macrochirus*. *L. macrochirus* exhibited the greatest spanwise change in fin ray cross-sectional aspect ratio (AR), from laterally compressed proximal fin segments (AR

1.7) to dorsoventrally compressed distal sections (AR<0.5), which would increase flexibility in the distal region of the fin due to a decrease in second moment of area (Figure 4.8). All fin elements *S. acanthias* and all but the distal segments of *L. macrochirus* had significantly higher aspect ratios than *P. orbignyi* fin rays at the same spanwise position. The material properties of fin rays certainly differ between species, but the largely uncalcified cartilage of stingray fins (Schaefer and Summers, 2005) are composed of the most flexible material; low aspect ratio fin rays complement this material and should yield more flexible fin rays in *P. orbignyi* than in other species. As fin ray cross-sectional area decreases from proximal to distal for all species, higher flexibility is generally expected from distal fin regions (Figure 4.7, 4.9).

The pectoral fin musculature of *P. orbignyi* differs dramatically from the systems of fin control in *S. acanthias* and *L. macrochirus.* Neither sharks nor actinopterygians have significant musculature in the pectoral fin itself (Figure 4.3, 4.7). In sharks, muscles at the base of the fin are sufficient to control fin pitch and yaw, the movements required to adjust pectoral fin trim during axial locomotion (Compagno, 1999). Actinopterygians possess a novel system by which muscles at the fin base can control distal fin curvature, due to the bilaminar structure of hemitrichia within each lepidotrich (Lauder, 2006). Batoids lack the unique actinopterygian system, but rajiform locomotion requires far more control of the distal fin than provided by the shark-like pectoral musculature. In *P. orbignyi*, each of the 100 fin radials is associated with four layers of muscle (dorsal and ventral pairs of profundus and superficialis), allowing direct actuation of the fin. Like the fin rays of all species, these muscles decrease in cross-sectional area with fin span, but add significant mass to the fin of *P. orbignyi* compared to *L. macrochirus*. The construction of the elaborate batoid fin skeleton has been recognized as a significant energetic cost, and so too is the development of their intricate pectoral musculature.

The pectoral fins of freshwater stingray *P. orbignyi* show spanwise and chordwise structural variations that correspond to the locomotor demands on different fin regions. In particular, the anterior fin is stiffened by passive structural changes, as it has more robust fin radials, fewer interradial joints, and a distally-shifted position of fin ray branching. Muscle fiber orientations present the potential for active stiffening as well. Both active and passive stiffening of the anterior fin correspond to the locomotor role of this region, which maintains a steady leading edge during undulatory locomotion. Mid-disc and posterior regions of the fin are relatively more flexible. Structure also predisposes stingray pectoral fins to a spanwise increase in flexibility; distal radials are shorter, yielding more interradial joints per unit length in the distal fin, and the cross-sectional area of all fin elements (radials and muscles) decreases with span. The segmentation and branching of pectoral fin rays in *P. orbignyi* is far more reminiscent of actinopterygian (*L. macrochirus*) fin structures than those of a closer shark relative (*S. acanthias*). However, stingrays control pectoral fin conformation via muscles throughout the fin span, in contrast to both other species. The structure of stingray pectoral fins represents convergent evolution and localized morphological adaptations closely correlated with the fins' locomotor function. In addition to a better understanding of locomotor diversity in fishes, these findings may also prove useful in biomimetic design, as an example of structure-function connections in a biological propulsor.

Acknowledgements

I am grateful to the Hanken Laboratory at Harvard University, particularly H. Maddin and Z.R. Lewis for histology methods and facilities, and would also like to thank A. Williston of the Ichthyology Collections at the Harvard Museum of Comparative Zoology and G.V. Lauder. This

project was supported by a Robert A. Chapman Memorial Scholarship and funding from the Harvard University Department of Organismic and Evolutionary granted to E.L. Blevins.

References

Abramoff, M. D., Magalhaes, P. J. and Ram, S. J. (2004). Image Processing with ImageJ. *Biophotonics International.* **11**(7) 36-42.

Blevins, E., Lauder, G. V. (2012). Rajiform locomotion: three-dimensional kinematics of the pectoral fin surface during swimming by freshwater stingray Potamotrygon orbignyi. *J. Exp. Biol.* **215**, 3231-3241.

Breder, C. M. (1926). The locomotion of fishes. *Zoologica* **50**, 159–297.

Calvert, R. A. (1983). Comparative anatomy and functional morphology of the pectoral fin of stingrays. Masters thesis, Duke University.

Compagno, L. J. V. (1999). Endoskeleton. In *Sharks, Skates and Rays: The Biology of Elasmobranch Fishes* (ed. W. C. Hamlett), pp. 69-92. Baltimore, MD: John Hopkins University Press.

Dingerkus, G. and Uhler, L. D. (1977). Enzyme clearing of Alcian blue stained whole small vertebrates for demonstration of cartilage. *Stain Technol*. **52**, 229–232.

Heine, C. E. (1992). Mechanics of flapping fin locomotion in the cownose ray, *Rhinoptera bonasus* (Elasmobranchii: Myliobatidae). PhD thesis, Duke University.

Koester, D. M. and Spirito, C. P. (2003). Punting: An unusual mode of locomotion in the Little Skate, *Leucoraja erinacea* (Chondrichthyes: Rajidae). *Copeia.* **3**, 553-561.

Lauder, G. V. (2006). Locomotion. In *The Physiology of Fishes*, Third Edition, (D. H. Evans and J. B. Claiborne, eds.), pp. 3-46. Boca Raton: CRC Press.

Liem, K. F., and Summers, A. P. (1999). Muscular system: gross anatomy and functional morphology of muscles. In *Sharks, Skates and Rays: The Biology of Elasmobranch Fishes* (ed. W. C. Hamlett), pp. 93-114. Baltimore, MD: John Hopkins University Press.

Lucifora, L. O. and Vassallo A. I. (2002). Walking in skates (Chondrichthyes, Rajidae): Anatomy, behaviour and analogies to tetrapod locomotion. *Biol. J. Linn. Soc.* **77**, 35–41.

Macesic, L. J. and Kajiura, S. M. (2010). Comparative punting kinematics and pelvic fin musculature of benthic batoids. *J. Morph.* **271**, 1219-1228.

Macesic, L. J., Mulvaney, D., and Blevins, E. L. Synchronized Swimming: Coordination of pelvic and pectoral fins during augmented punting by benthic batoids. *In revision.*

Mallory, F. B. (1901). A contribution to staining methods. I. A differential stain for connective-tissue fibrillae and reticulum. II. Chloride of iron haematoxylin for nuclei and fibrin. III. Phosphotungstic acid haematoxylin for neuroglia fibres. *J. Exp. Med.* **5**, 15.

Presnell, J. K. and Schreibman, M. P. (1997). *Humason's animal tissue techniques, 5th ed.* Baltimore, MD: Johns Hopkins University Press.

Rosenberger, L. J. (2001). Pectoral fin locomotion in Batoid fishes: undulation versus oscillation. *J. Exp. Biol*. **204**, 379-394.

Rosenberger, L. J. and Westneat, M. W. (1999). Functional morphology of undulatory pectoral fin locomotion in the stingray *Taenuria lymma*. *J. Exp. Biol.* **202**, 3523-3539.

Schaefer, J. T. and Summers A. P. (2005). Batoid wing skeletal structure: novel morphologies, mechanical implications, and phylogenetic patterns. *J. Morph.* **264**(3), 298-313.

Taft, N. K. (2011). Functional implications of variation in pectoral fin ray morphology between fishes with different patterns of pectoral fin use. *J. Morph.* **272**, 1144–1152.

Taft, N., Lauder, G. V. and Madden, P.G. (2008). Functional regionalization of the pectoral fin of the benthic longhorn sculpin during station holding and swimming. *J. Zool.* **276**, 159-167.

Wilga, C. D. and Lauder, G. V. (2002). Function of the heterocercal tail in sharks: quantitative wake dynamics during steady horizontal swimming and vertical maneuvering. *J. Exp. Biol*. **205**, 2365-2374.

Wilga, C. D., Maia, A., Nawelaerts, S., and Lauder, G. (2012). Prey handling using whole-body fluid dynamics in batoids. *Zoology*. **115**, 47-57.

Appendix

S1: Mean Excursions of All Points (mm)

Notes:
Point locations are shown in the point map below, and can be precisely determined from each point's XY coordinates in S2.
Excursion is equivalent to 1/2 amplitude, and was calculated as the three-dimensional distance between the maximum and minimum positions of each point during one wave cycle. Excursion occurs almost exclusively in the z-direction.
The mean values presented here are for all swimming sequences, pooled (N=24), as excursion did not differ significantly between swimming speed for any point except pt. 31 (see text for details).

Map of Point Locations on the Pectoral Fin:

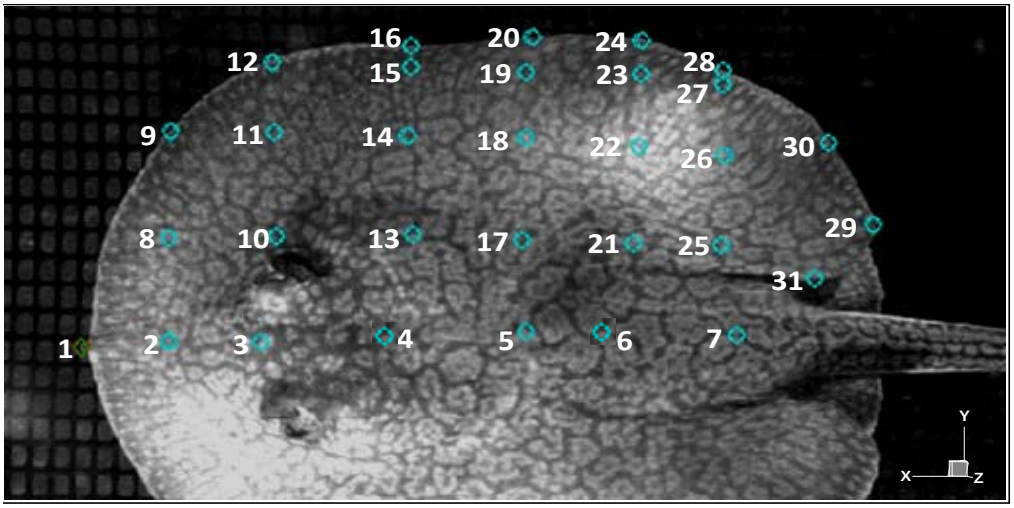

Point ID Number (See Point Map, or S2 for XY coordinates)	Mean Excursion (mm)	S.E.M.
1	3.81	0.24
2	2.68	0.24
3	0.00	0.00
4	4.03	0.46
5	3.11	0.18
6	4.10	0.13
7	4.64	0.32
8	3.45	0.30
9	5.29	0.45
10	2.58	0.19
11	5.88	0.57
12	8.52	0.96
13	3.02	0.23
14	7.73	0.67
15	16.57	1.15
16	18.83	1.47
17	3.29	0.20
18	8.59	0.57
19	20.41	1.11
20	28.19	1.25
21	3.87	0.24
22	11.25	0.88
23	24.52	1.25
24	31.68	0.88
25	6.55	0.86
26	15.86	1.18
27	22.64	1.94
28	29.96	1.15
29	14.93	1.35
30	24.38	1.34
31	7.29	0.52

S2: Sample Dataset for One Pectoral Wave Cycle (xyz coordinates for each point in mm)

Time	pt1_X	pt1_Y	pt1_Z	pt2_X	pt2_Y	pt2_Z	pt3_X	pt3_Y	pt3_Z	pt4_X	pt4_Y	pt4_Z	pt5_X	pt5_Y	pt5_Z	pt6_X	pt6_Y
0	-30.5317	2.04E-14	3.81	-15.0485	0.404325	2.68	0	0	0	19.08707	-1.57928	4.03	38.17414	-3.15856	3.11	56.09911	-4.59524
1	-30.6151	8.88E-15	3.81	-15.1467	0.499365	2.68	0	0	0	19.10605	-1.56764	4.03	38.2121	-3.13528	3.11	56.11597	-4.39609
2	-30.591	0	3.81	-15.1668	0.485154	2.68	0	0	0	19.11022	-1.55258	4.03	38.22045	-3.10516	3.11	56.11581	-4.35968
3	-30.5404	0	3.81	-15.1869	0.505627	2.68	0	0	0	19.13052	-1.52684	4.03	38.26103	-3.05369	3.11	56.16508	-4.23118
4	-30.4962	0	3.81	-15.1869	0.496264	2.68	0	0	0	19.1469	-1.52199	4.03	38.2938	-3.04398	3.11	56.20639	-4.2149
5	-30.4723	0	3.81	-15.1268	0.567019	2.68	0	0	0	19.13349	-1.55071	4.03	38.26698	-3.10142	3.11	56.20374	-4.32595
6	-30.5059	0	3.81	-15.1892	0.534831	2.68	0	0	0	19.10434	-1.59955	4.03	38.20868	-3.19911	3.11	56.13099	-4.46039
7	-30.507	1.07E-14	3.81	-15.2738	0.474561	2.68	0	0	0	19.11483	-1.59245	4.03	38.22966	-3.18491	3.11	56.14413	-4.4455
8	-30.6061	1.07E-14	3.81	-15.3684	0.475763	2.68	0	0	0	19.08216	-1.66604	4.03	38.16432	-3.33209	3.11	56.08542	-4.64351
9	-30.6715	1.78E-14	3.81	-15.4108	0.43007	2.68	0	0	0	19.07248	-1.69293	4.03	38.14496	-3.38586	3.11	56.06912	-4.75655
10	-30.7857	0	3.81	-15.4979	0.543634	2.68	0	0	0	19.02671	-1.71972	4.03	38.05342	-3.43944	3.11	55.98783	-4.83407
11	-30.689	1.07E-14	3.81	-15.4171	0.542171	2.68	0	0	0	19.04866	-1.78789	4.03	38.09732	-3.57578	3.11	56.0312	-5.00426
12	-30.5421	1.15E-14	3.81	-15.4083	0.47671	2.68	0	0	0	19.04512	-1.74398	4.03	38.09024	-3.48795	3.11	56.03857	-4.89143
13	-30.3588	0	3.81	-15.3106	0.462913	2.68	0	0	0	19.08592	-1.65843	4.03	38.17185	-3.31687	3.11	56.13385	-4.63676
14	-30.3063	1.24E-14	3.81	-15.2951	0.438746	2.68	0	0	0	19.09626	-1.61779	4.03	38.19251	-3.23558	3.11	56.15909	-4.5381
15	-30.2468	0	3.81	-15.2624	0.366522	2.68	0	0	0	19.13269	-1.64106	4.03	38.26539	-3.28211	3.11	56.22299	-4.51196
16	-30.2076	0	3.81	-14.9996	0.609502	2.68	0	0	0	19.1195	-1.76231	4.03	38.23901	-3.52462	3.11	56.19647	-4.86426
17	-30.1418	8.88E-15	3.81	-14.9347	0.584052	2.68	0	0	0	19.1179	-1.73848	4.03	38.2358	-3.47697	3.11	56.21727	-4.78895
18	-30.1183	8.88E-15	3.81	-14.8925	0.590629	2.68	0	0	0	19.10997	-1.77665	4.03	38.21995	-3.55329	3.11	56.20886	-4.87862
19	-30.1765	1.87E-14	3.81	-14.9653	0.591736	2.68	0	0	0	19.09048	-1.789	4.03	38.18096	-3.578	3.11	56.15543	-4.91286
20	-30.0339	0	3.81	-14.9213	0.520393	2.68	0	0	0	19.11077	-1.74854	4.03	38.22153	-3.49707	3.11	56.22186	-4.8121
21	-29.9978	0	3.81	-14.9524	0.562692	2.68	0	0	0	19.10611	-1.71564	4.03	38.21221	-3.43129	3.11	56.2421	-4.69422
22	-30.0347	1.24E-14	3.81	-14.9691	0.561133	2.68	0	0	0	19.11187	-1.63428	4.03	38.22374	-3.26855	3.11	56.25397	-4.47718
23	-29.9071	1.33E-14	3.81	-14.8533	0.570368	2.68	0	0	0	19.12526	-1.72505	4.03	38.25051	-3.4501	3.11	56.29936	-4.74591
24	-29.8343	0	3.81	-14.7768	0.538439	2.68	0	0	0	19.11926	-1.72841	4.03	38.23853	-3.45681	3.11	56.30103	-4.72765
25	-29.8656	1.51E-14	3.81	-14.815	0.564861	2.68	0	0	0	19.07748	-1.70801	4.03	38.15496	-3.41602	3.11	56.23233	-4.67685
26	-29.8662	1.60E-14	3.81	-14.8245	0.488709	2.68	0	0	0	19.07147	-1.82168	4.03	38.14294	-3.64335	3.11	56.23995	-4.95791
27	-29.7997	-4.00E-15	3.81	-14.8368	0.431204	2.68	0	0	0	19.0868	-1.78761	4.03	38.1736	-3.57521	3.11	56.2884	-4.84377
28	-29.7284	0	3.81	-14.8247	0.432066	2.68	0	0	0	19.10141	-1.73153	4.03	38.20282	-3.46306	3.11	56.34473	-4.69175
29	-29.7555	0	3.81	-14.7138	0.510505	2.68	0	0	0	19.07261	-1.68545	4.03	38.14522	-3.3709	3.11	56.2342	-4.61128
30	-29.6709	1.24E-14	3.81	-14.6696	0.489549	2.68	0	0	0	19.09566	-1.71992	4.03	38.19132	-3.43985	3.11	56.27546	-4.70256
31	-29.5869	0	3.81	-14.6306	0.475183	2.68	0	0	0	19.10924	-1.73442	4.03	38.21847	-3.46884	3.11	56.29532	-4.74118
32	-29.6352	4.00E-15	3.81	-14.7624	0.535429	2.68	0	0	0	19.08482	-1.78444	4.03	38.16964	-3.56889	3.11	56.25168	-4.81996
33	-29.6566	-4.00E-15	3.81	-14.7631	0.418361	2.68	0	0	0	19.07255	-1.82121	4.03	38.14511	-3.64241	3.11	56.20739	-4.91166
34	-29.5975	0	3.81	-14.5647	0.506189	2.68	0	0	0	19.07994	-1.84292	4.03	38.15988	-3.68584	3.11	56.23399	-4.94452
35	-29.5394	-5.77E-15	3.81	-14.5168	0.541862	2.68	0	0	0	19.10347	-1.7911	4.03	38.20694	-3.5822	3.11	56.30309	-4.7928
36	-29.5789	0	3.81	-14.5787	0.459461	2.68	0	0	0	19.09931	-1.68137	4.03	38.19862	-3.36274	3.11	56.30092	-4.46273
37	-29.5037	1.55E-14	3.81	-14.5603	0.484758	2.68	0	0	0	19.11233	-1.70746	4.03	38.22466	-3.41493	3.11	56.31499	-4.54081
38	-29.5041	1.33E-14	3.81	-14.5316	0.448025	2.68	0	0	0	19.13087	-1.69294	4.03	38.26175	-3.38589	3.11	56.36595	-4.49301
39	-29.5325	4.00E-15	3.81	-14.5487	0.453742	2.68	0	0	0	19.11609	-1.71119	4.03	38.23218	-3.42238	3.11	56.3556	-4.50684
40	-29.54	9.33E-15	3.81	-14.5765	0.356255	2.68	0	0	0	19.11954	-1.72547	4.03	38.23909	-3.45093	3.11	56.33841	-4.5399
41	-29.6702	0	3.81	-14.5409	0.471833	2.68	0	0	0	19.08287	-1.7305	4.03	38.16573	-3.46099	3.11	56.25118	-4.58168
42	-29.7082	1.24E-14	3.81	-14.5814	0.477712	2.68	0	0	0	19.07113	-1.66581	4.03	38.14227	-3.33161	3.11	56.22483	-4.42829
43	-29.6657	1.95E-14	3.81	-14.5698	0.391121	2.68	0	0	0	19.06407	-1.70104	4.03	38.12814	-3.40208	3.11	56.24919	-4.50814
44	-29.6391	1.20E-14	3.81	-14.4934	0.480044	2.68	0	0	0	19.09106	-1.67353	4.03	38.18212	-3.34707	3.11	56.28756	-4.42228
45	-29.6133	5.77E-15	3.81	-14.4921	0.427832	2.68	0	0	0	19.12305	-1.63033	4.03	38.2461	-3.26067	3.11	56.36324	-4.33234
46	-29.6871	0	3.81	-14.4856	0.390338	2.68	0	0	0	19.12091	-1.58461	4.03	38.24182	-3.16922	3.11	56.3529	-4.16133
47	-29.7262	7.99E-15	3.81	-14.5749	0.423618	2.68	0	0	0	19.0983	-1.67575	4.03	38.19661	-3.35151	3.11	56.20656	-4.47431
48	-29.7519	2.00E-14	3.81	-14.5221	0.338157	2.68	0	0	0	19.09199	-1.70377	4.03	38.18398	-3.40755	3.11	56.20172	-4.53693
49	-29.7261	2.07E-14	3.81	-14.5069	0.377194	2.68	0	0	0	19.12666	-1.67933	4.03	38.25332	-3.35866	3.11	56.27819	-4.46708
50	-29.7932	1.87E-14	3.81	-14.5992	0.353857	2.68	0	0	0	19.09244	-1.60927	4.03	38.18487	-3.21854	3.11	56.19189	-4.30012
51	-29.737	7.33E-15	3.81	-14.5295	0.25177	2.68	0	0	0	19.12402	-1.64793	4.03	38.24804	-3.29586	3.11	56.24512	-4.39084
52	-29.7087	2.00E-15	3.81	-14.5331	0.31821	2.68	0	0	0	19.15123	-1.61153	4.03	38.30247	-3.22306	3.11	56.31999	-4.29365
53	-29.7195	9.99E-15	3.81	-14.5046	0.265237	2.68	0	0	0	19.18746	-1.5729	4.03	38.37492	-3.14579	3.11	56.42715	-4.20364
54	-29.836	1.35E-14	3.81	-14.6041	0.279259	2.68	0	0	0	19.1405	-1.5838	4.03	38.28101	-3.1676	3.11	56.39205	-4.20379
55	-29.7783	0	3.81	-14.5228	0.27789	2.68	0	0	0	19.10021	-1.64574	4.03	38.20041	-3.29148	3.11	56.39483	-4.28887
56	-29.7593	1.44E-14	3.81	-14.5966	0.304555	2.68	0	0	0	19.09117	-1.69566	4.03	38.18234	-3.39133	3.11	56.3025	-4.43486
57	-29.7918	7.77E-15	3.81	-14.6481	0.307619	2.68	0	0	0	19.10062	-1.60522	4.03	38.20124	-3.21045	3.11	56.30635	-4.20001
58	-29.7881	1.42E-14	3.81	-14.5746	0.259644	2.68	0	0	0	19.12465	-1.67014	4.03	38.2493	-3.34029	3.11	56.35368	-4.35404
59	-29.5648	-1.11E-15	3.81	-14.6169	0.25465	2.68	0	0	0	19.16732	-1.63479	4.03	38.33463	-3.26957	3.11	56.43333	-4.18793
60	-29.5634	6.77E-15	3.81	-14.6389	0.145688	2.68	0	0	0	19.14688	-1.62511	4.03	38.29376	-3.25023	3.11	56.38443	-4.18853
61	-29.6287	5.33E-15	3.81	-14.5813	0.327534	2.68	0	0	0	19.14406	-1.57248	4.03	38.28812	-3.14497	3.11	56.40193	-4.0544
62	-29.5403	1.54E-14	3.81	-14.5599	0.392823	2.68	0	0	0	19.17341	-1.63392	4.03	38.34682	-3.26785	3.11	56.41784	-4.20944
63	-29.6166	-4.44E-15	3.81	-14.6214	0.401636	2.68	0	0	0	19.17452	-1.66896	4.03	38.34904	-3.33792	3.11	56.41243	-4.34011
64	-29.5844	-2.33E-15	3.81	-14.6684	0.326186	2.68	0	0	0	19.18237	-1.68499	4.03	38.36474	-3.36997	3.11	56.4447	-4.37252
65	-29.64	3.50E-15	3.81	-14.6569	0.323754	2.68	0	0	0	19.18236	-1.67969	4.03	38.36472	-3.35937	3.11	56.4092	-4.35048
66	-29.7536	-9.99E-16	3.81	-14.7342	0.328593	2.68	0	0	0	19.1629	-1.7195	4.03	38.3258	-3.43899	3.11	56.36094	-4.45389
67	-29.5778	-5.55E-15	3.81	-14.7258	0.286806	2.68	0	0	0	19.19438	-1.7135	4.03	38.38875	-3.42701	3.11	56.41123	-4.41498
68	-29.543	1.98E-14	3.81	-14.5767	0.330097	2.68	0	0	0	19.2369	-1.60404	4.03	38.4738	-3.20808	3.11	56.50087	-4.13325
69	-29.4747	1.86E-14	3.81	-14.5093	0.42559	2.68	0	0	0	19.28025	-1.56675	4.03	38.56051	-3.1335	3.11	56.60053	-4.03494
70	-29.5261	7.74E-15	3.81	-14.5341	0.424247	2.68	0	0	0	19.27223	-1.45072	4.03	38.54446	-2.90144	3.11	56.62495	-3.77283
71	-29.4528	1.58E-14	3.81	-14.5243	0.393086	2.68	0	0	0	19.30304	-1.46173	4.03	38.60608	-2.92347	3.11	56.7569	-3.78601
72	-29.4309	5.77E-15	3.81	-14.6149	0.252699	2.68	0	0	0	19.28353	-1.54675	4.03	38.56706	-3.09351	3.11	56.71808	-3.9645
73	-29.5483	1.61E-15	3.81	-14.527	0.479314	2.68	0	0	0	19.2796	-1.61209	4.03	38.5592	-3.22418	3.11	56.70355	-4.11708
74	-29.5052	6.83E-15	3.81	-14.6319	0.47679	2.68	0	0	0	19.22966	-1.56665	4.03	38.45932	-3.1333	3.11	56.62124	-3.99672
75	-29.4351	1.09E-14	3.81	-14.6227	0.378248	2.68	0	0	0	19.26007	-1.5494	4.03	38.52015	-3.09881	3.11	56.65383	-3.93492
76	-29.3945	1.72E-14	3.81	-14.4308	0.352139	2.68	0	0	0	19.29849	-1.54628	4.03	38.59698	-3.09255	3.11	56.73738	-3.91772
77	-29.314	1.81E-14	3.81	-14.499	0.400836	2.68	0	0	0	19.28789	-1.57531	4.03	38.57577	-3.15062	3.11	56.70199	-4.03487
78	-29.3381	1.33E-14	3.81	-14.554	0.406594	2.68	0	0	0	19.32225	-1.59344	4.03	38.6445	-3.18688	3.11	56.73538	-4.01947
79	-29.3681	1.89E-15	3.81	-14.5522	0.261124	2.68	0	0	0	19.3313	-1.56199	4.03	38.6626	-3.12398	3.11	56.75985	-3.97874
80	-29.3366	1.25E-14	3.81	-14.5282	0.407497	2.68	0	0	0	19.29791	-1.6092	4.03	38.59582	-3.2184	3.11	56.72545	-4.08565

Notes:
Coordinates are given in millimeters.
The movement of all points is standardized to the movement of pt. 3 (the head).
The location of points on the pectoral fin can be determined from their xy coordinates, or using the point map below.
Data is given for approximately one cycle of the propulsive wave, and is animated in S3.

pt6_Z	pt7_X	pt7_Y	pt7_Z	pt8_X	pt8_Y	pt8_Z	pt9_X	pt9_Y	pt9_Z	pt10_X	pt10_Y	pt10_Z	pt11_X	pt11_Y	pt11_Z	pt12_X	pt12_Y
4.1	74.02408	-6.03192	4.64	-14.7355	15.12331	3.45	-13.8973	30.39379	5.29	0.250766	14.73647	2.58	0.955058	29.63675	5.88	1.543575	43.6642
4.1	74.01984	-5.65691	4.64	-14.8404	15.02552	3.45	-14.1688	30.34335	5.29	0.177235	14.753	2.58	0.713908	29.68687	5.88	1.311694	43.78884
4.1	74.01116	-5.61419	4.64	-14.8562	15.01049	3.45	-14.2011	30.25619	5.29	0.153333	14.75494	2.58	0.69824	29.70323	5.88	1.267377	43.79598
4.1	74.06912	-5.40866	4.64	-14.8925	14.95998	3.45	-14.3588	30.33059	5.29	0.176531	14.80622	2.58	0.653198	29.75518	5.88	1.076454	43.83791
4.1	74.11898	-5.38582	4.64	-14.7842	15.02682	3.45	-14.2385	30.33607	5.29	0.146722	14.82132	2.58	0.723598	29.773	5.88	1.110828	43.88588
4.1	74.14051	-5.55048	4.64	-14.692	15.11107	3.45	-14.1348	30.50934	5.29	0.32206	14.87876	2.58	0.77435	29.83831	5.88	1.244916	43.99081
4.1	74.05329	-5.72167	4.64	-14.6543	15.13473	3.45	-13.9637	30.49552	5.29	0.278442	14.86004	2.58	0.845831	29.80393	5.88	1.275438	44.00195
4.1	74.05859	-5.7061	4.64	-14.5813	15.21979	3.45	-13.8758	30.65086	5.29	0.321394	14.97916	2.58	0.876296	29.83779	5.88	1.306006	43.98318
4.1	74.00653	-5.95493	4.64	-14.6354	15.1613	3.45	-13.8054	30.53277	5.29	0.282113	14.919	2.58	0.926138	29.80096	5.88	1.365494	43.94658
4.1	73.99329	-6.12724	4.64	-14.6171	15.11801	3.45	-13.7884	30.41157	5.29	0.235464	14.87315	2.58	0.874898	29.74725	5.88	1.672598	43.8961
4.1	73.92224	-6.2287	4.64	-14.6758	15.13136	3.45	-13.8187	30.54451	5.29	0.153213	14.88514	2.58	0.934996	29.76677	5.88	1.604113	43.89021
4.1	73.96508	-6.43274	4.64	-14.6349	15.16415	3.45	-13.7502	30.36798	5.29	0.1837	14.81773	2.58	1.036981	29.72772	5.88	1.830308	43.7718
4.1	73.98689	-6.29492	4.64	-14.6703	15.08887	3.45	-13.7401	30.26895	5.29	0.264617	14.73448	2.58	0.981408	29.75291	5.88	1.642508	43.89949
4.1	74.09586	-5.95665	4.64	-14.5664	15.0355	3.45	-13.7394	30.13509	5.29	0.276493	14.9018	2.58	0.975442	29.83158	5.88	1.565306	43.8992
4.1	74.12567	-5.84062	4.64	-14.5223	15.06187	3.45	-13.8394	30.10592	5.29	0.339715	14.94931	2.58	1.005766	29.83439	5.88	1.635008	43.94396
4.1	74.1806	-5.74181	4.64	-14.5261	15.09271	3.45	-13.755	29.93851	5.29	0.365826	14.9704	2.58	1.007322	29.84001	5.88	1.629547	43.8552
4.1	74.15394	-6.20389	4.64	-14.319	15.09126	3.45	-13.6184	29.95944	5.29	0.405557	14.90189	2.58	1.2238	29.81976	5.88	1.858362	43.78608
4.1	74.19875	-6.10094	4.64	-14.278	15.10622	3.45	-13.5535	29.79194	5.29	0.441817	14.9164	2.58	1.216373	29.82242	5.88	1.742693	43.77921
4.1	74.19778	-6.20395	4.64	-14.314	15.05493	3.45	-13.5484	29.70737	5.29	0.421907	14.84463	2.58	1.249822	29.82152	5.88	1.908735	43.61512
4.1	74.12989	-6.24772	4.64	-14.2811	15.0801	3.45	-13.2486	30.0785	5.29	0.367281	14.83975	2.58	1.299737	29.78326	5.88	1.858088	43.51854
4.1	74.22219	-6.12713	4.64	-14.2281	15.02986	3.45	-13.1646	30.10791	5.29	0.52452	14.76407	2.58	1.309022	29.78514	5.88	1.994855	43.50046
4.1	74.27198	-5.95716	4.64	-14.1542	15.0992	3.45	-13.1113	30.16651	5.29	0.505512	14.92742	2.58	1.311676	29.85594	5.88	1.985792	43.4341
4.1	74.2842	-5.68581	4.64	-14.1479	15.09003	3.45	-12.9263	30.32668	5.29	0.443475	14.94672	2.58	1.295527	29.83062	5.88	2.096564	43.54197
4.1	74.3482	-6.04172	4.64	-13.9487	15.07693	3.45	-12.7874	30.41876	5.29	0.674328	14.81849	2.58	1.51121	29.87229	5.88	2.423433	43.52133
4.1	74.36354	-5.99849	4.64	-13.9184	15.0877	3.45	-12.8658	30.41659	5.29	0.622822	14.8236	2.58	1.554933	29.80242	5.88	2.533841	43.5563
4.1	74.3097	-5.93767	4.64	-13.9446	15.12545	3.45	-12.8646	30.41693	5.29	0.548307	14.88613	2.58	1.532975	29.83114	5.88	2.609859	43.60125
4.1	74.33695	-6.27246	4.64	-13.884	15.04927	3.45	-12.8096	30.26495	5.29	0.51297	14.75525	2.58	1.623318	29.69707	5.88	2.885441	43.42695
4.1	74.40321	-6.11232	4.64	-13.8586	15.0376	3.45	-12.7047	30.47318	5.29	0.627018	14.82496	2.58	1.656053	29.71494	5.88	2.880584	43.59724
4.1	74.48664	-5.92044	4.64	-13.7926	15.06564	3.45	-12.7276	30.44663	5.29	0.658406	14.82617	2.58	1.628181	29.73841	5.88	2.922109	43.63358
4.1	74.32318	-5.85166	4.64	-13.7852	15.07657	3.45	-12.6642	30.37591	5.29	0.594987	14.90645	2.58	1.649722	29.74474	5.88	2.897553	43.66587
4.1	74.35959	-5.96528	4.64	-13.6553	14.96285	3.45	-12.5074	30.69555	5.29	0.638464	14.80533	2.58	1.816326	29.68977	5.88	3.072902	43.61684
4.1	74.37216	-6.01353	4.64	-13.6439	15.04337	3.45	-12.4905	30.68545	5.29	0.662188	14.83586	2.58	1.901072	29.71139	5.88	3.205131	43.61952
4.1	74.33372	-6.07103	4.64	-13.7222	15.03856	3.45	-12.7306	30.74148	5.29	0.609965	14.78313	2.58	1.81087	29.73508	5.88	3.093935	43.59717
4.1	74.26966	-6.18092	4.64	-13.6475	14.94814	3.45	-12.7551	30.62231	5.29	0.635949	14.77923	2.58	1.895143	29.57029	5.88	3.230658	43.59205
4.1	74.3081	-6.2032	4.64	-13.5945	14.95745	3.45	-12.4021	30.80872	5.29	0.658468	14.72058	2.58	1.895276	29.58053	5.88	3.347401	43.51422
4.1	74.39924	-6.00341	4.64	-13.5804	14.99201	3.45	-12.2362	30.81198	5.29	0.716779	14.77023	2.58	1.943666	29.54744	5.88	3.321462	43.49456
4.1	74.40321	-5.56272	4.64	-13.6449	14.96439	3.45	-12.4309	30.69653	5.29	0.684566	14.81341	2.58	1.839585	29.61298	5.88	3.19637	43.40765
4.1	74.40532	-5.6667	4.64	-13.5774	14.96569	3.45	-12.4663	30.52633	5.29	0.744213	14.79164	2.58	1.8855	29.57115	5.88	3.158542	43.43924
4.1	74.47014	-5.60014	4.64	-13.5239	14.87215	3.45	-12.5662	30.38353	5.29	0.813156	14.79243	2.58	1.949081	29.47177	5.88	3.064289	43.40049
4.1	74.47903	-5.59131	4.64	-13.5327	14.90268	3.45	-12.4795	30.39417	5.29	0.812382	14.74192	2.58	1.952509	29.5578	5.88	3.539286	43.52773
4.1	74.43772	-5.62888	4.64	-13.5419	14.88503	3.45	-12.6665	30.23211	5.29	0.776084	14.71965	2.58	1.983074	29.40458	5.88	3.4522	43.60573
4.1	74.33662	-5.70236	4.64	-13.6284	14.82868	3.45	-12.6441	30.23103	5.29	0.63598	14.56814	2.58	1.903131	29.38244	5.88	3.390933	43.61673
4.1	74.30739	-5.52496	4.64	-13.5997	14.87692	3.45	-12.5202	30.49326	5.29	0.636762	14.59594	2.58	1.851809	29.4284	5.88	3.244517	43.63054
4.1	74.37024	-5.61419	4.64	-13.5365	14.91017	3.45	-12.4137	30.52562	5.29	0.695111	14.51065	2.58	1.956889	29.35434	5.88	3.307535	43.64133
4.1	74.393	-5.49749	4.64	-13.5351	14.89374	3.45	-12.5398	30.62584	5.29	0.749757	14.55748	2.58	1.956483	29.36985	5.88	3.266587	43.63178
4.1	74.48039	-5.40401	4.64	-13.5719	14.91003	3.45	-12.4939	30.64	5.29	0.73161	14.65963	2.58	2.011716	29.39063	5.88	3.119755	43.5991
4.1	74.46398	-5.15344	4.64	-13.5388	14.96252	3.45	-12.5943	30.63954	5.29	0.795034	14.76646	2.58	1.92943	29.38725	5.88	2.976429	43.65887
4.1	74.21652	-5.59711	4.64	-13.5967	14.85211	3.45	-12.4931	30.63398	5.29	0.783588	14.65162	2.58	2.016801	29.31583	5.88	3.167224	43.41125
4.1	74.21946	-5.66632	4.64	-13.5975	14.84163	3.45	-12.5998	30.62823	5.29	0.68325	14.56561	2.58	1.959694	29.21067	5.88	2.963434	43.24298
4.1	74.30306	-5.57551	4.64	-13.5227	14.87577	3.45	-12.6377	30.5937	5.29	0.85637	14.61547	2.58	2.079871	29.17261	5.88	3.175155	43.10554
4.1	74.19891	-5.3817	4.64	-13.6087	14.96693	3.45	-12.9005	30.53092	5.29	0.796365	14.64723	2.58	1.98989	29.21328	5.88	3.046101	43.19054
4.1	74.24221	-5.48582	4.64	-13.474	14.94824	3.45	-12.8256	30.42752	5.29	0.828823	14.62585	2.58	2.091667	29.14509	5.88	3.104688	42.94082
4.1	74.33751	-5.36425	4.64	-13.5066	14.98338	3.45	-12.9137	30.36889	5.29	0.941391	14.63076	2.58	2.105991	29.17164	5.88	3.234606	42.9463
4.1	74.47938	-5.2615	4.64	-13.5675	14.9396	3.45	-12.715	30.40083	5.29	0.901538	14.58607	2.58	2.110852	29.14095	5.88	3.439953	42.92649
4.1	74.50309	-5.23998	4.64	-13.6752	14.9785	3.45	-12.7964	30.48175	5.29	0.707273	14.5416	2.58	2.018522	29.16888	5.88	3.274584	42.9705
4.1	74.58926	-5.28625	4.64	-13.5552	14.97828	3.45	-12.8521	30.34885	5.29	0.757731	14.59328	2.58	2.069934	29.08586	5.88	3.048961	42.90161
4.1	74.42266	-5.47839	4.64	-13.66	14.78126	3.45	-12.7921	30.3718	5.29	0.935543	14.60618	2.58	2.132728	29.04283	5.88	3.3162	42.8099
4.1	74.41146	-5.18958	4.64	-13.7106	14.91162	3.45	-12.8968	30.34283	5.29	0.867262	14.68839	2.58	2.010754	29.08392	5.88	3.098021	42.84044
4.1	74.45805	-5.36779	4.64	-13.6978	14.82819	3.45	-12.934	30.18645	5.29	0.966896	14.67289	2.58	2.122013	29.02048	5.88	3.503034	42.89054
4.1	74.53203	-5.10628	4.64	-13.8046	14.74637	3.45	-12.723	30.16192	5.29	1.01727	14.69149	2.58	2.049948	28.98313	5.88	3.460278	42.98255
4.1	74.4751	-5.12684	4.64	-13.7927	14.74233	3.45	-12.8839	30.28342	5.29	1.024067	14.66637	2.58	1.992622	29.02702	5.88	3.266485	42.95173
4.1	74.51574	-4.96383	4.64	-13.8569	14.81574	3.45	-12.8852	30.32813	5.29	0.82722	14.78395	2.58	2.023785	29.03935	5.88	3.043088	43.0441
4.1	74.48886	-5.15104	4.64	-13.7916	14.73462	3.45	-12.7524	30.24236	5.29	0.849137	14.75779	2.58	2.118753	28.94367	5.88	3.093488	42.91285
4.1	74.47581	-5.3423	4.64	-13.8342	14.7317	3.45	-12.8026	30.17934	5.29	0.784879	14.70443	2.58	2.227557	28.88692	5.88	3.1076	42.76771
4.1	74.52467	-5.37507	4.64	-13.7075	14.82287	3.45	-12.651	30.28956	5.29	0.823589	14.70053	2.58	2.196735	28.88257	5.88	3.045728	42.54948
4.1	74.45367	-5.3416	4.64	-13.8093	14.77237	3.45	-12.657	30.27114	5.29	0.791235	14.71253	2.58	2.149338	28.85441	5.88	3.125413	42.66384
4.1	74.39608	-5.46879	4.64	-13.856	14.78586	3.45	-12.652	30.3079	5.29	0.883061	14.70665	2.58	2.185528	28.8251	5.88	2.99619	42.73152
4.1	74.4337	-5.40295	4.64	-13.839	14.72809	3.45	-12.5437	30.2227	5.29	0.919578	14.70871	2.58	2.215912	28.85131	5.88	3.190689	42.68617
4.1	74.52795	-5.05843	4.64	-13.8301	14.72701	3.45	-12.4663	30.17865	5.29	0.942187	14.85076	2.58	2.251635	28.90065	5.88	3.088695	42.69798
4.1	74.64055	-4.93638	4.64	-13.7305	14.79235	3.45	-12.4764	30.19338	5.29	1.112518	14.9383	2.58	2.300067	28.94485	5.88	3.142096	42.70766
4.1	74.70544	-4.64421	4.64	-13.782	14.83935	3.45	-12.6498	30.07971	5.29	0.928748	14.96214	2.58	2.187906	28.95883	5.88	2.96646	42.69374
4.1	74.90772	-4.64855	4.64	-13.7136	14.82072	3.45	-12.6843	30.09885	5.29	0.888524	14.91492	2.58	2.237266	28.91912	5.88	2.74915	42.65786
4.1	74.8691	-4.83549	4.64	-13.7402	14.74224	3.45	-12.591	29.97981	5.29	0.999432	14.89763	2.58	2.280079	28.84848	5.88	2.862951	42.6594
4.1	74.8479	-5.00998	4.64	-13.7192	14.75707	3.45	-12.5925	29.99691	5.29	0.874968	14.82085	2.58	2.305823	28.78159	5.88	2.648156	42.69779
4.1	74.78317	-4.86014	4.64	-13.7734	14.81392	3.45	-12.7284	29.9113	5.29	0.70132	14.80138	2.58	2.218606	28.86114	5.88	2.591905	42.511
4.1	74.78752	-4.77103	4.64	-13.7493	14.7769	3.45	-12.704	29.83531	5.29	0.78509	14.83117	2.58	2.281393	28.86558	5.88	2.527716	42.52933
4.1	74.87778	-4.7429	4.64	-13.637	14.76426	3.45	-12.3747	29.94778	5.29	0.85626	14.77246	2.58	2.341435	28.83686	5.88	2.440318	42.45374
4.1	74.82821	-4.91911	4.64	-13.6703	14.74729	3.45	-12.3697	29.7779	5.29	0.96282	14.79134	2.58	2.460415	28.76505	5.88	2.451479	42.22606
4.1	74.82625	-4.85205	4.64	-13.6196	14.75027	3.45	-12.4912	29.6736	5.29	0.965681	14.80784	2.58	2.439822	28.8293	5.88	2.455572	42.08506
4.1	74.8571	-4.83351	4.64	-13.61	14.74073	3.45	-12.5029	29.68096	5.29	0.89514	14.82896	2.58	2.409251	28.76977	5.88	2.509222	42.06216
4.1	74.85508	-4.95289	4.64	-13.592	14.74308	3.45	-12.5556	29.77396	5.29	0.946814	14.72359	2.58	2.371081	28.7132	5.88	2.568679	42.1909

pt12_Z	pt13_X	pt13_Y	pt13_Z	pt14_X	pt14_Y	pt14_Z	pt15_X	pt15_Y	pt15_Z	pt16_X	pt16_Y	pt16_Z	pt17_X	pt17_Y	pt17_Z	pt18_X	pt18_Y
8.52	20.23251	14.45137	3.02	21.08564	28.27083	7.73	22.00378	42.95673	16.57	22.55987	47.93175	18.83	38.99402	12.0462	3.29	40.4927	26.10087
8.52	20.11499	14.58535	3.02	20.95229	28.53326	7.73	21.71421	43.14381	16.57	22.24387	48.17089	18.83	38.88694	12.31806	3.29	40.27587	26.35214
8.52	20.11453	14.57797	3.02	20.93944	28.57097	7.73	21.74593	43.03297	16.57	22.14571	48.19858	18.83	38.85701	12.35191	3.29	40.2839	26.34994
8.52	20.09092	14.64694	3.02	20.97037	28.65897	7.73	21.56437	43.16881	16.57	21.89993	48.29809	18.83	38.90237	12.39872	3.29	40.28101	26.53918
8.52	20.145	14.71667	3.02	20.94535	28.69924	7.73	21.48686	43.20821	16.57	21.85594	48.12753	18.83	38.95228	12.37643	3.29	40.30953	26.58998
8.52	20.18214	14.68026	3.02	21.11314	28.70394	7.73	21.67489	43.27859	16.57	21.85228	48.15674	18.83	39.00625	12.371	3.29	40.45024	26.5479
8.52	20.17359	14.60358	3.02	21.16909	28.70155	7.73	21.76103	43.24799	16.57	21.83721	48.06466	18.83	39.00118	12.17664	3.29	40.46429	26.46791
8.52	20.19916	14.6089	3.02	21.23307	28.81441	7.73	21.76617	43.29292	16.57	21.83896	48.13966	18.83	39.00022	12.22459	3.29	40.60443	26.52524
8.52	20.19913	14.51482	3.02	21.30504	28.76934	7.73	21.8599	43.26016	16.57	21.79984	48.08244	18.83	38.95083	12.07193	3.29	40.6676	26.3605
8.52	20.17217	14.44184	3.02	21.36503	28.70599	7.73	21.87072	43.26534	16.57	22.01913	47.85517	18.83	38.91644	12.01442	3.29	40.70314	26.29724
8.52	20.09982	14.41887	3.02	21.32746	28.69928	7.73	21.84878	43.29439	16.57	21.89882	47.89722	18.83	38.8941	12.01704	3.29	40.7069	26.26998
8.52	20.16792	14.33241	3.02	21.34528	28.59374	7.73	22.00767	43.27204	16.57	21.89939	47.82711	18.83	38.95331	11.9155	3.29	40.80851	26.12103
8.52	20.16669	14.38903	3.02	21.29164	28.67498	7.73	21.96694	43.40498	16.57	21.90063	47.78518	18.83	38.93808	11.91151	3.29	40.78613	26.21088
8.52	20.13232	14.57848	3.02	21.32062	28.83223	7.73	21.80867	43.56648	16.57	21.69608	47.82099	18.83	38.99474	12.10637	3.29	40.75253	26.42167
8.52	20.15538	14.63918	3.02	21.32929	28.95149	7.73	21.90587	43.76826	16.57	21.43692	47.85318	18.83	39.02329	12.22743	3.29	40.8396	26.50185
8.52	20.21942	14.6381	3.02	21.37525	28.95248	7.73	21.84156	43.83758	16.57	21.37989	47.89341	18.83	38.9981	12.30254	3.29	40.83332	26.59445
8.52	20.2821	14.47168	3.02	21.5435	28.85823	7.73	22.1382	43.81258	16.57	21.73094	47.97459	18.83	39.04162	12.06843	3.29	41.04781	26.30692
8.52	20.32907	14.53032	3.02	21.56424	28.94789	7.73	22.07638	43.85059	16.57	21.60853	48.02804	18.83	39.02503	12.05018	3.29	41.00299	26.40293
8.52	20.37714	14.42771	3.02	21.65562	28.91697	7.73	22.1234	43.83259	16.57	21.56323	47.98182	18.83	39.05057	11.96864	3.29	41.12152	26.30845
8.52	20.3027	14.40483	3.02	21.60065	28.94589	7.73	22.26447	44.00266	16.57	21.39363	47.94473	18.83	39.04204	11.99507	3.29	41.17879	26.32605
8.52	20.34768	14.49108	3.02	21.64819	28.97361	7.73	22.28665	44.12395	16.57	21.2409	48.00132	18.83	39.0646	12.08956	3.29	41.19107	26.39917
8.52	20.31347	14.53262	3.02	21.63977	29.07557	7.73	22.22951	44.25312	16.57	21.07222	48.04049	18.83	39.06735	12.10002	3.29	41.23709	26.50138
8.52	20.25722	14.63506	3.02	21.62004	29.19801	7.73	22.21769	44.5226	16.57	20.93312	48.13473	18.83	39.12132	12.18756	3.29	41.16332	26.72627
8.52	20.33463	14.58644	3.02	21.786	29.1182	7.73	22.466	44.46089	16.57	21.04934	48.04883	18.83	39.24411	12.01914	3.29	41.39636	26.47194
8.52	20.43418	14.5079	3.02	21.75524	29.10634	7.73	22.58381	44.72346	16.57	21.29769	48.23928	18.83	39.21816	12.04255	3.29	41.44496	26.46994
8.52	20.33338	14.55369	3.02	21.69525	29.19102	7.73	22.58758	44.88105	16.57	21.2981	48.60295	18.83	39.14243	12.01759	3.29	41.39178	26.57329
8.52	20.40723	14.39031	3.02	21.80823	29.03821	7.73	22.74514	44.89143	16.57	21.40901	48.56815	18.83	39.19159	11.76361	3.29	41.47326	26.36968
8.52	20.40401	14.4676	3.02	21.81383	29.1411	7.73	22.67861	45.07928	16.57	21.38693	48.94935	18.83	39.23219	11.89091	3.29	41.54231	26.37309
8.52	20.39737	14.53469	3.02	21.79498	29.15368	7.73	22.50229	45.20164	16.57	21.20899	49.29867	18.83	39.2402	12.01857	3.29	41.51739	26.52764
8.52	20.33309	14.63986	3.02	21.73557	29.26518	7.73	22.37991	45.37702	16.57	21.01527	49.65721	18.83	39.19217	12.15011	3.29	41.53053	26.64927
8.52	20.3799	14.58728	3.02	21.7793	29.20656	7.73	22.65552	45.65201	16.57	21.17788	49.85462	18.83	39.32474	12.03721	3.29	41.6184	26.57108
8.52	20.45274	14.59495	3.02	21.85162	29.22246	7.73	22.67488	45.75263	16.57	21.14858	50.05036	18.83	39.3225	11.98763	3.29	41.65748	26.55627
8.52	20.40606	14.55071	3.02	21.77478	29.15879	7.73	22.53633	45.86267	16.57	20.98044	50.20818	18.83	39.19138	11.97868	3.29	41.65624	26.52065
8.52	20.38656	14.49897	3.02	21.7383	29.04975	7.73	22.52659	45.91389	16.57	20.9732	50.32018	18.83	39.17465	11.93427	3.29	41.62364	26.45558
8.52	20.35309	14.42551	3.02	21.76746	29.0652	7.73	22.38328	45.94513	16.57	21.12846	50.54382	18.83	39.20351	11.89319	3.29	41.62809	26.38735
8.52	20.3604	14.52621	3.02	21.79646	29.01589	7.73	22.30638	46.0749	16.57	21.0384	50.71568	18.83	39.20832	12.03617	3.29	41.71585	26.48724
8.52	20.26352	14.68554	3.02	21.57667	29.26003	7.73	21.9893	46.32243	16.57	20.76939	51.0967	18.83	39.18553	12.239	3.29	41.51413	26.7192
8.52	20.26943	14.60827	3.02	21.6346	29.15586	7.73	21.95526	46.29655	16.57	20.70648	51.03363	18.83	39.20781	12.15101	3.29	41.66074	26.64361
8.52	20.3344	14.64101	3.02	21.69147	29.16587	7.73	21.90864	46.32737	16.57	20.76307	51.12648	18.83	39.1675	12.19835	3.29	41.6486	26.69624
8.52	20.39626	14.595	3.02	21.64298	29.0709	7.73	21.9694	46.4637	16.57	20.71416	51.08066	18.83	39.17829	12.16474	3.29	41.67156	26.61497
8.52	20.33176	14.55815	3.02	21.57531	29.01818	7.73	21.89371	46.41446	16.57	20.72234	51.16555	18.83	39.13327	12.16524	3.29	41.67447	26.57663
8.52	20.22456	14.52743	3.02	21.44428	28.9769	7.73	21.79305	46.46405	16.57	20.63231	51.13074	18.83	39.15761	12.03082	3.29	41.55099	26.56743
8.52	20.15174	14.63397	3.02	21.44505	29.04241	7.73	21.49104	46.50858	16.57	20.5265	51.16961	18.83	39.18505	12.15527	3.29	41.42828	26.68743
8.52	20.16141	14.68054	3.02	21.43425	28.95403	7.73	21.62347	46.28468	16.57	20.52393	51.02634	18.83	39.18039	12.09335	3.29	41.51613	26.54125
8.52	20.17038	14.71144	3.02	21.39484	28.98115	7.73	21.48591	46.23136	16.57	20.83062	51.13209	18.83	39.19579	12.14309	3.29	41.53428	26.56995
8.52	20.2518	14.72535	3.02	21.51489	28.98569	7.73	21.32991	46.29709	16.57	20.78418	51.08509	18.83	39.16523	12.24537	3.29	41.50298	26.67533
8.52	20.14959	14.82641	3.02	21.32739	29.04896	7.73	21.11784	46.51296	16.57	20.79624	51.24927	18.83	39.15436	12.35544	3.29	41.3366	26.80347
8.52	20.15025	14.71211	3.02	21.36132	28.92683	7.73	21.45196	46.37078	16.57	21.05167	50.93838	18.83	39.13382	12.1982	3.29	41.4149	26.57252
8.52	20.1683	14.66534	3.02	21.46471	28.79382	7.73	21.48696	46.41353	16.57	20.83381	50.65399	18.83	39.14492	12.12988	3.29	41.37429	26.46494
8.52	20.23935	14.63952	3.02	21.41442	28.81102	7.73	21.5187	46.43137	16.57	20.7532	50.53824	18.83	39.16413	12.20747	3.29	41.29868	26.52909
8.52	20.12566	14.74543	3.02	21.31324	28.97595	7.73	21.40815	46.49122	16.57	20.54398	50.60835	18.83	39.01903	12.36252	3.29	41.17872	26.56733
8.52	20.18508	14.70762	3.02	21.45687	28.87734	7.73	21.58107	46.36891	16.57	20.62986	50.35548	18.83	39.17739	12.17965	3.29	41.22188	26.52804
8.52	20.19006	14.77906	3.02	21.43111	28.89421	7.73	21.55977	46.3062	16.57	20.57631	50.25764	18.83	39.26955	12.19916	3.29	41.24046	26.60755
8.52	20.14648	14.80227	3.02	21.38637	28.90495	7.73	21.62858	46.27123	16.57	20.53584	50.09895	18.83	39.26108	12.27913	3.29	41.21781	26.63879
8.52	20.04249	14.79635	3.02	21.30131	28.83828	7.73	21.61778	46.19254	16.57	20.49004	49.9661	18.83	39.08466	12.27221	3.29	41.1264	26.51834
8.52	19.99819	14.73311	3.02	21.36217	28.76786	7.73	21.72648	46.04875	16.57	20.40695	49.83553	18.83	39.12293	12.25858	3.29	41.15252	26.49379
8.52	20.10093	14.66572	3.02	21.36376	28.70994	7.73	21.79267	45.74387	16.57	20.7	49.62604	18.83	39.12325	12.18844	3.29	41.12132	26.34248
8.52	20.02	14.74671	3.02	21.39089	28.78596	7.73	21.80117	45.91485	16.57	20.59325	49.628	18.83	39.0137	12.41727	3.29	40.95373	26.54359
8.52	20.13504	14.6825	3.02	21.43212	28.66957	7.73	21.98296	45.73812	16.57	20.67852	49.33981	18.83	39.15798	12.2381	3.29	41.00205	26.38411
8.52	20.1042	14.77855	3.02	21.36019	28.78029	7.73	22.09681	45.82253	16.57	20.72808	49.25165	18.83	39.27817	12.27579	3.29	40.87003	26.53696
8.52	20.07256	14.80245	3.02	21.38823	28.71933	7.73	22.10443	45.68322	16.57	20.89379	49.09255	18.83	39.38328	12.25709	3.29	40.89523	26.48831
8.52	20.00894	14.89235	3.02	21.31627	28.85208	7.73	22.32195	45.79131	16.57	20.70627	48.97929	18.83	39.36372	12.34724	3.29	40.80393	26.6153
8.52	20.01143	14.80312	3.02	21.46417	28.63597	7.73	22.53315	45.58088	16.57	20.98443	48.81988	18.83	39.40232	12.2623	3.29	40.85814	26.4726
8.52	19.99606	14.76896	3.02	21.48871	28.56527	7.73	22.66429	45.42412	16.57	20.89231	48.47917	18.83	39.36594	12.22002	3.29	40.86539	26.36611
8.52	20.02766	14.75869	3.02	21.49493	28.5782	7.73	22.79539	45.18361	16.57	21.05517	48.37092	18.83	39.36434	12.22478	3.29	40.83752	26.28853
8.52	20.06703	14.80083	3.02	21.53928	28.51834	7.73	22.77836	44.99766	16.57	21.1325	48.28606	18.83	39.28122	12.26363	3.29	40.70147	26.28714
8.52	20.03401	14.77669	3.02	21.48632	28.50497	7.73	22.85214	44.85521	16.57	21.38904	47.95961	18.83	39.23971	12.11577	3.29	40.65866	26.19941
8.52	20.04352	14.75639	3.02	21.49699	28.44311	7.73	22.87035	44.64111	16.57	21.19818	47.64265	18.83	39.28803	12.15969	3.29	40.71151	26.21703
8.52	20.08932	14.90739	3.02	21.52597	28.57594	7.73	22.88936	44.5135	16.57	21.0638	47.57364	18.83	39.28865	12.37392	3.29	40.65509	26.43156
8.52	20.20744	14.99677	3.02	21.58934	28.70276	7.73	22.99044	44.34628	16.57	21.20573	47.43811	18.83	39.29635	12.48799	3.29	40.78254	26.561
8.52	20.16829	15.14251	3.02	21.51002	28.72869	7.73	22.98648	44.36156	16.57	21.0324	47.4818	18.83	39.24389	12.54275	3.29	40.64573	26.80069
8.52	20.15801	15.11734	3.02	21.61511	28.727	7.73	23.17362	44.39398	16.57	21.0791	47.28284	18.83	39.31583	12.55724	3.29	40.64346	26.77329
8.52	20.15035	15.0235	3.02	21.64376	28.53769	7.73	23.31164	44.08384	16.57	21.13782	46.95828	18.83	39.31364	12.45878	3.29	40.62795	26.65437
8.52	20.09489	14.96626	3.02	21.6371	28.53103	7.73	23.45487	43.88887	16.57	21.16913	46.63892	18.83	39.19272	12.37191	3.29	40.67276	26.55066
8.52	19.9654	15.06662	3.02	21.604	28.53121	7.73	23.40228	43.818	16.57	21.18876	46.91488	18.83	39.16111	12.34582	3.29	40.49152	26.65158
8.52	19.9437	15.07524	3.02	21.53133	28.59547	7.73	23.36198	43.62672	16.57	21.28102	46.98946	18.83	39.37013	12.30196	3.29	40.58151	26.70565
8.52	20.16574	15.09764	3.02	21.68322	28.52948	7.73	23.37216	43.39563	16.57	21.16586	47.12497	18.83	39.53102	12.24463	3.29	40.60637	26.71434
8.52	20.17689	14.98734	3.02	21.68524	28.4276	7.73	23.32057	43.06049	16.57	21.51691	46.96451	18.83	39.53803	12.17204	3.29	40.60646	26.59727
8.52	20.07076	15.13153	3.02	21.76658	28.44193	7.73	23.47707	43.14688	16.57	21.42469	47.14906	18.83	39.40003	12.30589	3.29	40.64844	26.65154
8.52	20.11087	15.19359	3.02	21.76493	28.4543	7.73	23.41958	43.04265	16.57	21.2008	47.11287	18.83	39.2785	12.35081	3.29	40.56096	26.66885
8.52	20.03637	15.11856	3.02	21.82508	28.34501	7.73	23.51879	42.97868	16.57	21.36768	47.07511	18.83	39.30372	12.20674	3.29	40.55621	26.63136

pt18_Z	pt19_X	pt19_Y	pt19_Z	pt20_X	pt20_Y	pt20_Z	pt21_X	pt21_Y	pt21_Z	pt22_X	pt22_Y	pt22_Z	pt23_X	pt23_Y	pt23_Z	pt24_X	pt24_Y
8.59	42.255	41.32032	20.41	43.6719	47.22761	28.19	57.64594	8.814449	3.87	59.63687	23.08073	11.25	60.65012	37.66587	24.52	61.83263	46.56673
8.59	42.21317	41.50279	20.41	43.58142	47.12065	28.19	57.6632	8.992287	3.87	59.43799	23.30705	11.25	60.57075	38.03824	24.52	62.16051	46.49816
8.59	42.43521	41.51774	20.41	43.64237	46.90194	28.19	57.63486	9.012503	3.87	59.39054	23.43013	11.25	60.64896	38.08536	24.52	62.40179	46.45609
8.59	42.46687	41.35745	20.41	43.27734	46.78445	28.19	57.7457	9.023318	3.87	59.24484	23.66029	11.25	60.76207	38.41051	24.52	62.81399	46.5749
8.59	42.5408	41.32381	20.41	43.31741	46.44266	28.19	57.69003	9.089435	3.87	59.22898	23.73759	11.25	61.17896	38.71316	24.52	63.24718	46.47215
8.59	42.85445	41.03812	20.41	43.23469	46.08118	28.19	57.6674	9.026049	3.87	59.45671	23.72176	11.25	61.52119	38.78627	24.52	63.20846	46.37463
8.59	43.09156	40.78822	20.41	43.23805	45.74432	28.19	57.62666	8.912513	3.87	59.55338	23.59516	11.25	61.87776	38.75916	24.52	63.81488	45.97232
8.59	43.19953	40.68186	20.41	43.54789	45.77301	28.19	57.67379	8.817208	3.87	59.66593	23.69086	11.25	62.10628	38.77061	24.52	64.34916	45.5172
8.59	43.40565	40.38384	20.41	43.83646	45.36867	28.19	57.66889	8.564821	3.87	59.59978	23.5458	11.25	62.36464	38.5729	24.52	64.6326	45.01747
8.59	43.41686	40.05485	20.41	43.55717	45.13995	28.19	57.57965	8.475305	3.87	59.54081	23.51831	11.25	62.59856	38.48034	24.52	64.88639	44.4213
8.59	43.48439	39.93463	20.41	43.63213	44.81376	28.19	57.51138	8.419402	3.87	59.54816	23.46908	11.25	62.78475	38.43831	24.52	65.05936	43.97394
8.59	43.69204	39.5414	20.41	43.98198	44.75237	28.19	57.55975	8.205893	3.87	59.72921	23.32183	11.25	63.11707	37.74361	24.52	65.46528	43.49766
8.59	43.82875	39.5587	20.41	43.7451	44.70087	28.19	57.57661	8.303806	3.87	59.65649	23.57333	11.25	63.38454	37.81442	24.52	65.62617	43.41197
8.59	43.67861	39.57166	20.41	43.79993	44.84797	28.19	57.66173	8.563415	3.87	59.6956	23.74097	11.25	63.35071	37.93705	24.52	65.49644	43.18741
8.59	43.78743	39.60449	20.41	43.58476	44.91504	28.19	57.70562	8.670058	3.87	59.64018	23.88209	11.25	63.53697	37.97063	24.52	65.79585	43.04666
8.59	43.79372	39.50128	20.41	43.53139	44.76454	28.19	57.71992	8.727452	3.87	59.55595	24.05687	11.25	63.68247	37.95842	24.52	65.86347	42.90048
8.59	43.92456	39.16515	20.41	43.65654	44.54367	28.19	57.76374	8.370728	3.87	59.74189	23.62355	11.25	64.32178	37.62912	24.52	66.22263	42.27641
8.59	43.94971	39.0778	20.41	43.45341	44.47093	28.19	57.74521	8.470427	3.87	59.75061	23.85462	11.25	64.43258	37.61103	24.52	66.35586	42.0454
8.59	43.96349	38.72312	20.41	43.35576	44.33104	28.19	57.71029	8.361587	3.87	59.91781	23.5985	11.25	64.64923	37.46356	24.52	66.35581	41.84838
8.59	44.05258	38.65345	20.41	43.16157	44.31723	28.19	57.74342	8.278598	3.87	59.90458	23.52988	11.25	64.74798	37.25523	24.52	66.39469	41.65395
8.59	44.11508	38.59369	20.41	42.96871	44.41814	28.19	57.75623	8.332617	3.87	60.06381	23.73407	11.25	64.83929	37.24564	24.52	66.48111	41.64146
8.59	44.06063	38.49673	20.41	42.94878	44.39352	28.19	57.78657	8.474328	3.87	60.0303	23.81714	11.25	64.93174	37.26685	24.52	66.71919	41.62977
8.59	43.95124	38.57576	20.41	42.60594	44.3586	28.19	57.77505	8.766955	3.87	60.21549	24.10456	11.25	65.21774	37.82573	24.52	66.58329	41.77245
8.59	44.15553	38.25506	20.41	42.58067	44.01379	28.19	58.05137	8.681599	3.87	60.47747	23.78446	11.25	65.54876	37.33368	24.52	66.78621	41.41358
8.59	44.09495	38.13217	20.41	42.45828	44.06645	28.19	58.11152	8.638761	3.87	60.50615	23.82712	11.25	65.52784	37.3412	24.52	67.1221	41.11396
8.59	43.97087	38.31439	20.41	42.17539	44.12355	28.19	58.03557	8.65799	3.87	60.53294	23.93597	11.25	65.42137	37.21135	24.52	67.10321	41.2033
8.59	44.22008	37.97223	20.41	42.14818	43.579	28.19	58.01287	8.341998	3.87	60.66481	23.51948	11.25	65.71081	36.75894	24.52	67.30715	40.7856
8.59	44.18327	38.04543	20.41	41.90067	43.64877	28.19	57.9821	8.455826	3.87	60.77183	23.55289	11.25	65.71506	36.67806	24.52	67.2244	40.90321
8.59	44.13466	38.23169	20.41	42.02907	43.69839	28.19	58.06124	8.533129	3.87	60.73779	23.83944	11.25	65.87102	36.79893	24.52	67.05434	40.9051
8.59	44.01599	38.41835	20.41	41.86058	43.68858	28.19	58.03694	8.618092	3.87	60.80989	24.00216	11.25	65.79941	36.90607	24.52	66.85354	40.9498
8.59	44.20655	38.56154	20.41	41.79594	43.68488	28.19	58.07411	8.553867	3.87	60.88151	23.98955	11.25	66.05682	36.70004	24.52	67.09102	40.85739
8.59	44.13186	38.70637	20.41	41.84236	43.99728	28.19	58.08971	8.561885	3.87	60.89005	24.00449	11.25	66.173	36.52379	24.52	67.16188	40.58214
8.59	44.01721	38.79833	20.41	41.76969	44.24244	28.19	58.00799	8.603474	3.87	60.86749	23.93087	11.25	66.07812	36.33123	24.52	67.04511	40.36396
8.59	43.94384	38.9457	20.41	41.66696	44.63715	28.19	58.00198	8.460133	3.87	60.81462	23.90572	11.25	66.14406	36.17727	24.52	67.15967	40.0991
8.59	43.864	39.1376	20.41	41.67169	45.282	28.19	58.10276	8.40104	3.87	61.01223	23.89153	11.25	66.26606	35.99151	24.52	67.18446	39.96625
8.59	43.7885	39.45729	20.41	41.60235	46.06465	28.19	58.09463	8.508172	3.87	60.88041	24.11108	11.25	66.1556	35.9253	24.52	67.02279	39.98024
8.59	43.53321	39.94362	20.41	41.3455	47.00276	28.19	57.99643	8.87368	3.87	61.02409	24.35354	11.25	66.02753	36.08996	24.52	66.76189	40.19152
8.59	43.49348	40.03571	20.41	41.52788	47.34524	28.19	58.00255	8.84254	3.87	61.19788	24.41798	11.25	66.08516	35.83435	24.52	66.80322	39.91054
8.59	43.60407	40.12223	20.41	41.57898	48.15103	28.19	58.22984	8.591642	3.87	61.20055	24.4148	11.25	66.0255	35.7814	24.52	66.72883	39.67897
8.59	43.59397	40.21683	20.41	41.5736	48.62201	28.19	58.17994	8.611966	3.87	61.2331	24.18309	11.25	66.01148	35.63864	24.52	66.74992	39.56658
8.59	43.50489	40.37303	20.41	41.49028	49.2743	28.19	58.1287	8.612356	3.87	61.37206	24.04326	11.25	66.16211	35.59332	24.52	66.60503	39.43172
8.59	43.60309	40.71296	20.41	41.55593	49.49394	28.19	58.09631	8.572226	3.87	61.10471	24.06301	11.25	66.00312	35.57782	24.52	66.52514	39.49292
8.59	43.47458	41.0507	20.41	41.50731	50.2216	28.19	58.10217	8.693224	3.87	61.07553	24.28598	11.25	66.05297	35.7837	24.52	66.48778	39.73616
8.59	43.41128	41.06443	20.41	41.40452	50.63784	28.19	58.11571	8.640125	3.87	61.21326	24.20407	11.25	66.05767	35.69015	24.52	66.39405	39.99633
8.59	43.27185	41.22969	20.41	41.29835	50.95615	28.19	58.14394	8.697627	3.87	61.30094	24.25816	11.25	65.94022	35.79858	24.52	66.22802	40.5024
8.59	43.19564	41.41529	20.41	41.12046	51.34658	28.19	58.17225	8.797405	3.87	61.34122	24.34804	11.25	66.07483	35.76272	24.52	66.09157	41.06672
8.59	42.98347	41.72476	20.41	40.93384	51.99442	28.19	58.13206	8.968722	3.87	61.17722	24.5275	11.25	65.9421	36.05139	24.52	65.16997	42.31779
8.59	42.97479	41.57758	20.41	40.9374	52.15614	28.19	58.13662	8.702292	3.87	61.24326	24.22164	11.25	65.99808	35.82489	24.52	65.25308	42.80276
8.59	42.83062	41.53399	20.41	40.6526	52.28736	28.19	58.13735	8.631243	3.87	61.33886	24.20949	11.25	65.8394	35.80157	24.52	65.03146	43.33095
8.59	42.74907	41.64417	20.41	40.55085	52.64139	28.19	58.2004	8.679343	3.87	61.18735	24.31322	11.25	65.90453	36.13252	24.52	64.96337	44.00438
8.59	42.44332	41.97142	20.41	40.47972	52.92114	28.19	58.11062	8.868737	3.87	61.10052	24.39144	11.25	65.84653	36.73126	24.52	64.82396	44.66084
8.59	42.42183	41.8693	20.41	40.39749	52.91861	28.19	58.16248	8.787386	3.87	61.08588	24.39573	11.25	65.91228	36.80548	24.52	64.67117	45.20121
8.59	42.25277	42.00788	20.41	40.17409	52.99783	28.19	58.21373	8.902387	3.87	61.03811	24.63591	11.25	65.82929	37.17193	24.52	64.57991	45.87584
8.59	42.07802	42.06301	20.41	40.36977	53.13474	28.19	58.25565	8.946839	3.87	60.96576	24.68476	11.25	65.66082	37.43796	24.52	64.39393	46.45893
8.59	41.83202	42.07324	20.41	40.05104	53.10339	28.19	58.16592	8.948186	3.87	61.0039	24.49178	11.25	65.39849	37.60999	24.52	64.35102	46.72473
8.59	41.7819	42.04751	20.41	40.07568	53.04469	28.19	58.22859	8.901072	3.87	60.9675	24.58209	11.25	65.12053	37.84116	24.52	64.21254	47.05061
8.59	41.73805	42.01382	20.41	40.08507	52.91307	28.19	58.2463	8.742337	3.87	60.85963	24.58536	11.25	65.03622	37.85517	24.52	64.0528	47.23505
8.59	41.42479	42.18222	20.41	39.87664	52.9753	28.19	58.21359	9.005677	3.87	60.90039	24.63575	11.25	64.73876	38.25075	24.52	63.63702	47.8172
8.59	41.43568	42.06949	20.41	39.91038	52.82136	28.19	58.28633	8.811039	3.87	60.97949	24.46368	11.25	64.72265	38.3273	24.52	63.59732	47.77768
8.59	41.20914	42.19425	20.41	40.08914	53.22766	28.19	58.28741	9.037447	3.87	60.85832	24.75987	11.25	64.50937	38.69669	24.52	63.21997	48.11484
8.59	41.00482	42.24242	20.41	40.09679	53.10389	28.19	58.29843	9.044397	3.87	60.9125	24.61332	11.25	64.30552	38.80639	24.52	62.92051	48.16429
8.59	40.79726	42.36844	20.41	39.94047	53.16574	28.19	58.22968	9.165025	3.87	60.87309	24.61478	11.25	64.0522	39.02734	24.52	62.46411	48.39562
8.59	40.85515	42.25351	20.41	40.3529	52.84386	28.19	58.28535	9.02686	3.87	60.88599	24.43938	11.25	63.99227	38.92051	24.52	62.45437	48.1971
8.59	40.88127	42.19162	20.41	40.42309	52.58734	28.19	58.35528	8.920761	3.87	60.89483	24.27085	11.25	63.86731	38.8371	24.52	62.3166	48.05094
8.59	40.85343	42.15142	20.41	40.65886	52.50189	28.19	58.36029	8.829256	3.87	60.97395	24.22066	11.25	63.70177	38.85166	24.52	62.14552	48.02281
8.59	40.80403	42.24829	20.41	40.96903	52.392	28.19	58.34624	8.861599	3.87	60.77049	24.22107	11.25	63.498	38.87872	24.52	61.84892	48.01346
8.59	40.82931	42.14391	20.41	41.11946	52.19228	28.19	58.30699	8.814057	3.87	60.56583	24.1695	11.25	63.31426	38.77826	24.52	61.74387	47.88201
8.59	40.80345	42.32564	20.41	41.09055	52.09611	28.19	58.34033	8.872027	3.87	60.64636	24.11515	11.25	63.12886	38.86333	24.52	61.51641	47.94381
8.59	40.75147	42.45125	20.41	41.08652	52.14511	28.19	58.43323	9.177451	3.87	60.65983	24.34743	11.25	62.93899	39.08546	24.52	60.82731	48.47595
8.59	40.78903	42.5594	20.41	41.23628	52.04659	28.19	58.51554	9.236788	3.87	60.59815	24.48165	11.25	62.80902	39.18516	24.52	60.44766	48.69976
8.59	40.74995	42.82506	20.41	41.45471	52.02874	28.19	58.45649	9.445999	3.87	60.61345	24.58837	11.25	62.48282	39.39922	24.52	60.09	49.00852
8.59	40.91699	42.74536	20.41	41.663	51.75812	28.19	58.47537	9.467688	3.87	60.64009	24.57183	11.25	62.34852	39.38077	24.52	59.5755	49.13019
8.59	41.10801	42.63593	20.41	41.82771	51.32748	28.19	58.48653	9.282267	3.87	60.51163	24.41133	11.25	62.29435	39.08992	24.52	59.49245	48.96058
8.59	41.21061	42.44117	20.41	42.04966	50.98955	28.19	58.44222	9.19236	3.87	60.3882	24.33874	11.25	62.21135	38.90178	24.52	59.4048	48.87412
8.59	41.12846	42.45724	20.41	42.04709	50.71456	28.19	58.41956	9.351344	3.87	60.24579	24.32441	11.25	61.97455	38.90461	24.52	59.65119	48.88694
8.59	41.22716	42.38241	20.41	42.52985	50.50932	28.19	58.44145	9.415237	3.87	60.16613	24.39312	11.25	61.92233	38.92789	24.52	59.7576	48.88637
8.59	41.2977	42.27381	20.41	42.77705	50.25867	28.19	58.52284	9.438683	3.87	60.07834	24.41267	11.25	61.84115	38.90829	24.52	59.98028	48.7687
8.59	41.62384	42.25618	20.41	43.14139	49.66253	28.19	58.5567	9.223168	3.87	60.17346	24.3135	11.25	61.84324	38.65808	24.52	60.17861	48.63836
8.59	41.73147	42.1218	20.41	43.29872	49.54277	28.19	58.58268	9.323659	3.87	60.1523	24.28481	11.25	61.94387	38.79154	24.52	60.0691	48.70248
8.59	41.92554	42.23113	20.41	43.38365	49.27578	28.19	58.52024	9.36117	3.87	60.04444	24.35019	11.25	61.86554	38.8714	24.52	60.78415	48.35752
8.59	42.33069	42.09303	20.41	43.47683	48.77004	28.19	58.50868	9.243188	3.87	59.94796	24.21255	11.25	61.91223	38.80437	24.52	60.77237	48.24464

pt24_Z	pt25_X	pt25_Y	pt25_Z	pt26_X	pt26_Y	pt26_Z	pt27_X	pt27_Y	pt27_Z	pt28_X	pt28_Y	pt28_Z	pt29_X	pt29_Y	pt29_Z	pt30_X	pt30_Y
31.68	74.44085	3.709679	6.55	76.22066	20.07592	15.86	76.979	30.6622	22.64	77.19361	33.21458	29.96	96.71154	7.278198	14.93	91.50886	24.28991
31.68	74.33011	4.034095	6.55	76.1635	20.21456	15.86	76.7	31.06604	22.64	77.02878	33.66955	29.96	96.83481	7.641523	14.93	91.27783	24.67652
31.68	74.58299	3.816108	6.55	76.03945	20.1448	15.86	76.6275	31.09823	22.64	76.99046	33.81579	29.96	96.86993	7.367289	14.93	91.0165	24.57444
31.68	74.5079	4.050637	6.55	75.88833	20.1891	15.86	76.47838	31.31391	22.64	76.9025	34.16401	29.96	96.49036	7.899829	14.93	90.81154	24.65092
31.68	74.58321	4.112793	6.55	75.77848	20.12739	15.86	76.37232	31.43004	22.64	77.10534	34.08216	29.96	96.41221	7.859294	14.93	91.16966	24.33168
31.68	74.62321	4.002341	6.55	75.80002	19.90154	15.86	76.42668	31.3009	22.64	77.29649	33.99643	29.96	96.38271	7.796201	14.93	91.11425	23.89675
31.68	74.56688	3.801094	6.55	75.74347	19.63054	15.86	76.3474	31.17715	22.64	77.52264	33.86232	29.96	96.39991	7.311729	14.93	91.1556	23.37842
31.68	74.51134	3.821961	6.55	75.82514	19.47104	15.86	76.45006	31.23111	22.64	77.60069	34.04431	29.96	96.34514	7.351818	14.93	91.06298	23.00691
31.68	74.46913	3.566562	6.55	75.70599	19.13987	15.86	76.55255	31.00243	22.64	77.83613	33.88202	29.96	96.31156	6.97057	14.93	91.06359	22.29209
31.68	74.43093	3.429002	6.55	75.58852	18.9219	15.86	76.64379	30.88494	22.64	77.72774	33.97439	29.96	96.25406	6.934159	14.93	91.0728	21.74803
31.68	74.34545	3.317133	6.55	75.57131	18.69847	15.86	76.73322	30.887	22.64	78.18805	33.66158	29.96	96.3407	6.56467	14.93	90.87452	21.06706
31.68	74.35397	3.14574	6.55	75.65383	18.44809	15.86	76.91457	30.80865	22.64	78.39395	33.37317	29.96	96.42542	6.348862	14.93	90.7388	20.38597
31.68	74.32544	3.241933	6.55	75.56918	18.56353	15.86	77.02733	31.06671	22.64	78.48091	33.68838	29.96	96.42186	6.626422	14.93	90.74496	20.00484
31.68	74.37787	3.592839	6.55	75.57723	18.77785	15.86	77.33065	31.64523	22.64	78.63031	34.07338	29.96	96.39852	7.17229	14.93	90.67633	20.13068
31.68	74.4217	3.676401	6.55	75.54186	18.96531	15.86	77.4609	31.82904	22.64	78.76899	34.28127	29.96	96.50433	7.229441	14.93	90.45641	20.06548
31.68	74.35337	3.733798	6.55	75.50035	19.05577	15.86	77.57479	31.91689	22.64	78.85773	34.3932	29.96	96.52954	7.341861	14.93	90.39984	19.9125
31.68	74.38497	3.297149	6.55	75.56638	18.54392	15.86	77.86431	31.48821	22.64	79.18594	33.95048	29.96	96.42337	6.765137	14.93	90.36526	19.19364
31.68	74.39846	3.424212	6.55	75.57209	18.66785	15.86	78.01921	31.83699	22.64	79.17415	34.19123	29.96	96.38204	7.098476	14.93	90.16162	19.34786
31.68	74.43497	3.284533	6.55	75.57114	18.60953	15.86	78.14623	31.68412	22.64	79.4864	33.91444	29.96	96.60549	6.516177	14.93	90.31149	19.0634
31.68	74.39551	3.192194	6.55	75.51527	18.55324	15.86	78.26473	31.6484	22.64	79.66671	33.83024	29.96	96.63178	6.258132	14.93	90.15698	19.11874
31.68	74.44735	3.35328	6.55	75.56214	18.65312	15.86	78.5621	31.90078	22.64	79.95967	34.23239	29.96	96.48291	6.246071	14.93	90.27674	19.05606
31.68	74.37776	3.50177	6.55	75.56968	18.91985	15.86	78.66992	32.02672	22.64	80.21405	34.19566	29.96	96.62608	6.368241	14.93	90.12627	19.32033
31.68	74.35124	3.784385	6.55	75.54822	19.18601	15.86	78.68102	32.30745	22.64	80.11666	34.70039	29.96	96.51852	6.674591	14.93	89.98937	19.78926
31.68	74.41324	3.464472	6.55	75.64832	18.92408	15.86	79.23882	32.19746	22.64	80.62505	34.12362	29.96	96.63397	6.128485	14.93	90.24259	19.04547
31.68	74.47313	3.44223	6.55	75.67335	18.93868	15.86	79.32784	32.21253	22.64	80.76079	34.13701	29.96	96.74379	5.937169	14.93	90.22034	19.29485
31.68	74.38086	3.499744	6.55	75.65428	19.06527	15.86	79.34114	32.29439	22.64	80.90704	33.98088	29.96	96.69335	5.891576	14.93	90.37171	19.15486
31.68	74.41658	3.177668	6.55	75.74033	18.75377	15.86	79.51814	31.9346	22.64	81.02785	33.73833	29.96	96.67657	5.277379	14.93	90.40434	18.94297
31.68	74.52608	3.257393	6.55	75.83845	18.88293	15.86	79.91377	32.16566	22.64	81.08627	34.08726	29.96	96.59356	5.277096	14.93	90.30708	19.20642
31.68	74.53708	3.456054	6.55	75.81024	19.16651	15.86	79.92994	32.47544	22.64	81.33479	34.14411	29.96	96.53298	5.403531	14.93	90.33474	19.63334
31.68	74.50612	3.62942	6.55	75.70716	19.2733	15.86	79.76082	32.77246	22.64	81.57888	34.15776	29.96	96.3786	5.401282	14.93	90.04382	20.02072
31.68	74.54062	3.565979	6.55	75.73173	19.26281	15.86	79.96156	32.61902	22.64	81.79901	33.90688	29.96	96.5103	4.789925	14.93	90.08718	20.10732
31.68	74.51665	3.535229	6.55	75.80866	19.23907	15.86	80.00526	32.54287	22.64	81.95462	33.78725	29.96	96.41011	4.547757	14.93	90.0706	20.22073
31.68	74.46679	3.497243	6.55	75.73288	19.30351	15.86	80.03806	32.42677	22.64	81.86426	33.63534	29.96	96.38319	4.277567	14.93	89.91175	20.33971
31.68	74.36826	3.438016	6.55	75.82219	19.17862	15.86	80.31221	32.28149	22.64	81.82614	33.48542	29.96	95.91297	3.977718	14.93	89.92476	20.20055
31.68	74.347	3.423609	6.55	75.8939	19.20067	15.86	80.47302	32.16435	22.64	81.86836	33.48852	29.96	95.9347	3.835483	14.93	90.1065	20.1149
31.68	74.38195	3.587502	6.55	75.99129	19.44142	15.86	80.76683	32.26573	22.64	81.70274	33.80813	29.96	95.88484	3.917585	14.93	90.09806	20.28677
31.68	74.46582	3.941548	6.55	75.88194	19.94171	15.86	80.62556	32.67935	22.64	81.83362	34.04854	29.96	95.82853	4.342232	14.93	90.07771	20.7077
31.68	74.47173	3.854836	6.55	75.995	19.87832	15.86	80.94651	32.40725	22.64	82.22907	33.68855	29.96	95.8163	4.063512	14.93	90.45736	20.26904
31.68	74.51914	3.919674	6.55	76.08352	20.02867	15.86	80.95753	32.45819	22.64	82.38096	33.76469	29.96	95.61662	4.069106	14.93	90.34536	20.44655
31.68	74.47153	3.891345	6.55	76.07777	20.00418	15.86	81.09117	32.78197	22.64	82.68678	33.60113	29.96	95.76611	3.747014	14.93	90.49249	20.2245
31.68	74.45555	3.876965	6.55	76.12465	19.93484	15.86	81.34521	32.65482	22.64	82.64925	33.4707	29.96	95.42245	3.73407	14.93	90.45227	20.31915
31.68	74.39376	3.866509	6.55	76.0307	20.07581	15.86	81.1759	32.77386	22.64	82.54846	33.54634	29.96	95.39406	3.627334	14.93	90.28761	20.49072
31.68	74.26203	4.181713	6.55	76.04754	20.27197	15.86	80.92176	33.11232	22.64	82.26039	33.92412	29.96	95.40381	3.799353	14.93	90.48191	20.45545
31.68	74.33148	4.107713	6.55	76.0596	20.19845	15.86	81.27618	32.73313	22.64	82.471	33.79257	29.96	95.31418	3.92399	14.93	90.38052	20.62935
31.68	74.36645	3.923763	6.55	76.11032	20.194	15.86	81.50004	32.68329	22.64	82.34841	34.1659	29.96	95.50327	3.864911	14.93	90.65624	20.53836
31.68	74.34975	4.043572	6.55	76.1828	20.39976	15.86	81.46699	32.84647	22.64	82.45004	34.27688	29.96	95.32229	3.870774	14.93	90.73525	20.57792
31.68	74.27608	4.301174	6.55	76.11435	20.68887	15.86	81.453	33.05788	22.64	82.41428	34.4662	29.96	95.21488	4.418723	14.93	90.85546	20.85823
31.68	74.23838	3.988686	6.55	76.23089	20.33091	15.86	81.4968	32.7478	22.64	82.41355	34.15602	29.96	95.17408	3.947417	14.93	90.91676	20.65157
31.68	74.24488	3.950217	6.55	76.25218	20.31155	15.86	81.55977	32.70176	22.64	82.4536	33.87505	29.96	95.11764	4.000638	14.93	90.79494	20.72372
31.68	74.2966	4.138987	6.55	76.38436	20.54323	15.86	81.71567	32.65785	22.64	82.3103	33.93293	29.96	94.93343	4.002886	14.93	90.99759	20.65336
31.68	74.22563	4.27874	6.55	76.32982	20.79129	15.86	81.50605	32.95196	22.64	82.3197	34.09829	29.96	94.78779	4.334323	14.93	90.81821	21.0878
31.68	74.286	4.17023	6.55	76.52995	20.70299	15.86	81.72946	32.7352	22.64	82.59751	33.91159	29.96	94.89908	4.182308	14.93	90.78463	21.13186
31.68	74.49396	4.267162	6.55	76.76017	20.80182	15.86	81.63586	32.94074	22.64	82.62832	34.08558	29.96	95.19202	4.172239	14.93	91.23472	21.04741
31.68	74.55828	4.408785	6.55	76.78644	20.92454	15.86	81.74914	32.96776	22.64	82.68548	34.1682	29.96	95.12917	4.315196	14.93	91.52321	21.09205
31.68	74.39165	4.377276	6.55	76.74388	20.96286	15.86	81.74402	32.90481	22.64	82.36239	34.27355	29.96	95.16125	4.338391	14.93	91.41915	21.22347
31.68	74.33816	4.248598	6.55	76.8919	20.95284	15.86	81.83403	32.84744	22.64	82.61004	34.11237	29.96	95.25878	4.133593	14.93	91.40977	21.39342
31.68	74.33698	4.069424	6.55	77.00807	20.81871	15.86	81.75041	32.7397	22.64	82.58046	34.0482	29.96	95.46525	3.939665	14.93	91.16581	21.47945
31.68	74.3048	4.349348	6.55	76.97065	21.18626	15.86	81.7661	33.0172	22.64	82.33664	34.56253	29.96	95.27066	4.375176	14.93	91.45114	21.5282
31.68	74.34688	4.10392	6.55	77.18523	21.03767	15.86	81.92258	32.85857	22.64	82.51384	34.36755	29.96	95.25397	4.298697	14.93	91.83122	21.28765
31.68	74.30877	4.402679	6.55	77.21098	21.29462	15.86	81.77226	33.28692	22.64	82.30165	34.84853	29.96	95.13449	4.469283	14.93	91.8127	21.82131
31.68	74.26866	4.407816	6.55	77.17857	21.37804	15.86	81.62394	33.45928	22.64	81.89548	35.17147	29.96	95.21685	4.502317	14.93	91.83706	21.89726
31.68	74.42355	4.463081	6.55	77.22208	21.4712	15.86	81.49396	33.73537	22.64	81.6289	35.43832	29.96	95.29519	4.699183	14.93	92.12446	22.03978
31.68	74.53538	4.248264	6.55	77.38763	21.40409	15.86	81.49658	33.70341	22.64	81.76469	35.52834	29.96	95.37839	4.429617	14.93	92.22073	22.04214
31.68	74.5961	3.979988	6.55	77.43247	21.23724	15.86	81.25942	33.6304	22.64	81.53067	35.66008	29.96	95.46323	4.241243	14.93	92.01184	22.17844
31.68	74.62729	3.892581	6.55	77.54546	21.21097	15.86	81.07428	33.88374	22.64	81.52039	35.79258	29.96	95.51321	4.280791	14.93	92.14593	22.16873
31.68	74.57012	3.972135	6.55	77.55399	21.26501	15.86	80.70065	34.23958	22.64	81.12657	36.13213	29.96	95.33098	4.219763	14.93	92.57497	21.97571
31.68	74.41219	3.887861	6.55	77.57548	21.17456	15.86	80.59463	34.25269	22.64	80.85216	36.38057	29.96	95.30304	3.959782	14.93	92.44351	22.08646
31.68	74.58103	3.963365	6.55	77.65688	21.3059	15.86	80.531	34.53078	22.64	81.02945	36.75712	29.96	95.3856	4.200164	14.93	92.53727	22.36679
31.68	74.55698	4.313503	6.55	77.72729	21.68392	15.86	80.22382	35.14744	22.64	80.69925	37.40269	29.96	95.45551	4.626848	14.93	92.41967	22.93337
31.68	74.60357	4.520388	6.55	77.80588	21.81889	15.86	80.18277	35.49387	22.64	80.62464	37.74498	29.96	95.65772	4.693716	14.93	92.66553	23.06895
31.68	74.59864	4.733552	6.55	77.6921	22.14398	15.86	79.81259	35.98083	22.64	80.37383	38.16605	29.96	95.61474	5.183518	14.93	92.42556	23.57996
31.68	74.56024	4.760991	6.55	77.68168	22.20253	15.86	79.6298	36.1773	22.64	79.91667	38.53411	29.96	95.74616	5.304931	14.93	92.35921	23.79763
31.68	74.55497	4.603514	6.55	77.64331	21.93057	15.86	79.64244	36.17617	22.64	79.92583	38.35927	29.96	95.72315	5.170694	14.93	92.43583	23.70575
31.68	74.57569	4.337368	6.55	77.65301	21.83028	15.86	79.57461	36.11418	22.64	79.81832	38.30526	29.96	95.75337	5.087175	14.93	92.34501	23.73752
31.68	74.58971	4.487682	6.55	77.67533	22.05535	15.86	79.31235	36.21793	22.64	79.52972	38.3141	29.96	95.67769	5.316371	14.93	92.19982	24.04121
31.68	74.50572	4.576556	6.55	77.66468	22.20555	15.86	79.33674	36.19306	22.64	79.46521	38.21655	29.96	95.96787	5.420244	14.93	92.21676	24.3526
31.68	74.82208	4.568503	6.55	77.73929	22.32276	15.86	79.29558	36.09916	22.64	79.53267	38.13135	29.96	96.04161	5.60467	14.93	92.54325	24.35887
31.68	74.81344	4.334326	6.55	77.73077	22.10731	15.86	79.21115	35.74213	22.64	79.67308	37.88431	29.96	96.26	5.567977	14.93	92.376	24.35263
31.68	74.66445	4.366513	6.55	77.64272	22.15771	15.86	78.93602	35.72332	22.64	79.60943	37.61152	29.96	96.21028	5.781177	14.93	92.31598	24.55729
31.68	74.63647	4.531881	6.55	77.64047	22.26288	15.86	79.18305	35.606	22.64	79.56419	37.56921	29.96	96.33557	5.910523	14.93	92.16174	24.75209
31.68	74.73759	4.266945	6.55	77.51976	22.09347	15.86	78.99853	35.22468	22.64	79.35918	37.24855	29.96	96.37827	5.902545	14.93	92.11969	24.80226

pt30_Z	pt31_X	pt31_Y	pt31_Z
24.38	87.52615	1.058607	7.29
24.38	87.66078	1.405109	7.29
24.38	87.75215	1.266406	7.29
24.38	87.61936	1.371157	7.29
24.38	87.64793	1.347322	7.29
24.38	87.7211	1.135294	7.29
24.38	87.68078	0.833227	7.29
24.38	87.73241	0.703136	7.29
24.38	87.69758	0.350036	7.29
24.38	87.69715	0.151375	7.29
24.38	87.66157	-0.05847	7.29
24.38	87.73047	-0.36614	7.29
24.38	87.80671	-0.2535	7.29
24.38	87.88939	0.100775	7.29
24.38	87.92592	0.168535	7.29
24.38	87.99108	0.231742	7.29
24.38	88.01373	-0.33837	7.29
24.38	88.04382	-0.23906	7.29
24.38	88.03114	-0.41882	7.29
24.38	88.01611	-0.51711	7.29
24.38	88.0189	-0.38281	7.29
24.38	88.13259	-0.32115	7.29
24.38	88.12902	-0.02465	7.29
24.38	88.19416	-0.37732	7.29
24.38	88.26167	-0.40959	7.29
24.38	88.19486	-0.38067	7.29
24.38	88.05743	-0.94735	7.29
24.38	88.01565	-0.8754	7.29
24.38	87.98298	-0.69984	7.29
24.38	87.90791	-0.63695	7.29
24.38	87.9028	-0.76682	7.29
24.38	87.80415	-0.71194	7.29
24.38	87.62595	-0.75812	7.29
24.38	87.60555	-0.93225	7.29
24.38	87.59366	-0.92748	7.29
24.38	87.50649	-0.85625	7.29
24.38	87.48794	-0.5121	7.29
24.38	87.42365	-0.60998	7.29
24.38	87.54153	-0.58534	7.29
24.38	87.41615	-0.55512	7.29
24.38	87.35053	-0.58137	7.29
24.38	87.038	-0.44161	7.29
24.38	86.98656	-0.25149	7.29
24.38	87.08026	-0.44483	7.29
24.38	87.13167	-0.28802	7.29
24.38	87.11751	-0.18005	7.29
24.38	86.96854	0.23813	7.29
24.38	86.96462	-0.16249	7.29
24.38	87.08983	-0.32173	7.29
24.38	87.19577	-0.29394	7.29
24.38	87.03514	-0.01133	7.29
24.38	87.0867	-0.1922	7.29
24.38	87.1428	-0.10751	7.29
24.38	87.33878	-0.09645	7.29
24.38	87.30331	-0.23175	7.29
24.38	87.35553	-0.37135	7.29
24.38	87.21472	-0.36437	7.29
24.38	87.11113	-0.02933	7.29
24.38	87.25223	-0.27056	7.29
24.38	87.34553	-0.01257	7.29
24.38	87.37094	-0.06657	7.29
24.38	87.28757	0.10381	7.29
24.38	87.32304	-0.0929	7.29
24.38	87.27705	-0.20483	7.29
24.38	87.17856	-0.25279	7.29
24.38	86.9757	-0.34648	7.29
24.38	86.87074	-0.57345	7.29
24.38	86.87492	-0.30983	7.29
24.38	86.84123	0.180412	7.29
24.38	87.19985	0.127252	7.29
24.38	87.15672	0.542813	7.29
24.38	87.35382	0.485707	7.29
24.38	87.16411	0.355403	7.29
24.38	87.13075	0.14113	7.29
24.38	86.98273	0.257778	7.29
24.38	86.97179	0.490959	7.29
24.38	86.97355	0.592538	7.29
24.38	87.126	0.312462	7.29
24.38	87.19668	0.481943	7.29
24.38	87.10468	0.692817	7.29
24.38	87.26272	0.520127	7.29

Description of S3: 3-D Animation of Stingray Pectoral Fin

Notes:

- S3 is an animation based on the xyz data given in S2.
- Anterior is to the right, showing the propulsive wave of undulation passing down the right pectoral fin from anterior to posterior.
- Colors depict mean velocity of each point between frames; note that this differs from wavespeed, which is the velocity of the propulsive wave crossing the disc (see text). Warmer colors indicate higher velocities; units are mm/s.
- Sequences were filmed at 250 frames s^{-1}, but data was downsampled by a factor of five prior to animation—the animation uses every fifth timestep of the data in S2.